Hashemite Kingdom of Jordan

Scientific Research Support Fund

Hashemite University

Jordan Journal of Earth and Environmental Sciences

JJEES

An International Peer-Reviewed Scientific Journal

Financed by the Scientific Research Support Fund

http://jjees.hu.edu.jo/

Volume (9) Number (1) ISSN 1995-6681 April 2018 / Sha'ban 1439

Jordan Journal of Earth and Environmental Sciences (JJEES)

JJEES is an International Peer-Reviewed Research Journal, Issued by Deanship of Scientific Research, The Hashemite University, in corporation with, the Jordanian Scientific Research Support Fund, the Ministry of Higher Education and Scientific Research.

Editorial Board:

The International Advisory Board:

Editorial Board Support Team:

Submission address:

Manuscripts should be submitted electronically to the following e-mail:

jjees@hu.edu.jo

For more information and previous issues:

www.jjees.hu.edu.jo

Hashemite Kingdom of Jordan

Scientific Research Support Fund

Hashemite University

Jordan Journal of Earth and Environmental Sciences

JJEES

An International Peer-Reviewed Scientific Journal

Financed by the Scientific Research Support Fund

Volume 9 Number (1)

http:// jjees.hu.edu.jo/

ISSN 1995-6681

المجلة الأردنية لعلوم الأرض والبيئة
Jordan Journal of Earth and Environmental Sciences (JJEES)
http://jjees.hu.edu.jo

Hashemite University

Deanship of Scientific Research

TRANSFER OF COPYRIGHT AGREEMENT

Journal publishers and authors share a common interest in the protection of copyright: authors principally because they want their creative works to be protected from plagiarism and other unlawful uses, publishers because they need to protect their work and investment in the production, marketing and distribution of the published version of the article. In order to do so effectively, publishers request a formal written transfer of copyright from the author(s) for each article published. Publishers and authors are also concerned that the integrity of the official record of publication of an article (once refereed and published) be maintained, and in order to protect that reference value and validation process, we ask that authors recognize that distribution (including through the Internet/WWW or other on-line means) of the authoritative version of the article as published is best administered by the Publisher.

To avoid any delay in the publication of your article, please read the terms of this agreement, sign in the space provided and return the complete form to us at the address below as quickly as possible.

Article entitled:----------

Corresponding author: ----------

To be published in the journal: Jordan Journal of Earth & Environmental Sciences (JJEES)

I hereby assign to the Hashemite University the copyright in the manuscript identified above and any supplemental tables, illustrations or other information submitted therewith (the "article") in all forms and media (whether now known or hereafter developed), throughout the world, in all languages, for the full term of copyright and all extensions and renewals thereof, effective when and if the article is accepted for publication. This transfer includes the right to adapt the presentation of the article for use in conjunction with computer systems and programs, including reproduction or publication in machine-readable form and incorporation in electronic retrieval systems.
Authors retain or are hereby granted (without the need to obtain further permission) rights to use the article for traditional scholarship communications, for teaching, and for distribution within their institution.

☐ **I am the sole author of the manuscript**

☐ **I am signing on behalf of all co-authors of the manuscript**

☐ **The article is a 'work made for hire' and I am signing as an authorized representative of the employing company/institution**

Please mark one or more of the above boxes (as appropriate) and then sign and date the document in black ink.

Signed:_____ **Name printed:** _____

Title and Company (if employer representative) : _____

Date: _____

Data Protection: By submitting this form you are consenting that the personal information provided herein may be used by the Hashemite University and its affiliated institutions worldwide to contact you concerning the publishing of your article.

Please return the completed and signed original of this form by mail or fax, or a scanned copy of the signed original by e-mail, retaining a copy for your files, to:

Deanship of Scientific Research
The Hashemite University P.O. Box 150458, P.C.13115, Zarqa, Jordan
Tel.: 00962 53903333/ Ext. 4235
Fax: 00962 53826823
E-mail: jjees@hu.edu.jo

Subscription

Jordan Journal of Earth & Environmental Sciences (ISSN 1995-6681)
An International Peer- Reviewed Research Journal
Published by the Deanship of Scientific Research - The Hashemite University

Name:	الاســـــــــــم:
Specialty:.....	التخصـــــــــص:
Address:.....	العنـــــــــوان:
P.O. Box:.....	صنـــدوق البريـــــد:
City & Postal Code:	المدينة: الرمز البريدي:
Country:.....	الـــــــــــدولة:
Phone:.....	رقـــم الهاتـــــف:
Fax No:.....	رقـــم الفاكـــــس:
E-mail:.....	البريـــد الإلكترونـــي:
Method of payment:	طريقـــــة الدفـــع:
Amount Enclosed:.....	المبلـــغ المرفـــق:
Signature:.....	التوقيـــــــــع:

Cheques should be paid to Deanship of Research - The Hashemite University

I would like to subscribe to the Journal:

For

- ☐ One year
- ☐ Two years
- ☐ Three years

One year Subscription Rates

	Inside Jordan	Outside Jordan
Individuals	10JD	70$
Students	5JD	35$
Institutions	20JD	90$

Correspondence

Subscriptions and sales:

Professor Issa Makhlouf
Deanship of Scientific Research
The Hashemite University P.O. Box 150458, P.C.13115, Zarqa, Jordan
Tel.: 00962 53903333/ Ext. 4235
Fax: 00962 53826823
E-mail: jjees@hu.edu.jo

JJEES
Jordan Journal of Earth and Environmental Sciences

JJEES
Jordan Journal of Earth and Environmental Sciences

Volume 9, (Number 1), April, 2018
ISSN 1995-6681
Pages 1 - 11

An Assessment of Heavy Metal Soil Contamination in a Steel Factory and the Surrounding Area in Erbil City

Nashmeel Saeed Khudhur[1], Shelan Mustafa Khudhur[1], and Idrees Nadir Ahmad[2]

[1] Department of Environmental Science, College of Science, University of Salahaddin, Erbil, Kurdistan Region, Iraq
[2] Department of Geology, College of Science, University of Salahaddin, Erbil, Kurdistan Region, Iraq

Received 5 May, 2017; Accepted 16 April, 2018

Abstract

The objective of the current study is to assess the soil contamination caused by a steel factory to the surrounding areas in Erbil city. The highest value of all metals (with the exception of Al) was observed in the Erbil Steel Company (E.S.C.). The mean concentration of heavy metals followed this pattern: Fe > Al > Zn > Mn > Ti > Pb > Cu > Ni > Cr > V > Co > As ≥ Mo > Cd. Only the concentration of Ni (70-181 ppm) exceeded the WHO limits in all the studied sites. Soil pollution was assessed using many indices including: index of geoaccumulation (I_{geo}), enrichment factor (EF), contamination factor (CF), degree of contamination (C_{deg}), pollution load index (PLI), element contamination index (ECI) and the overall metal contamination index (MCI) using Al as a reference element. In comparison with the local soil backgrounds from Erbil city, moderate contamination was observed generally in the Sahdawa, Shamamal and Sardasht areas with As, Co, Cr, Mn, Mo, Ni, Ti, V and Zn. However, Sahdawa was found considerably contaminated by Pb (CF = 4.79). Sites (2-8) have a considerable degree of contamination ($16 \leq C_{deg} < 32$). PLI in all the studied sites (except for Sardasht) indicated a deterioration in the site quality (PLI > 1). The R-mode factor analysis extracted three factors: first, the metals coming mainly from the E.S.C. activities accounting for 72.292 % of the total variance. Second, the lithogenic factor accounting for 14.638 % of the total variance, and finally the sampling date accounting for 6.667% of the total variance.

Keywords: Soil pollution; Heavy metals; Steel factory.

1. Introduction

Environmental pollution is the addition of substances by human activities to the environment creating health risks to humans or damaging the natural ecosystems (Radojevic and Bashkin, 2006). The soil ecosystem is considered as a complex, living, and dynamic component that may get polluted from anthropogenic activities (e.g industrial areas). When the toxic metals, trace elements and other organic substances are accumulated on the soil, the pollutants get deposited on the soil surface (Sharma and Raju, 2013). These pollutants are sometimes carried by wind and rain from a pollution source to a great distance. (Stanley et al., 2014).

One of the industrial establishments that emit pollutants in the form of dust and gases which find their way into the soil is steel factories. Iron is the second most abundant metal on earth, and is present in very insoluble compounds (oxides-hydroxides) in aerobic environments (Howard, 1999). Most of the living systems need iron, since this metal has two readily available ionization states, Fe(II) and Fe(III), and is thus often used as a cofactor for oxidation-reduction enzymes (Guerinot, 1994). High concentrations of metals including iron may inhibit and kill microorganisms, because it catalyzes the production of free radicals (Byers and Arceneaux, 1998). The production of steel is vital for the economic growth, but its production is a major source of pollution. Steel production is often associated with significant dust particle pollution which can remain airborne and can spread over large areas through wind and rain accumulating in soils and plants (Mlitan, 2013). Dust from steel and other industrial factories lead to considerable changes in the soil pH and the accumulation of emitted metals in soil which may affect both the composition and physiological processes of microorganisms (Wuana and Okieimen, 2011). Solid and liquid wastes, including fumes generated from the steel plant and the raw materials usually contain notable amounts of heavy metals such as arsenic (As), cadmium (Cd), mercury (Hg), manganese (Mn), copper (Cu), cobalt (Co), nickel (Ni), zinc (Zn), lead (Pb) and bismuth (Bi) which may be released into the environment and cause environmental health problems (Namuhani and Kimumwe, 2015). With the global changes resulting in new challenges for the environmental protection and conservation, there is a big need for baseline data to evaluate the potential risks of the released pollutants as a result of steel production to the ecosystems (Amune et al., 2012). From a public health standpoint, it is extremely important to assert that heavy metals are transported via food chains either from domestic or wild animals, or directly from crops to humans (Radojevic and Bashkin, 2006). In the Kurdistan Region and many other areas of the world, there is a fundamental conflict between the need to develop the national economy, and the potentially

* Corresponding author. e-mail: nashmeel.khudhur@su.edu.krd

adverse environmental effects that may be associated with such economic and industrial growth.

This study is aimed at investigating the possible problems of pollution with heavy metals deposited from the Erbil Steel Factory in the surrounding environment over the last years. The analysis will be done using different contamination index methods of geoaccumulation index (I_{geo}), enrichment factor (EF), contamination factor (CF), degree of contamination (C_{deg}), pollution load index (PLI), element contamination index (ECI) and the overall metal contamination index (MCI) using Al as a reference element to differentiate the natural components from the anthropogenic ones. In addition, the soil contamination risk assessment will be investigated based on a comparison between a measured level of contamination in the soils with uncontaminated local soil values and the average soil backgrounds.

2. Materials And Methods

2.1. The Study Area

Erbil, the capital of the Iraqi Kurdistan Region is situated 414 meters above the sea level, on longitude 43º 15' E and latitude 35º 11' N to 37º 24 N' (WFP, 2002). Erbil soils are calcareous, originating from limestone and dolomite in different formations. The topsoil is calcareous with a 1-2% organic matter and exists in areas with hot-dry summers and cold rainy winters (FAO, 2001). The Erbil climate is somehow similar to the Irano-Turanian type of the semi-arid zones, characterized by cold winters, mild-growing periods in spring and hot summers (Khudhur and Khudhur, 2015).

The Erbil Steel Company (ESC) is the most prominent heavy-industry establishment in the Kurdistan Region of Iraq. It was constructed in 2006 in the Northern Iraq. Steel production started in December of 2007 with an annual production capacity of 240000 tons (ESC, 2016). The company is situated to the west of Erbil city. Originally the company started working only with the gathered iron scrap developing afterwards, into one of the biggest iron-production compounds in the region (Khudhur et al., 2016). For the sake of the present study, nine sites were selected on the basis of distance from the factory. The coordinates of the locations were taken by GPS (GARMIN) with accuracy of 5m (Table 1). The studied sites are: (1) Erbil Steel Company, (2) Khazna, (3) Tarjan, (4) Binberz, (5) Nogharan, (6) Sahdawa, (7) Qaryatagh, (8) Shamamal and (9) Sardasht and the last sample was collected from the Garden Soil in the College of Science used as control (Figure 1).

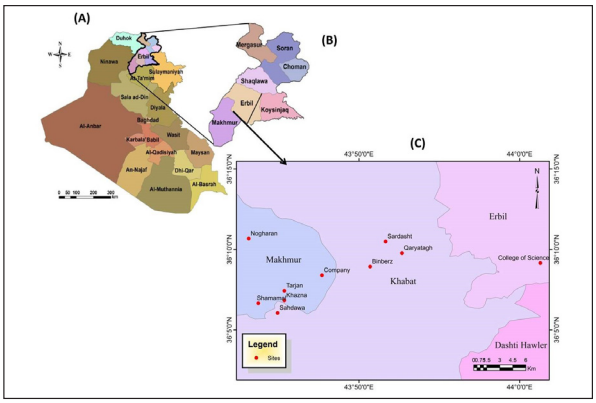

Figure 1. Map showing: (A) Iraq, (B) Erbil city and (C) the studied area.

Table 1. Detailed sampling locations around Erbil Steel Company.

Site No.	Site name	Coordination of locations	
		North	East
S1	Erbil Steel Company (E.S.C.)	36° 08' 24.00"	43° 47' 42.00"
S2	Khazna	36° 06' 50.40"	43° 45' 21.60"
S3	Tarjan	36° 07' 26.40"	43° 45' 21.60"
S4	Binberz	36° 08' 56.40"	43° 50' 42.00"
S5	Nogharan	36° 10' 40.80"	43° 43' 08.40"
S6	Sahdawa	36° 06' 03.60"	43° 44' 56.40"
S7	Qaryatagh,	36° 09' 46.80"	43° 52' 40.80"
S8	Shamamal	36° 06' 39.60"	43° 43' 44.40"
S9	Sardasht	36° 10' 30.00"	43° 51' 39.60"
S10	Science College (Control)	36° 09' 10.80"	43° 51' 39.60"

2.2. The Soil Sampling

Surface soil samples were collected from soils exposed to both waste and air effluents of the Steel Factory during the winter of 2014. In each case, the soil was scraped (5-15 cm depth) into a clean plastic bag using a stainless steel spoon. A total of three pooled samples were taken from each location collecting thirty samples from all the study areas. Soils were air-dried at room temperature (25 C°), then crushed and sieved through 2-mm stainless sieve to remove debris (Sheppard and Addison, 2008).

2.3. Analysis of some Physiochemical Characteristics of the Soil

Soil texture and particle-size distribution, moisture content, pH value, and organic matter were determined according to the methods described by (Ryan, et al. 2001). Soil texture and particle-size distribution were determined by hydrometer method; moisture content was determined by gravimetric method; soil pH was determined by using calibrated pH-meter (JENWAY 3505) and the soil organic matter was determined by Walkly-Black procedure (1934).

2.4. Determination of Heavy Metal Concentration in the Soil

The soil samples were analysed for fourteen metals including: aluminium (Al), arsenic (As), cadmium (Cd), cobalt (Co), chromium (Cr), copper (Cu), iron (Fe), manganese (Mn), molybdenum (Mo), nickel (Ni), lead (Pb), titanium (Ti), vanadium (V) and zinc (Zn). The soil samples were digested in aqua regia using 3:1 nitric to hydrochloric acids as given in (ALS, 2015). Metals in the final solutions were determined using ICP-Mass Spectroscopy (ICP-MS).

2.5. Soil Contamination Assessment Methods

The assessment of soil contamination was carried out by various methods. For the sake of this study, different indices have been applied to assess the heavy-metal distribution and contamination in the Erbil Steel Company and the related area. The indices used are: geoaccumulation index (I_{geo}), enrichment factor (EF), contamination factor (CF), degree of contamination (C_{deg}), pollution load index (PLI), element contamination index (ECI) and the overall metal contamination index (MCI). A normalized indices approach for element concentration is adopted in this study using world uncontaminated background soils, namely average soil backgrounds (Kabata-Pendias and Mukherjee, 2007), and local soil backgrounds (Alnaqshabandi, 2014) (table 2). Also

Aluminium as a metal of normalization was employed for the sake of this study.

Table 2. Background concentration of heavy metals in earth crust (Alnaqshabandi, 2014 and Kabata-Pendias and Mukherjee, 2007).

Elements \ Background		Local	Average soil
Al	%	1.85	3.995
Fe		2.43	1.749
Ti		0.04	0.7038
As	ppm	6.23	6.83
Cd		0.25	0.41
Co		14.35	11.3
Cr		70	59.5
Cu		22.75	38.9
Mn		591	488
Mo		0.59	1.1
Ni		107.5	29
Pb		8.35	27
V		52.4	129
Zn		52.75	70

2.5.1. Index of Geoaccumulation (Igeo)

The index of geoaccumulation (I_{geo}) is a quantitative measure of the extent of metal pollution in the studied soil. It is calculated using the geo-accumulation index proposed by Muller (1969) and given by (Nowrouzi and Pourkhabbaz, 2014). This index (I_{geo}) of heavy metal is calculated using the following mathematical relation:

$$I_{geo} = \log_2 [C_n/1.5B_n] \quad \text{..... (1)}$$

where C_n is the measured total concentration in the soil with the metal n,. B_n is the background value for the metal n,; the factor 1.5 (correction factor) is used because of possible variations of the background data due to lithological variations.

2.5.2. Enrichment Factor

The Enrichment Factor (EF) is a normalization method proposed by Simex and Helz (1981) to assess the concentration of the metals (Salah et al., 2012). For the present study, EF has been chosen to normalize metal concentrations using Al. The EF is defined as follows:

$$EF = (M/Al)_{Sample} / (M/Al)_{Background} \quad \text{..... (2)}$$

Where $(M/Al)_{Sample}$ is the ratio of metal and Al concentrations in the sample $(M/Al)_{Background}$ is the ratio of metal and Al concentrations of the background.

2.5.3. Contamination Factor (CF)

The contamination Factor (CF) is the concentration of each metal in the soil divided by the background concentration of the metal (concentration in unpolluted soil).

$$CF = C_{Heavy\ metal} / C_{Background} \quad \text{..... (3)}$$

The background concentrations were calculated from the heavy metal concentration in unaffected soils of the studied area (Bambara et al., 2015).

2.5.4. Degree of Contamination (C_{deg})

It is a modified and generalized form of the degree of contamination (C_{deg}) formula (Aikpokpodion et al., 2010); this formula was also proposed by (Hakanson, 1980). It is calculated by the following equation:

$$C_{deg} = \sum(C_m / B_m)^i \quad \text{..... (4)}$$

where i represents the respective metals (i.e. Al, As, Cd, Co, Cr, Cu, Fe, Mn, Mo, Ni, Pb, Ti, V and Zn), C_m is the measured concentration in the soil, and B_m is the background concentration value of metal (m) within the area of study. For the C_{deg}, Hakanson recognized four descriptive classes, where by $C_{deg} < 8$ implies a low degree of contamination. C_{deg} 8-16 means a moderate degree of contamination. C_{deg} 16-32 indicates a considerable degree of contamination and $C_{deg} \geq 32$ implies a very high degree of contamination.

2.5.5. Pollution Load Index (PLI)

The Pollution load index (PLI) provides an empirical index that comparatively assesses the level of heavy metal pollution. The PLI for the various sampling areas were determined as the geometric mean of all assessed CF of a sampling site (Afrifa et al., 2013).

$$PLI = (CF_1 \times CF_2 \times CF_3 \times .... \times CF_n)^{1/n} \quad \text{..... (5)}$$

$_n$ is the number of metal index providing a simple, comparative means for assessing the level of heavy metal pollution. A value of PLI < 1 denotes perfection. PLI = 1 indicates that only baseline levels of pollutants are present, and PLI > 1 would indicate deterioration of the site quality (Bambara et al., 2015).

2.5.6. The Element Contamination Index and the Metal Contamination Index

The Element contamination index (ECI) and the overall metal contamination index (MCI) are expressions of a single metal contamination within a sample or combined metal contamination for a sample relative to the background values of the respective metal (Singh et al., 2015) . They are expressed as:

$$ECI = (C_m - B_m / B_m) \quad \text{..... (6)}$$

$$MCI = \sum(C_m - B_m / B_m)^i \quad \text{..... (7)}$$

Where i C_m and B_m are as defined earlier. According to (Aikpokpodion et al., 2010), MCI was designed to describe general trace elements contamination. MCI of < 5 implies a very low contamination; MCI = 5-10 means low contamination; MCI = 10-25 denotes medium contamination; MCI = 25-50 means high contamination; MCI = 50-100 implies a very high contamination and MCI > 100 implies an extremely high contamination.

2.6. Statistical Analysis

Results were processed and analyzed using Microsoft Excel 2010 and SPSS Statistical Analysis Package for Windows®. Data is reported as mean ± standard error of the mean. For physicochemical properties, one-way analysis of variance (ANOVA) was performed and the multiple comparisons among the studied sites were done by using Duncan's test. A p-value of <0.05 is considered significant. Arc GIS "Geographic Information system" (version 10.2) was used for mapping the heavy metal distribution in the studied areas. The concentration of heavy metals and physicochemical properties of the studied soil samples were treated statistically by Person's correlation coefficient and R-mode factor analysis to determine the relation between these elements in the different locations of the study area.

3. Results and Discussion

3.1. Soil Physicochemical Properties

Soil water affects the moisture available to organisms, aeration status, nature and amount of soluble materials, osmotic pressure, and the pH of the soil solution (Paul, 2007). The current study has showed a moisture range of

10.26±0.040 and 21.98±0.058 % in control soil and Sardasht area respectively. Significant differences ($p<0.05$) were observed among the studied sites (table 3). This result is consistent with other finding in earlier studies conducted by Khudhur et al. (2016) on the soils of these areas. Particle-size distribution and soil texture classes were presented in table (3). Different soil texture classes were found varying from loam, sandy loam, and sandy clay loam to loamy sand.

Results show that the soil pH ranged between 7.48 and 8.83 (table 3) and this finding suggests that the studied soils are mostly in neutral to sub-alkaline condition which can be attributed to the high content of carbonate, ash and cinders of anthropogenic origin, and to the alkali components in the atmosphere which may eventually deposit on the ground and affect the soil pH (Al Obaidy and Al Mashhadi, 2013).

The soil organic matter of the Erbil Steel Company was significantly different ($p<0.05$) from the other sites, and has the highest organic matter content of 48.20±4.447 $g.Kg^{-1}$ (table 3). Zhang and Wang (2007) confirm this observation by stating that when the heavy metal pollution in the soil increases, the particulate organic matter and its proportion in the total soil organic C increase as well. Heavy metals are largely enriched with particulate organic matter, which could impact the further mineralization of soil organic matter.

Table 3. Physicochemical properties of the studied soils as (mean ± S.E.).

Site No.	Site name	Moisture %	Particle size distribution			Texture class	pH	Soil organic matter $g.Kg^{-1}$
			Clay %	Silt %	Sand %			
S1	E.S.C.	14.04±0.176^{cd}	23.39	32.17	44.44	Loam	8.83±0.176^{a}	48.20±4.447^{a}
S2	Khazna	15.76±0.069^{bc}	5.99	22.46	71.55	Sandy Loam	7.48±0.069^{e}	10.24±0.136^{def}
S3	Tarjan	20.44±0.023^{ab}	28.33	22.04	49.63	Sandy Clay Loam	7.79±0.023^{d}	20.21±0.289^{c}
S4	Binberz	20.07±0.136^{ab}	21.87	40.62	37.51	Loam	7.87±0.136^{cd}	2.77±0.000^{f}
S5	Nogharan	16.39±0.087^{bc}	6.01	27.04	66.95	Sandy Loam	8.15±0.087^{bc}	30.63±0.365^{b}
S6	Sahdawa	21.89±0.075^{a}	19.42	38.85	41.73	Loam	8.13±0.075^{bc}	32.79±0.454^{b}
S7	Qaryatagh	13.96±0.058^{cd}	17.63	35.26	47.11	Loam	8.10±0.058^{bc}	7.30±0.056^{ef}
S8	Shamamal	14.26±0.072^{cd}	14.62	35.10	50.28	Loam	8.13±0.072^{bc}	14.75±0.200^{cde}
S9	Sardasht	21.98±0.058^{a}	3.25	22.72	74.04	Loamy Sand	8.10±0.058^{bc}	35.83±0.477^{b}
S10	Control	10.26±0.040^{d}	17.87	33.19	48.93	Loam	8.38±0.040^{b}	16.63±0.000^{cd}
Maximum		21.98	28.33	40.62	74.04		8.83	48.20
Minimum		10.26	3.25	22.04	37.51		7.48	2.77

**Different letters means significant differences between the studied sites $p<0.05$.*

3.2. Soil Metal Contents

Heavy metals are especially dangerous because of their persistence and toxicity. Soil acts as a sink for heavy metals through sorption, complexation, and precipitation reactions. Due to proximity to humans, accumulation of harmful substances in urban soils is of great concern. Heavy metals may be transferred to human bodies by way of ingestion, inhalation and dermal contact, or through the food chain (Salah et al., 2013). According to the United Nation Environmental Program (UNEP), Percy et al. (1997) sited in (Elgawad et al., 2007) reported that out of the forty heavy metals in the earth, arsenic (As), cadmium (Cd), chromium (Cr), copper (Cu), lead (Pb), mercury (Hg) and nickel (Ni) are the most common heavy metals that are considered pollutants. In particular the metals arsenic, antimony, lead, mercury, copper, chromium and chromium VI, as the soluble compound of chromium, can have adverse harmful effects on human health and the environment and should thus be tested (PUMA safe, 2009). As shown in table (table 4), the concentrations of detected metals showed variable values depending on the sampling sites. It is worth mentioning that in comparison to the other sites, the soil samples collected in the factory exhibited higher concentration of metals (except for aluminum). Those results are consistent with the findings of Khudhur et al. (2016) in the Steel Company. The increment of soil metals in the same area may be a result of precipitation of iron and steel factory dusts over the years (Mlitan, 2013). Moreover, the highest Al content was detected in the Binberz soil. This difference could be relevant to the climate, soil origin, composition or human activities (Mlitan, 2013).

The highest value of all the studied metals (except for Al) was observed in Erbil Steel Company. The results showed variations in the concentrations of the elements, which possibly indicate the effects of the soil type, type of the parent rocks and anthropogenesis and industrial activities The release of industrial wastes directly into the environment without any treatment or fuel incinerator products can also be regarded as other sources of the soil pollution (Mohammed and Abdullah, 2016). The lowest values of most of the studied metals are as follows: Al (1.13 %), Fe (1.87 %), As (4 ppm), Co (11 ppm), Cr (52 ppm), Mn (395 ppm), Ni (70 ppm), Pb (9 ppm) and V (39 ppm). They were observed in the Sardasht soil. The results regarding As, Cr and Mn contents are in agreement with those of Rahman et al. (2012); the results of Cd and Cu agree with those of (Asaah et al., 2006) and the lowest Cd and Co and the

highest Cr values are in consistence with those of Odat (2015). The world median content of Cr in soils has been established as 54 ppm due to its abundance in the parent material. The Cr content of surface soils is known to have increased due to pollution by various sources. Moreover, the ranges of As (4-13 ppm), Cr (52-134 ppm) and Ni (70-181 ppm) agree with the ranges obtained by Mohammed and Abdullah (2016) in Baghdad. The lowest values of Ti (0.03 %), Cu (25 ppm) and Zn (61 ppm) were observed in Nogharan, Qaryatagh and Binberz respectively. The values of 0.5 and 1 ppm as lowest values for both Cd and Mo were observed in all of the studied sites with the exception of the Erbil Steel Company.

The results of the occurrence of the metals in all the studied sites indicated that Fe has emerged as the dominant metal, while Cd has the lowest concentration. The studied metals have shown the following sequence: Fe > Al > Zn > Mn > Ti > Pb > Cu > Ni > Cr > V > Co > As ≥ Mo > Cd.

The WHO concentration limits in the soil are 100 ppm for Pb, 3 ppm for Cd, 50 ppm for Ni, 150 ppm for Cr, 40 ppm for As and 300 ppm for Zn (Bambara et al., 2015). The concentration of Pb, Cd, Cr and Zn obtained in the studied sites (with the exception of Erbil Steel Company) are less than the WHO concentration limits. The concentration of Ni in all of the studied sites has exceeded the WHO limits, whereas the concentration of As has not reached the WHO limits in all the studied sites.

Table 4. Mean contents of heavy metals in the studied soils.

Metals \ Site No.		S1	S2	S3	S4	S5	S6	S7	S8	S9	S10	Maximum	Minimum
Al	%	1.32	1.93	1.8	2.17	1.68	1.89	2.13	1.81	1.13	1.65	2.17	1.13
Fe	%	8.76	2.47	2.38	2.48	2.13	2.51	2.46	2.63	1.87	2.06	8.76	1.87
Ti	%	0.1	0.04	0.04	0.05	0.03	0.04	0.04	0.07	0.06	0.04	0.1	0.03
As	ppm	13	5	5	6	5	5	7	11	4	5.5	13	4
Cd	ppm	8.4	0.5	0.5	0.5	0.5	0.5	0.5	0.5	0.5	0.5	8.4	0.5
Co	ppm	20	15	15	15	13	15	14	17	11	12	20	11
Cr	ppm	134	68	68	68	62	70	67	91	52	52	134	52
Cu	ppm	258	28	30	27	31	36	25	45	26	27	258	25
Mn	ppm	1420	531	556	510	500	633	528	630	395	518	1420	395
Mo	ppm	13	1	1	1	1	1	1	1	1	1	13	1
Ni	ppm	181	109	104	102	88	105	101	142	70	88	181	70
Pb	ppm	294	13	15	9.5	15	40	12	14	9	12	294	9
V	ppm	59	49	47	53	43	45	52	53	39	40.5	59	39
Zn	ppm	7485	71	73	61	92	93	66	67	70	81.5	7485	61

3.3. Results of the Soil Contamination Assessment

3.3.1. Index of Geoaccumulation (Igeo)

The calculated I_{geo} values are shown in table (5a). Compared to the local soil background, the I_{geo} values indicated uncontaminated/moderately contaminated soils for: As in both E.S.C. and Shamamal (I_{geo} = 0.48 and 0.24); Cr, Mn and Ni in E.S.C. (I_{geo} = 0.35, 0.68 and 0.17); Cu in Sahdawa and Shamamal (I_{geo} = 0.08 and 0.40); Pb in Khazna, Tarjan, Nogharan and Shamamal (I_{geo} = 0.05, 0.26, 0.26 and 0.16); and Zn in Nogharan, Sahdawa and control soils (I_{geo} = 0.22, 0.23 and 0.04); Ti in both E.S.C. and Shamamal (I_{geo} = 0.74 and 0.22) as well as Cd and Mo in all sites (except for The Erbil Steel Company) and this result is consistent with Odat (2015). The non-contamination to moderate contamination in Khazna, Tarjan, Nogharan and Shamamal with Pb could be attributed to the road network on the west side of the Factory that supplies raw materials to the factory; the high heavy metal load on this side is attributed to anthropogenic effects such as the burning of fossil fuel, wear and tear of tires, and dust generation during transportation of raw materials (Namuhani and Kimumwe, 2015).Moderate contamination was proven in both E.S.C. with Fe (I_{geo} = 1.27) and Sahdawa with Pb (I_{geo} = 1.68). The Erbil Steel Company was found moderately/strongly contaminated with Cu (I_{geo} = 2.93), strongly contaminated with Mo (I_{geo} = 3.89) and strongly/extremely contaminated with Cd (I_{geo} = 4.51) and Pb (I_{geo} = 4.57).

Based on the average soil background, the I_{geo} values indicated uncontaminated/moderately contaminated soils for: As in E.S.C. and Shamamal (I_{geo} = 0.35 and 0.10); Co and Mn in E.S.C. (I_{geo} = 0.24 and 0.96) respectively; Cr in E.S.C. and Shamamal (I_{geo} = 0.59 and 0.03) and Ni in Sardasht soil. It is evident that the I_{geo} values for Fe (in E.S.C.) and Ni (except for E.S.C. and Sardasht) are ($1 < I_{geo} < 2$) (table 5b) and can be classified as moderately contaminated. The Erbil Steel Company was found moderately/strongly contaminated by Cu, Mo, Ni and Pb (I_{geo} = 2.15, 2.99, 2.07 and 2.87) respectively. It was found strongly contaminated by Cd (I_{geo} = 3.79) and extremely contaminated with Zn (I_{geo} = 6.18).

Table 5 a. Geoaccumulation Index (I_{geo}) of trace elements based on local and average soil backgrounds in the study area.

	Site No. \ Elements	Al	As	Cd	Co	Cr	Cu	Fe	Mn	Mo	Ni	Pb	Ti	V	Zn
Local background	S1	-1.08	0.48	4.51	-0.11	0.35	2.93	1.27	0.68	3.89	0.17	4.57	0.74	-0.42	6.59
	S2	-0.53	-0.91	0.42	-0.52	-0.63	-0.29	-0.56	-0.74	0.18	-0.57	0.05	-0.59	-0.68	-0.16
	S3	-0.63	-0.91	0.42	-0.52	-0.63	-0.19	-0.62	-0.68	0.18	-0.64	0.26	-0.59	-0.75	-0.12
	S4	-0.36	-0.64	0.42	-0.52	-0.63	-0.34	-0.56	-0.80	0.18	-0.66	-0.40	-0.26	-0.57	-0.38
	S5	-0.73	-0.91	0.42	-0.73	-0.76	-0.14	-0.78	-0.83	0.18	-0.88	0.26	-1.00	-0.87	0.22
	S6	-0.56	-0.91	0.42	-0.52	-0.59	0.08	-0.54	-0.49	0.18	-0.62	1.68	-0.59	-0.81	0.23
	S7	-0.38	-0.42	0.42	-0.62	-0.65	-0.45	-0.57	-0.75	0.18	-0.68	-0.06	-0.59	-0.60	-0.26
	S8	-0.62	0.24	0.42	-0.34	-0.21	0.40	-0.47	-0.50	0.18	-0.18	0.16	0.22	-0.57	-0.24
	S9	-1.30	-1.23	0.42	-0.97	-1.02	-0.39	-0.97	-1.17	0.18	-1.21	-0.48	0.00	-1.02	-0.18
	S10	-0.75	-0.77	0.42	-0.85	-1.02	-0.34	-0.83	-0.78	0.18	-0.88	-0.06	-0.78	-0.96	0.04
Average soil	S1	-2.19	0.35	3.79	0.24	0.59	2.15	1.75	0.96	2.99	2.07	2.87	-3.42	-1.72	6.18
	S2	-1.64	-1.04	-0.30	-0.18	-0.39	-1.06	-0.09	-0.47	-0.73	1.33	-1.65	-4.74	-1.99	-0.57
	S3	-1.74	-1.04	-0.30	-0.18	-0.39	-0.96	-0.14	-0.40	-0.73	1.26	-1.44	-4.74	-2.05	-0.53
	S4	-1.47	-0.78	-0.30	-0.18	-0.39	-1.12	-0.08	-0.52	-0.73	1.24	-2.10	-4.42	-1.88	-0.79
	S5	-1.84	-1.04	-0.30	-0.38	-0.53	-0.92	-0.30	-0.55	-0.73	1.02	-1.44	-5.16	-2.18	-0.19
	S6	-1.67	-1.04	-0.30	-0.18	-0.35	-0.70	-0.06	-0.21	-0.73	1.28	-0.02	-4.74	-2.11	-0.18
	S7	-1.50	-0.55	-0.30	-0.28	-0.42	-1.23	-0.09	-0.47	-0.73	1.22	-1.76	-4.74	-1.90	-0.67
	S8	-1.74	0.10	-0.30	0.00	0.03	-0.38	0.00	-0.22	-0.73	1.71	-1.54	-3.93	-1.88	-0.65
	S9	-2.42	-1.36	-0.30	-0.63	-0.78	-1.17	-0.49	-0.89	-0.73	0.69	-2.18	-4.16	-2.32	-0.59
	S10	-1.87	-0.90	-0.30	-0.50	-0.78	-1.12	-0.35	-0.50	-0.73	1.02	-1.76	-4.94	-2.27	-0.37

Table 5 b. Index of geoaccumulation (I_{geo}) for contamination levels in the soils.

I_{geo} Class	I_{geo} Value	Contamination Level
0	$I_{geo} \leq 0$	Uncontaminated
1	$0 < I_{geo} < 1$	Uncontaminated/moderately contaminated
2	$1 < I_{geo} < 2$	Moderately contaminated
3	$2 < I_{geo} < 3$	Moderately/strongly contaminated
4	$3 < I_{geo} < 4$	Strongly contaminated
5	$4 < I_{geo} < 5$	Strongly/extremely contaminated
6	$5 < I_{geo}$	Extremely contaminated

** Taken from (Rahman et al., 2012).*

3.3.2. Enrichment factor

The Enrichment Factor (EF) is the relative abundance of an element in a soil compared to the bedrock. The EF was calculated by a comparison of each tested metal concentration with that of a reference metal. The normally used reference metals are Mn, Al, and Fe. In this study Al was used to keep differences between natural from anthropogenic components. according to the hypothesis that the content components in the earth crust have not been troubled or disturbed by anthropogenic activity effects. Al is chosen as the element of normalization because natural sources and natural processes are approximated equal to (98%) of the all processes that the earth evolved; i.e. the natural sources greatly dominate its contribution (Shukur and Al-Tamimi, 2016).

The results of the Enrichment Factor of the studied metals are presented in table (6a). On the basis of the local soil backgrounds while taking Al as a reference element, and according to the contamination categories established by (Loska et al., 2003) given in table (6b), most of the studied areas (except for E.S.C.) have minimal enrichment. The contamination categories of EF showed that the Erbil Steel Company has moderate enrichment for As, Cr, Mn, Ni and Ti (EF = 2.92, 2.68, 3.37, 2.36 and 3.50) respectively; significant enrichment for Cu and Fe (EF = 15.89 and 5.05) respectively; very high enrichment for Mo (EF = 30.88), and extremely high enrichment for Cd, Pb and Zn (EF = 47.09, 49.35 and 198.9) respectively. Sardasht area showed moderate enrichment with Mo (EF = 2.77), Ti (EF = 2.46) and Zn (EF = 2.17). Shamamal and Sahdawa revealed moderate enrichment with Cu and Pb (EF = 2.02 and 4.69) respectively. Cadmium caused moderate enrichment in different sites including Tarjan (EF = 2.06), Nogharan (EF = 2.20), Shamamal (EF = 2.04), Sardasht (EF = 3.27) and garden soil (EF = 2.24). Generally speaking, the soils of the study area are mainly derived from the upper cretaceous carbonate rocks. However, carbonates in general have low concentrations of Pb and Cd, so the possible source of these metals may be anthropogenic. Since the soil samples have been taken along different distances from the Erbil Steel Company, it can be considered as the main source of the metals in the soils of the study area.

Based on the average soil background, all the studied areas (except for E.S.C.) are moderately enriched by the elements Cd, Co, Cr and Fe. Moderate enrichment by Mn in all the studied areas (except for E.S.C. and Binberz). Moderate enrichment of As, Cu, Mo, Pb and Zn was found in different areas (table 6a). The elements As, Co, Cr, Fe, and Mn are significantly enriched in the Erbil Steel Company.

All the studied areas showed significant enrichment of Ni. Mohammed and Abdullah (2016) stated that Ni in soil is strongly associated with Fe and Mn oxides. Also clay minerals, in particular montmorillonite, exhibit great capability to bind this metal. The elevated Ni concentrations may be related to oil combustion and agricultural activities (phosphate fertilizers) in these areas. The Erbil Steel Company showed very high enrichment due to the elements Cu (EF = 20.07), Mo (EF = 35.77) and Pb (EF = 32.96), and showed extremely high enrichment of both Cd and Zn, with EF > 40.

Table 6 a. Enrichment factor (EF) of trace elements based on local and average soil backgrounds in the study area using Al as a reference element.

	Elements / Site No.	Al	As	Cd	Co	Cr	Cu	Fe	Mn	Mo	Ni	Pb	Ti	V	Zn
Local background	S1	1.00	2.92	47.09	1.95	2.68	15.89	5.05	3.37	30.88	2.36	49.35	3.50	1.58	198.9
	S2	1.00	0.77	1.92	1.00	0.93	1.18	0.97	0.86	1.62	0.97	1.49	0.96	0.90	1.29
	S3	1.00	0.82	2.06	1.07	1.00	1.36	1.01	0.97	1.74	0.99	1.85	1.03	0.92	1.42
	S4	1.00	0.82	1.71	0.89	0.83	1.01	0.87	0.74	1.44	0.81	0.97	1.07	0.86	0.99
	S5	1.00	0.88	2.20	1.00	0.98	1.50	0.97	0.93	1.87	0.90	1.98	0.83	0.90	1.92
	S6	1.00	0.79	1.96	1.02	0.98	1.55	1.01	1.05	1.66	0.96	4.69	0.98	0.84	1.73
	S7	1.00	0.98	1.74	0.85	0.83	0.95	0.88	0.78	1.47	0.82	1.25	0.87	0.86	1.09
	S8	1.00	1.80	2.04	1.21	1.33	2.02	1.11	1.09	1.73	1.35	1.71	1.79	1.03	1.30
	S9	1.00	1.05	3.27	1.25	1.22	1.87	1.26	1.09	2.77	1.07	1.76	2.46	1.22	2.17
	S10	1.00	0.99	2.24	0.94	0.83	1.33	0.95	0.98	1.90	0.92	1.61	0.98	0.87	1.73
Average soil	S1	1.00	5.76	62.01	5.36	6.82	20.07	15.16	8.81	35.77	18.89	32.96	0.43	1.38	323.6
	S2	1.00	1.52	2.52	2.75	2.37	1.49	2.92	2.25	1.88	7.78	1.00	0.12	0.79	2.10
	S3	1.00	1.62	2.71	2.95	2.54	1.71	3.02	2.53	2.02	7.96	1.23	0.13	0.81	2.31
	S4	1.00	1.62	2.25	2.44	2.10	1.28	2.61	1.92	1.67	6.48	0.65	0.13	0.76	1.60
	S5	1.00	1.74	2.90	2.74	2.48	1.90	2.90	2.44	2.16	7.22	1.32	0.10	0.79	3.13
	S6	1.00	1.55	2.58	2.81	2.49	1.96	3.03	2.74	1.92	7.65	3.13	0.12	0.74	2.81
	S7	1.00	1.92	2.29	2.32	2.11	1.21	2.64	2.03	1.71	6.53	0.83	0.11	0.76	1.77
	S8	1.00	3.55	2.69	3.32	3.38	2.55	3.32	2.85	2.01	10.81	1.14	0.22	0.91	2.11
	S9	1.00	2.07	4.31	3.44	3.09	2.36	3.78	2.86	3.21	8.53	1.18	0.30	1.07	3.54
	S10	1.00	1.95	2.95	2.57	2.12	1.68	2.84	2.57	2.20	7.35	1.08	0.12	0.76	2.82

Table 6 b. Soil contamination categories based on enrichment factor (EF).

EF Value	Contamination Level
EF < 2	Minimal enrichment
EF = 2-5	Moderate enrichment
EF = 5-20	Significant enrichment
EF = 20-40	Very high enrichment
EF > 40	Extremely high enrichment

** Taken from (Loska et al., 2003).*

3.3.3. Contamination factor (CF)

The contamination factor was used to determine the contamination status of the soils. Generally the CF of the trace elements (Al, As, Co, Cr, Mn, Ni, Ti and V) of soil samples in the studied areas based on the local soil background was indicating low to moderate contamination except for Erbil Steel Company which showed considerable to very high contamination by Fe (CF = 3.60), Cd (CF = 33.60), Cu (CF = 11.34), Mo (CF = 22.03), Pb (CF = 35.21) and Zn (CF = 141.9) (table 7a). The accumulation of metals in these areas are strongly controlled by the nature of the substrate as well as the physicochemical conditions controlling dissolution and precipitation (Shukur and Al-Tamimi, 2016). The Soil of Sahdawa area revealed considerable contamination by Pb (CF<6) as given in table (7b).

Compared to the average soil backgrounds, the studied areas revealed low to moderate contamination by As and Cr. With the exception of Sardasht which revealed low contamination, the remaining areas are moderately contaminated by Co and Mn. All the studied sites (except for E.S.C.) have moderate contamination regarding the CF values for Cd and Fe. In Shamamal, moderate contamination by Cu (CF = 1.16) was found; in Sardasht by Ni (CF = 2.41) and in Sahdawa by Pb (CF = 1.48). Moderate contamination by Zn was revealed in the sites S2, S3, S5, S6, S9 and S10. Ni caused considerable contamination in all the studied sites except for E.S.C. and Sardasht where there is very high contamination with (CF = 6.24), and moderate contamination with (CF = 2.41) respectively. This can be attributed to the influence of industrial activities, agricultural runoff, and other anthropogenic inputs. The Erbil Steel Company was considerably contaminated by Fe (CF<6), and was very highly contaminated by Cd, Cu, Mo, Pb and Zn (CF > 6).

Table 7 a. Contamination factor (CF) of trace elements based on local and average soil backgrounds in the study area.

	Elements / Site No.	Al	As	Cd	Co	Cr	Cu	Fe	Mn	Mo	Ni	Pb	Ti	V	Zn
Local background	S1	0.71	2.09	33.60	1.39	1.91	11.34	3.60	2.40	22.03	1.68	35.21	2.50	1.13	141.9
	S2	1.04	0.80	2.00	1.05	0.97	1.23	1.02	0.90	1.69	1.01	1.56	1.00	0.94	1.35
	S3	0.97	0.80	2.00	1.05	0.97	1.32	0.98	0.94	1.69	0.97	1.80	1.00	0.90	1.38
	S4	1.17	0.96	2.00	1.05	0.97	1.19	1.02	0.86	1.69	0.95	1.14	1.25	1.01	1.16
	S5	0.91	0.80	2.00	0.91	0.89	1.36	0.88	0.85	1.69	0.82	1.80	0.75	0.82	1.74
	S6	1.0 2	0.80	2.00	1.05	1.00	1.58	1.03	1.07	1.69	0.98	4.79	1.00	0.86	1.76
	S7	1.15	1.12	2.00	0.98	0.96	1.10	1.01	0.89	1.69	0.94	1.44	1.00	0.99	1.25
	S8	0.98	1.77	2.00	1.18	1.30	1.98	1.08	1.07	1.69	1.32	1.68	1.75	1.01	1.27
	S9	0.61	0.64	2.00	0.77	0.74	1.14	0.77	0.67	1.69	0.65	1.08	1.50	0.74	1.33
	S10	0.89	0.88	2.00	0.84	0.74	1.19	0.85	0.88	1.69	0.82	1.44	0.88	0.77	1.55
Average soil	S1	0.33	1.90	20.49	1.77	2.25	6.63	5.01	2.91	11.82	6.24	10.89	0.14	0.46	106.9
	S2	0.48	0.73	1.22	1.33	1.14	0.72	1.41	1.09	0.91	3.76	0.48	0.06	0.38	1.01
	S3	0.45	0.73	1.22	1.33	1.14	0.77	1.36	1.14	0.91	3.59	0.56	0.06	0.36	1.04
	S4	0.54	0.88	1.22	1.33	1.14	0.69	1.42	1.05	0.91	3.52	0.35	0.07	0.41	0.87
	S5	0.42	0.73	1.22	1.15	1.04	0.80	1.22	1.02	0.91	3.03	0.56	0.04	0.33	1.31
	S6	0.47	0.73	1.22	1.33	1.18	0.93	1.44	1.30	0.91	3.62	1.48	0.06	0.35	1.33
	S7	0.53	1.02	1.22	1.24	1.13	0.64	1.41	1.08	0.91	3.48	0.44	0.06	0.40	0.94
	S8	0.45	1.61	1.22	1.50	1.53	1.16	1.50	1.29	0.91	4.90	0.52	0.10	0.41	0.96
	S9	0.28	0.59	1.22	0.97	0.87	0.67	1.07	0.81	0.91	2.41	0.33	0.09	0.30	1.00
	S10	0.41	0.81	1.22	1.06	0.87	0.69	1.17	1.06	0.91	3.03	0.44	0.05	0.31	1.16

Table 7 b. Soil contamination categories based on contamination factor (CF).

CF Value	Contamination Level
CF<1	Low contamination
1<CF<3	Moderate contamination
3<CF<6	Considerable contamination
CF>6	Very high contamination

** Taken from (Afrifa et al., 2013).*

3.3.4. Degree of Contamination (Cdeg)

The degree of contamination (C_{deg}) results of the soil samples in the studied area are presented in (Figure 2). Compared to the local soil backgrounds, the sites (2-8) have a considerable degree of contamination represented by (Aikpokpodion et al., 2010). Compared to the average soil backgrounds, the sites (2, 3, 4, 5 and 7) have a moderate degree of contamination ($8 \leq C_{deg} < 16$), while the sites 6 and 8 have a considerable degree of contamination ($16 \leq C_{deg} < 32$). On the basis of both local and average soil backgrounds, Sardasht and garden soil (control) have a moderate degree of contamination, while the Erbil Steel Company has a very high degree of contamination ($C_{deg} \geq 32$).

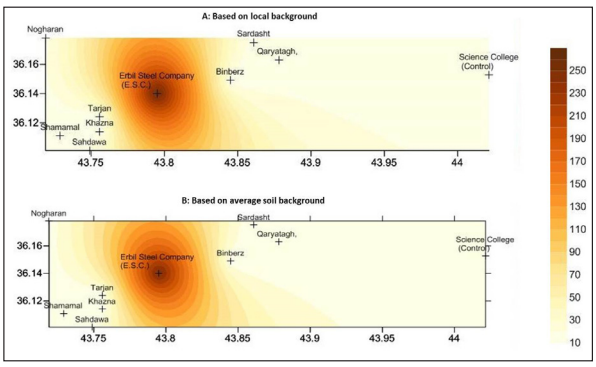

Figure 2. Degree of Contamination (C_{deg}) in the studied soils based on A: local soil backgrounds, and B: average soil backgrounds.

3.3.5. Pollution Load Index (PLI)

Pollution Load Index (PLI) was used to evaluate the extent of pollution by heavy metals in the environment. If PLI < 1, there is no heavy metal pollution (Tomlinson et al., 1980). The values of PLI > 1 imply that heavy metal pollution exists in the study areas. During this study the PLI values were > 1 on the basis of the local soil backgrounds in all the studied sites (except for Sardasht). The results indicated deterioration in the site quality (Figure 3) which can be attributed to the absence of dust collectors and a perimeter wall around the factory. Also all the fumes and gases from the factory are released into the environment. On the basis of soil average backgroundS, all the studied areas (except for E.S.C.) have denoted perfection (PLI < 1) and the Erbil steel company showed deterioration in the site quality (PLI = 3.40). These study findings are in consistent with the findings in studies conducted by Namuhani and Kimumwe (2015) around a steel-processing factory in Uganda.

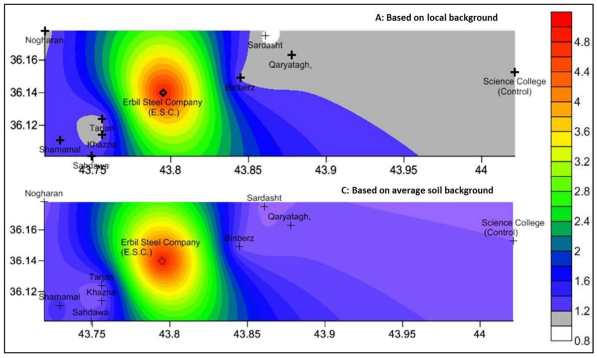

Figure 3. Pollution load index (PLI) in the studied area based on A: local soil backgrounds, and B: average soil backgrounds.

3.3.6. Element Contamination Index and Metal Contamination Index

According to the classification of MCI given by (Aikpokpodion et al., 2010), Sahdawa (MCI = 6.6) and Shamamal (MCI = 6.1), the soils revealed low contamination based on local soil backgrounds. The Erbil Steel Company showed extremely high contamination (MCI = 247.5 and 163.8) based on comparisons with local and average soil backgrounds respectively (Figure 4).

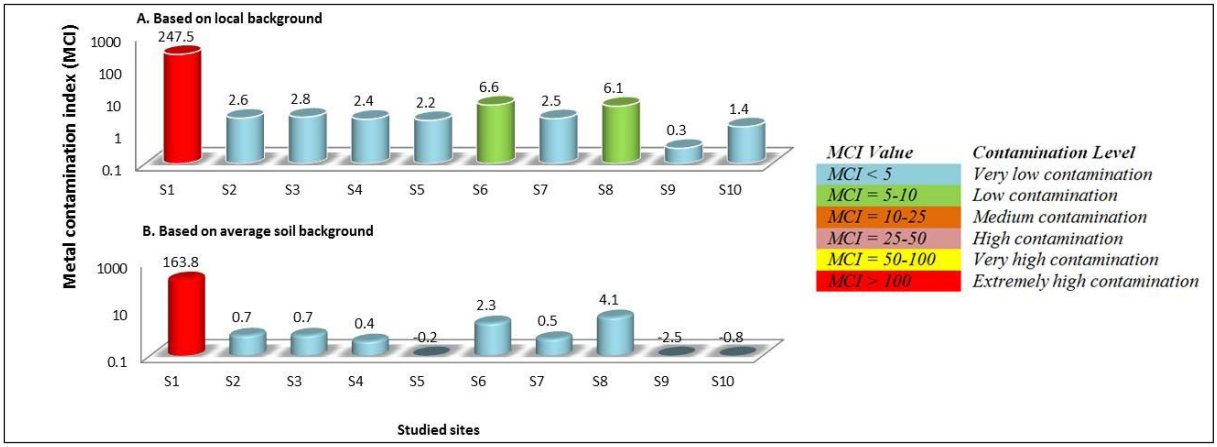

Figure 4. Metal contamination index (MCI) in the studied soils based on A: local soil backgrounds, and B: average soil backgrounds.

3.4. Results of the Statistical Correlation

Person's correlation analysis (table 8) showed high significant positive correlations ($p<0.01$) between soil organic matter and Al ($r = 0.82$). Generally there were strong positive correlations among the studied metals which may indicate that these metals are from the same source as stated by (Stanley et al., 2014). These results are also observed earlier by Khudhur et al. (2016). The strong association of Cd, Zn, and Cu indicates common sources, and that these metals may have been derived from anthropogenic sources, especially the industries (Rahman et al., 2012).

Table 8. Person's correlation among soil physicochemical properties and heavy metals in the studied areas.

	Al	As	Cd	Co	Cr	Cu	Fe	Mn	Mo	Ni	Pb	Ti	V	Zn
pH	-0.54	0.63	0.72	0.33	0.57	0.73	0.68	0.70	0.72	0.49	0.73	0.60	0.21	0.72
S.O.M.	-0.82**	0.26	0.64	0.23	0.45	0.65	0.58	0.59	0.64	0.31	0.67	0.50	-0.09	0.64
Moisture	-0.04	-0.47	-0.25	-0.18	-0.24	-0.25	-0.25	-0.28	-0.25	-0.34	-0.22	-0.11	-0.24	-0.25
Al	1	-0.15	-0.46	0.07	-0.22	-0.46	-0.38	-0.33	-0.46	-0.09	-0.45	-0.50	0.30	-0.46
As		1	0.75	0.85**	0.92**	0.79**	0.79**	0.82**	0.75	0.93**	0.74	0.84**	0.80**	0.75
Cd			1	0.73	0.89**	1.00**	0.99**	0.97**	1.00**	0.81**	0.99**	0.82**	0.61	1.00**
Co				1	0.94**	0.77**	0.80**	0.84**	0.73	0.97**	0.75	0.72	0.90**	0.73
Cr					1	0.92**	0.93**	0.95**	0.89**	0.98**	0.90**	0.86**	0.82**	0.89**
Cu						1	0.99**	0.98**	1.00**	0.84**	0.99**	0.84**	0.63	1.00**
Fe							1	0.99**	0.99**	0.86**	0.99**	0.83**	0.69	0.99**
Mn								1	0.97**	0.90**	0.98**	0.81**	0.69	0.97**
Mo									1	0.81**	0.99**	0.82**	0.61	1.00**
Ni										1	0.81**	0.80**	0.85**	0.81**
Pb											1	0.81**	0.60	1.00**
Ti												1	0.63	0.82**
V													1	0.61
Zn														1

** *Correlation is significant at the 0.01 level (2-tailed).*

The R-mode factor analysis enhances significant single-factor anomalies and helps to discriminate between element associations that have different underlying influences controlling their concentration. The analysis groups related variables into principal associations known as factors on the basis of their mutual correlation coefficients (Asaah et al., 2006). The data of seventeen studied variables in this study were subjected to R-mode analysis which accounted for 94% of the total data variance. Only variables with loadings > 0.5 were considered significant according to Likuku et al. (2013). The resulting varimax is summarized in Table 9. The extracted factors were as follows:

Factor 1: As, Cd, Co, Cr, Cu, Fe, Mn, Mo, Ni, Pb, Ti, V and Zn. This factor accounts for 72.292 % of the total data variance. These metals resulted mainly from the industrial activities of the Erbil Steel Company.

Factor 2: pH, soil organic matter, Al, Cd, Cu, Mo, Pb and Zn. This factor accounts for 14.638 % of the total data variance. This variance may indicate a lithogenic origin. The metals may have come mainly from either the domestic and municipal wastes discharged into the environment, or from the metallurgical and chemical industries in addition to the dumpsites, automobiles and fuel combustion in the study area.

Factor 3: pH and soil moisture. This factor accounts for 6.667% of the total data variance, which reflects the date of the study during the winter season.

Table 9. Varimax rotated component matrix of the studied metals in the soils around the Erbil Steel Company.

No.	Studied variables	Components			Communality
		1	2	3	
1	Ph	0.352	0.695	0.466	0.825
2	OM	0.201	0.921	-0.168	0.917
3	Moisture	-0.159	0.051	-0.966	0.961
4	Al	0.061	-0.928	0.015	0.865
5	As	0.849	0.153	0.379	0.888
6	Cd	0.778	0.580	0.154	0.966
7	Co	0.979	-0.015	0.010	0.958
8	Cr	0.946	0.275	0.107	0.982
9	Cu	0.801	0.567	0.152	0.987
10	Fe	0.843	0.494	0.141	0.975
11	Mn	0.855	0.465	0.165	0.975
12	Mo	0.778	0.580	0.154	0.966
13	Ni	0.951	0.121	0.185	0.953
14	Pb	0.782	0.585	0.120	0.969
15	Ti	0.765	0.453	0.026	0.791
16	V	0.944	-0.259	0.090	0.967
17	Zn	0.777	0.582	0.154	0.966
Eigenvalues		12.290	2.488	1.133	
Percentage of Variance %		72.292	14.638	6.667	
Cumulative Percent %		72.292	86.930	93.598	

Conclusion

The findings of the current study suggest that the soil samples from the Steel Factory exhibited higher concentration of metals (except for Al). The results of metal occurrence indicated that while Fe was the most dominant metal, Cd was the least dominant. The concentration of heavy metals (except in the Erbil Steel Company) did not appear to be of serious concern, with the exception of nickel which exceeded the permissible limits set by the WHO for all studied soils. Most of the studied sites have minimal enrichment, with the exception of Erbil Steel Company which showed moderate to extremely high enrichment by the studied metals which can be considered as the main source of the metals in the soils of the surrounding studied areas of Sardasht, Shamamal, Sahdawa, Tarjan and Nogharan. It is noticeable that the pH, soil organic matter and the metal contents are in parallel increasing together. On the whole, there were strong positive correlations among the studied metals which may indicate that the metals are from the same source, and may have been derived from anthropogenic sources. According to the R-mode factor analysis, three factors were extracted. The first one refers to the industrial activities of the Erbil Steel Company; the second factor indicates lithogenic factors, and the third factor reflects the date of the study during winter season. On the whole, the soils around the Erbil Steel Company were slightly polluted with heavy metals as a result of anthropogenic influences, in particular vehicular emissions. Accordingly, immediate measures need to be taken to prevent further soil pollution by the heavy metals coming from the Erbil Steel Company.

References

[1] Afrifa, C.G.; Ofosu, F.G.; Bamford, S.A.; Wordson, D.A.; Atiemo, S.M.; Aboh, I.J.K. and Adeti, J.P. 2013. Heavy metal contamination in surface soil dust at selected fuel filling stations in Accra, Ghana. Am. J. Sci. Ind. Res., 4(4): 404-413.

[2] Aikpokpodion, P.E.; Lajide, L. and Aiyesanmi, A.F. 2010. Heavy metals contamination in fungicide treated cocoa plantations in Cross River State, Nigeria. American-Eurasian J. Agric. & Environ. Sci., 8 (3): 268-274

[3] Al Obaidy, A. M. J. and Al Mashhadi, A. A. M. 2013. Heavy metal contaminations in urban soil within Baghdad City, Iraq, J. Environmental Protection, 4: 72-82.

[4] Alnaqshabandi, Z.S.A. 2014. Impact of wastewater irrigation on soils from selected locations in Kurdistan Region-Iraq. M.Sc. thesis, University of Salahaddin-Erbil.

[5] ALS, Geochemistry, Schedule of Services & Fees, 2015. Milton, QLD, Australia 4064. www.alsglobal.com

[6] Amune, M.; Christiana, O. and Kakulu, S. 2012. Impact of mining and agriculture on heavy metal levels in environmental samples in Okehi Local Government area of Kogi State. Int. J. Pure Appl. Sci. Technol., 12(2), 66-77.

[7] Asaah, V. A.; Abimbola, A. F. and Suh, C. E. 2006. Heavy metal concentrations and distribution in surface soils of the Bassa Industrial Zone 1, Douala, Cameroon. The Arabian Journal for Science and Engineering, 31(2 A): 147-158.

[8] Bambara, L.T.; Kabore, K.; Zoungrana, M.; Zougmore, F.; Cisse, O. and Bentil, N. 2015. Assessment of heavy metals contamination in agricultural soil of Loumbila and Paspanga, Burkina Faso. Int. J. Advanced Research in Science, Engineering and Technology. 2(1): 380-386.

[9] Byers, B.R. and Arceneaux, J.E.L. 1998. Microbial iron transport: iron acquisition by pathogenic microorganisms. Microbial Metal Ions Biol Syst. 35: 37-66.

[10] Elgawad, M.A.; Mohamed, H.A.; Shendi, M.M. and Ghabour, S.I. 2007. Status of some heavy metals in Fayoum district soils. The third Conf. for Sustainable Agricultural Development, Fac. of Agric., Fayoum Univ., 12-14 Nov. 2007. (507-526)

[11] ESC: Erbil Steel Company website: http://www.erbilsteel.com/2016

[12] FAO: Food and Agriculture Organization. 2001. Study of agro-ecological zoning for Diana, Mergasor, Barzan, and Sheruan-Mazn/Rubar Barazgird valley areas. FAO Representation in Iraq. FAO Coordination Office for Northern Iraq.

[13] Guerinot, M.L. 1994. Microbial iron transport. Annual Review of Microbiology. 48: 743-772.

[14] Hakanson, L. 1980. Ecological risk index for aquatic pollution control. A sedimentological approach. Water Res., 14(5): 975-1001.

[15] Howard, D.H. 1999. Acquisition, transport, and storage of iron by pathogenic fungi. Clinical Microbiology Reviews. 12(3): 394-404.

[16] Kabata-Pendias, A. and Mukherjee, A. B. 2007. Trace Elements from Soil to Human. Springer-Verlag Berlin Heidelberg.

[17] Khudhur, N.S.; Khudhur, S.M. and Ameen, N.O.A. 2016. A Study on soil bacterial population in steel company and some related area in Erbil city in relation to heavy metal pollution. Zanco J. Pure and Applied Sci., 28(5), 101-116.

[18] Khudhur, S. M. and Khudhur, N. S. 2015. Soil pollution assessment from industrial area of Erbil City. Journal of Zankoi Sulaimani, 17- 4 (Part-A): 225-238.

[19] Loska, K.; Wiechuła, D.; Barska, B.; Cebula, E. and Chojnecka, A. 2003. Assessment of arsenic enrichment of cultivated soils in Southern Poland, Polish Journal of Environmental Studies, 12(2), 187-192.

[20] Mlitan, A.B. 2013. Heavy metals and microbial toxicity of analysis of soil samples near iron and still factory (Misurata, Libya), 2nd International Conference on Chemical, Environmental and Biological Sciences (ICCEBS'2013) March 17-18, 2013 Dubai (UAE).

[21] Mohammed, M.S. and Abdullah, E.J. (2016). Heavy metals pollution assessment of the soil in the Northern Site of East Baghdad Oil Field, Iraq. Iraqi Journal of Science, 57(1A): 175-183.

[22] Namuhani, N. and Kimumwe, C. 2015. Soil contamination with heavy metals around Jinja Steel Rolling Mills in Jinja Municipality, Uganda. Journal of Health & Pollution, 5(9): 61-67.

[23] Nowrouzi, M. and Pourkhabbaz, A. 2014. Application of geoaccumulation index and enrichment factor for assessing metal contamination in the sediments of Hara Biosphere Reserve, Iran. Chemical Speciation and Bioavailability, 26(2), 99-105.

[24] Odat, S. 2015. Application of geoaccumulation index and enrichment factors on the assessment of heavy metal pollution along Irbid/Zarqa Highway-Jordan. Journal of Applied Sciences, 15(11): 1318-1321.

[25] Paul, E.A. 2007. Soil Microbiology, Ecology, and Biochemistry, Third edition, Elsevier Inc., UK.

[26] PUMA safe, 2009. Handbook of Environmental Standards. S.A.F.E. Team Global/Asia.

[27] Radojevic, M. and Bashkin, V.N. 2006. Practical Environmental Analysis, Second Edition, RSC Publishing.

[28] Rahman, S.; Khanam, D.; Adyel T.; Islam, M. Sh.; Mohammad Ahsan, A. and Akbor, M. A. (2012). Assessment of heavy metal contamination of agricultural soil around Dhaka Export Processing Zone (DEPZ), Bangladesh: Implication of Seasonal Variation and Indices, Appl. Sci., 2(3): 584-601.

[29] Ryan, J.; Estefan, G. and Rashid, A. 2001. Soil and Plant Analysis Laboratory Manual, Second Edition, International Center for Agricultural Research in the Dry Areas (ICARDA), Aleppo, Syria.

[30] Salah, E. A. M.; Zaidan, T. A. and Al-Rawi, A. S. 2012. Assessment of heavy metals pollution in the sediments of Euphrates River, Iraq. J. Water Resource and Protection, 4: 1009-1023.

[31] Salah, E.; Turki, A. and Noori, S. 2013. Heavy metals concentration in urban soils of Fallujah City, Iraq. Journal of Environment and Earth Science, 3(11): 100-112.

[32] Sharma, M.S. and Raju, N.S. 2013. Correlation of Heavy Metal contamination with Soil properties of Industrial areas of Mysore, Karnataka, India by Cluster analysis. Int. Res. J. Environment Sci., 2(10), 22-27.

[33] Sheppard, C.S. and Addison, J.A. 2008. Soil Sample Handling and Storage. In: Soil Sampling and Methods of Analysis, second edition, edited by Carter, M.R. and Gregorich, E.G., Taylor & Francis Group, LLC. Pp 39-49.

[34] Shukur, H. K. M. and Al-Tamimi, O. S. 2016. Assessment of contamination by heavy metals in soil of Laylan Area / NE of Iraq. Int. J. Advanced Research, 4(7): 505-512.

[35] Singh, P.K.; Verma, P.; Tiwari, A.K.; Sharma, S. and Purty, P. 2015. Review of Various Contamination Index Approaches to Evaluate Groundwater Quality with Geographic Information System (GIS). Int. J. Chem. Tech. Res., 7(4): 1920-1929.

[36] Stanley, H.O., Odu, N.N. and Immanuel, O.M. 2014. Impact of cement dust pollution on physicochemical and microbiological properties of soil around Lafarge cement Wapco, Ewekoro, southwestern Nigeria. Int. J. Advanced Biol. Res., 4(4), 400-404.

[37] WFP: World Food Programme. 2002. Statistical Report on Population of Iraqi Kurdistan Region. www.wfp.org

[38] Wuana, R.A. and Okieimen, F.E. 2011. Heavy metals in contaminated soils: a review of sources, chemistry, risks and best available strategies for remediation. International Scholarly Research Network. doi:10.5402/2011/402647.

[39] Zhang, M. K. and Wang, L.P. 2007. Impact of heavy metals pollution on soil organic matter accumulation. The Journal of Applied Ecology. 18(7):1479-83. https://www.ncbi.nlm.nih.gov/pubmed/17886638

JJEES
Jordan Journal of Earth and Environmental Sciences

Volume 9, (Number 1), April, 2018
ISSN 1995-6681
Pages 13 - 20

A Novel Technique for Hexavalent Chromium Reduction

Mohammed S. El-Ali Al-Waqfi[1] and Basim Ali Telfah[2]

[1]Technical Monitoring & Auditing Manager, Ministry of Water & Irrigation, Amman-Jordan
[2]Former Secretary General, Ministry of Water & Irrigation, Amman-Jordan

Received 30 June, 2017; Accepted 6 Feb, 2018

Abstract

This study presents a novel technique for the reduction of Cr(VI) to Cr(III) in an acidic aqueous medium. This technique is a batch treatment that utilizes an iron rotating disc as the reductant metal. The removal of the Cr(VI) under various conditions, including retention time, rotation rate, ion initial concentration and the initial pH of the solution, was investigated in this study. The effect of the shape of the rotating iron piece on the Cr(VI) reduction was also examined. It was found that the efficiency of removal of Cr(VI) initially, increased with increasing rate of rotation, retention time and the surface area of the disc until the dichromate ions were totally consumed or a state of equilibrium was reached. Conversely, the removal efficiency of Cr(VI) was found to decrease with the increasing of the solution pH and the initial concentration of Cr(VI). Almost the complete removal of Cr(VI) was achievable in a retention time of fifteen minutes at pH being 1.5 and the initial concentration reaching 100 ppm. Practically, the removal of the Cr(VI) become independent of the rotation rates above 600 rpm with the retention time being more than fifteen minutes. The use of a fan-shaped iron piece, unexpectedly, showed insignificant advantages over the rotating disc as the retention time increased.

Keywords: Cr (VI); Reduction; Low-cost reductants; Iron rotating disc

1. Introduction

Chromium is an inorganic pollutant of a prime concern to scientists and engineers working in the field of the environment and the conservation of water resources. It can exist in several forms; the most common and stable ones are Cr(VI) and Cr(III) as in dichromates ($Cr_2O_7^{2-}$) and chromium hydroxide ($Cr(OH)_3$). Chromium can make its way into waters and soils through chemical spills or inadequately treated industrial wastewaters. Cr(III) and Cr(VI) significantly differ in their toxicities, mobilities, and (bio)availabilities. Cr(III) is vital for glucose metabolism in our bodies. While it is essential in animal food, it is harmful to plants only at very high concentrations [Moore and Ramamoorthy, 1984], on the other hand, hexavalent chromium is exceptionally toxic to humans as well as to animals and plants. Also, Cr(VI) is considered by the US Toxicology Program as a pulmonary carcinogen. unlike Cr(III), which is relatively immobile and can simply be precipitated as hydroxide, Cr(VI) is easily transported through soils and aquatic environments [Richard and Bourg, 1991]. Furthermore, Cr(VI) is a strong oxidizing agent and can be absorbed through the skin. Despite their toxicity, Cr(VI) compounds are still extensively used in a wide range of industries (such as the tannery, corrosion inhibitors, stainless steel, inks, dyes, electroplating, etc) due to the good qualities and advantages of its applications.

The reduction of Cr(VI) to Cr(III) by S(IV) and Fe(II) followed by the precipitation of $Cr(OH)_3$ has been the most commonly used technology for the elimination of hexavalent chromium encountered in industrial wastewaters. Evaporative recovery of concentrated hexavalent chromium wastes was also proved, technically and economically, to be a viable treatment alternative. However, the increasingly stringent effluent standards made some industries utilize ion exchange for the disposal-off Cr(VI)-containing wastewaters. Lately, The application of other processes such as electrochemical and electro reduction of Cr(VI) using an iron metal has been extensively investigated (Eary and Ray, 1988; Cantrell et al., 1995; Powell et al., 1995; Sedlak and Chan, 1997; Blowes et al., 1997; Buergeand and Hug, 1997a; Beukes et al., 1999; Huang et al., 2008; Shamra et al., 2008;Yang et al., 2008; Abdo and Sedahmed, 1998; Demirbas et al., 2004;; Junyapoon and Weerapong, 2006; Chen et al., 215; Igcalinos and Besagas, 2016;).The reduction rates and the subsequent precipitation as hydroxide were adequately rapid and may, therefore, offer a practical treatment option for the industry (Gould, 1982; El-Shazly et al., 2005; Zhu et al., 216).

The currently used processes for the electrochemical reduction of Cr(VI) by iron, mostly employ the metal in the form of wool, chips or shots (small spheres) contained in packed columns, rotating chambers or tumble barrels. In such equipment, the iron surface is vulnerable to become covered with the metal oxidation secondary products as well as the settleable materials present in the effluents treated. Packed columns are, in particular, prone to clogging and flooding complications. Several workers have reported the formation of magnetite (Fe_3O_4), green rust ($Fe_4Fe_2(OH)_{12}SO_4.H_2O$), goethite (FeOOH) and ferric hydroxide ($Fe(OH)_3$) on the metal surface (Mackenzie et al., 1999; Scherer et al., 1998; Pratt et al., 1997; Lee et al., 2003; Ponder et al., 2000; Kendelewicz et al., 2000; Gilmore et al., 1998; Buerge and Hug, 1999 b). Furthermore, these equipments are relatively difficult to design and are associated with high power consumption and

* Corresponding author. e-mail: Mahammad_Al-waqfi@mwi.gov.jo

cost.

In view of the drawbacks associated with such techniques, an attempt was made to develop an easy, and efficient, as well as potentially economical method for the treatment of Cr(VI) which can be scaled up to suit the needs of small industrial firms, meeting at the same time the strict effluent standards. An iron-rotating disc was, therefore, chosen as the reductant metal. In addition to the elimination of the likely clogging problems associated with some of the current techniques, the rotating disc also provides a stirring action to the treated solution promoting the mass transfer of the fresh reactants to the metal's surface and the released ferrous ions to the bulk of the solution. The stirring action also hinders the concentration of reaction products in the vicinity of the disc, thereby lessening the tendency of formation of precipitates on the metal's surface. The formation of precipitates may unfavorably affect the reduction rate of hexavalent chromium to the trivalent state. In addition, the rotating disc has the advantage of providing an easily controllable and accessible surface area, an important parameter for scale up and design purposes. Moreover, with a properly designed continuous stirred reactor, the novel technique may be applied in a continuous treatment mode; making it adequate to industries with high discharges of Cr^{6+}. Finally, iron is an inexpensive and widely available material.

As is known, the position of iron and its ferrous ions in the electrochemical series is higher than that of hexavalent chromium, which implies that both types are capable of reducing Cr(VI) ions and displacing them from solution in a redox manner as follows (Patterson, 1985):

Reaction of dichromate with iron

$$Cr_2O_7^{2-} + 3Fe + 14H^+ \rightarrow 2Cr^{3+} + 3Fe^{2+} + 7H_2O \quad \text{.....(1)}$$

Reaction of ferrous ions with dichromate

$$Cr_2O_7^{2-} + 6Fe^{2+} + 14H^+ \rightarrow 2Cr^{3+} + 6Fe^{3+} + 7H_2O \quad \text{.....(2)}$$

Dissolved oxygen also reacts with iron and its ferrous ions as depicted in Equations (3) and (4) respectively.

$$2Fe + 4H^+ + O_2 \rightarrow 2Fe^{2+} + 2H_2O \quad \text{.....(3)}$$

$$4Fe^{2+} + 4H^+ + O_2 \rightarrow 4Fe^{3+} + 2H_2O \quad \text{.....(4)}$$

Eqs. (1) and (2) clearly imply that the reduction reactions of dichromate require acid and are thus pH dependent. As manifested by Eqs. (3) and (4), dissolved oxygen oxidizes the iron metal to the ferrous state, which is oxidized further to ferric ions. Consequently, well-aerated solutions are expected to consume more iron.

In this research paper, the reduction of Cr(VI) using an iron metal as a rotating disc was investigated. The studied parameters include the initial pH of a wastewater sample, the initial Cr(VI) concentration, the retention time, the rotation rate and the surface area of the rotating disc as well as its shape.

2. Materials and Methods

2.1. Materials

The polluted water sample studied was taken from a dichromate bright dip tank. In such a case, the dichromate solution is expected to contain, in addition to the sodium ions, ferrous and cadmium ions as a result of the bright dipping of cadmium- plated screws and nuts. The concentrations of cadmium and ferrous ions tend to increase with time due to the successive dichromate treatments of the cadmium plated items. As indicated by Eq. (2), the presence of high concentrations of Fe^{2+} can seriously interfere with the assessment of using the rotating disc as a means for the hexavalent chromium reduction. On the other hand, cadmium ions are expected to have an insignificant influence on the subsequent immobilization of the trivalent chromium ions resulting from the reduction process. Both cadmium and chromium hydroxides are precipitated upon the addition of sodium hydroxide to the solution. While pH at pH 1.5, the solubility of $Cr(OH)_3$ is minimal; cadmium hydroxide is relatively soluble (Patterson, 1985). The wastewater sample investigated was, therefore, taken from a freshly prepared dichromate bath so that high concentrations of Fe^{2+} and Cd^{2+} were avoided. The analysis of the studied sample is shown in Table 1.

Table 1. Analysis of the investigated wastewater sample.

Constituent	Concentration, mg/l
Cr(VI)	3000
Cd^{2+}	N.D.
Fe^{2+}	19
pH	11

2.1. Experimental set up and procedure

The bench-scale experimental setup used in the current study is shown in Fig. (1). It consisted of a 2000 ml beaker and a rotating disc made of mild steel (S.T37) fitted with a ¼ hp-variable speed motor via a rotating shaft made of stainless steel to avoid the interference of the shaft material in the reduction process. The variable speed motor was capable of providing rotation rates ranging from 0-1800 rpm (revolution per minute). The motor's speed was adjusted via a calibrated control knob incorporated in the motor assembly. Each time the motor's speed was adjusted, a taco meter was used for the verification of the rotation rate reading.

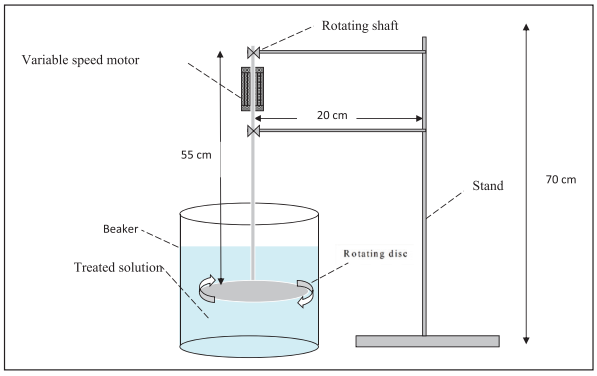

Figure 1. Schematic diagram of the experimental setup.

A horizontal arrangement of the rotating disc was selected to ensure axial symmetry and hence avoid the non-uniformity of the flow regime, generated by the rotating disc that might arise by the action of gravity. Such non-uniformity may interfere with the reduction process through affecting the mass transfer rates of the reacting species from the bulk of solution to the iron metal as well as the diffusion of the dissolved ferrous ions away from the metal's surface. The rotating shaft was therefore kept in an upright position by being clamped to a vertical stand.

At the beginning of each experiment, the iron disc was washed with distilled water and dried with air and degreased with benzene, then acetone to make sure neither fingerprints

nor traces of grease were left on the metal surface. Such traces of dirt act as a barrier preventing contact between the metal's surface and the solution interfering with the redox reactions, which are responsible for the treatment.

A forty-litre solution of hexavalent chromium was taken from the dichromate dip tank and was used as a stock solution. Different solutions of hexavalent chromium were prepared by diluting samples from the stock solution to the required initial concentrations. Solutions of concentrations of 1000, 750, 500, 300, 100 and 50 ppm of hexavalent chromium were made up.

A set of batch treatments on the sample solutions were conducted to investigate the effects of the different parameters on the removal efficiency of Cr(VI). The studied parameters included the initial pH of sample, the retention time, Cr(VI) initial concentration, the surface area of the disc, its shape, and the rotation rate. The initial pH of the samples was adjusted by using either 1 N NaOH or 1 N H_2SO_4. All experiments were conducted at room temperature. Also, the reproducibility of the results was tested by conducting a set of triplicated runs under the same experimental conditions.

Prior to chemical analysis, the treated samples were filtered through a 0.45 μm membrane filter and their pH was adjusted to a value of 8.5, so that trivalent chromium would form an insoluble precipitate (i.e., chromium hydroxide, $Cr(OH)_3$), which could then be easily removed, and thus the solution arrives at the lowest total chromium concentration; the optimum pH value at which the solubility of chromium hydroxide is minimal is 8.5. The filtrate was then analyzed for the determination of the remaining concentrations of Cr(VI) according to the Standard Methods for the Examination of Water and Wastewater, (21st edition) using a HACH Direct Reading Spectrophotometer (model DR2000). All the reagents used were of AR grade (HACH, USA). A microprocessor pH meter (model pH3000.WTW) was used for the measurement of pH.

2.3. Data Treatment

The removal efficiency of Cr(VI) was calculated according to the following equation,

$$\text{Removal efficiency}(\%) = \frac{\text{Initial concentration of } Cr(VI) - \text{remaining concentration of } Cr(VI)}{\text{initial concentration of } Cr(VI)} X100 \quad ....(5)$$

3. Results and Discussion

3.1. Effect of Retention Time

Figs.2 and 3 illustrate the variation of Cr(VI) removal with the retention (i.e., contact) time. At the beginning of the reduction process, the removal of Cr(VI) significantly increased and as time elapsed, a stage with almost constant removal efficiency was reached. As the reaction time proceeded further,anions were, increasingly, consumed in the reaction till they were totally removed or an equilibrium phase was reached. It is also apparent from Figs.2 and 3 that almost complete removal of Cr(VI) was almost achievable in about fifteen-minute time for the wastewater samples of low starting pH. Moreover, both figures indicate that the starting pH was a key factor in influencing the retention time required for attaining complete removal and/or reaching equilibrium stage; lower pH favored shorter times for attaining equilibrium conditions.

The initially observed sharp rise in the removal efficiency of Cr(VI) can be attributed to the intense evolution of hydrogen gas observed at the surface of the rotating disc at the onset of the reduction process as a result of the reaction of hydrogen ions with iron. The liberated hydrogen gas bubbles may have resulted in the development of local turbulent eddies, which in turn disturbed the diffusion boundary layer adjacent to the disc's surface and hence enhanced the mass transfer of fresh reactants from the solution bulk to the reductant metal surface. As the dichromate concentration decreased with time, the driving force for the diffusion from the solution bulk to the surface of the rotating disc progressively diminished, the reduction rate of Cr(VI) was retarded as demonstrated by the plateau part of the curves of Figs. 2 and 3.

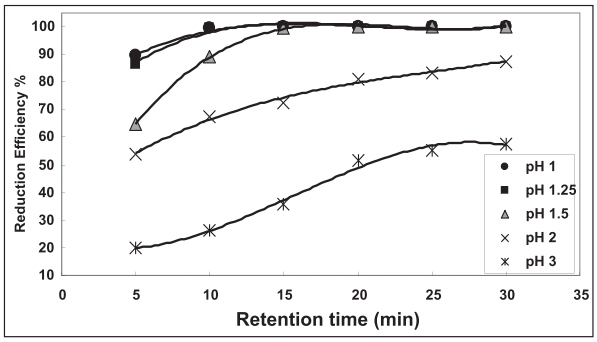

Figure 2. Effect of retention time on removal efficiency of Cr(VI) (initial concentration 50 mg/l, radius of RD 4.75 cm and rotation rate 600rpm).

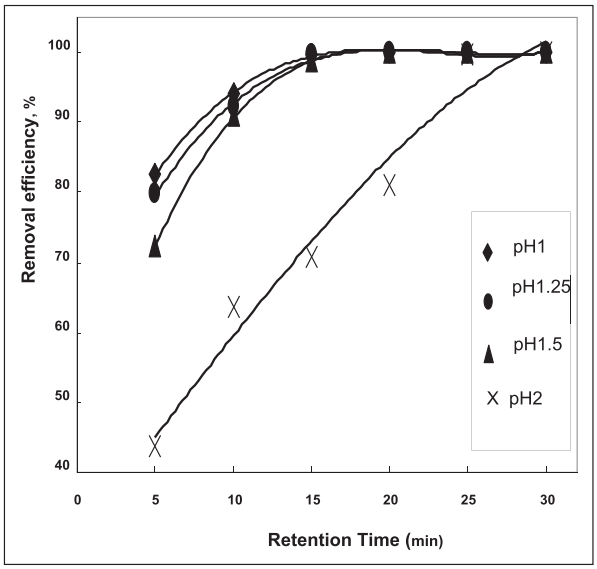

Figure 3. Effect of retention time on removal efficiency of Cr(VI) (initial concentration 50 mg/l, radius of RD 4.75 cm and rotation rate 600rpm).

3.2. Effect of Initial Concentration

As shown by Fig. 4, when the initial concentration of Cr(VI) increased, the removal efficiency was relatively reduced, and the time required for attaining high removals and/or approaching equilibrium state was, significantly, increased. This rise in the equilibrium retention time may be attributed to the growing deficiency in the excess hydrogen ions. As the redox reactions advance; the availability of excess hydrogen ions becomes vital for the occurrence of the reduction process. This was clearly supported by the significant increase in the pH of the treated samples with increasing retention time due to the progressive acid consumption by the redox reactions, as revealed by Fig. 5.

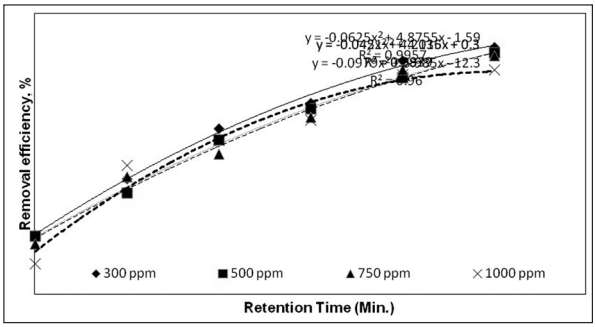

Figure 4. Effect of retention time on removal efficiency of Cr(VI) at different initial concentrations (initial pH 1.5, radius of RD 4.75 cm, rotation rate 600rpm).

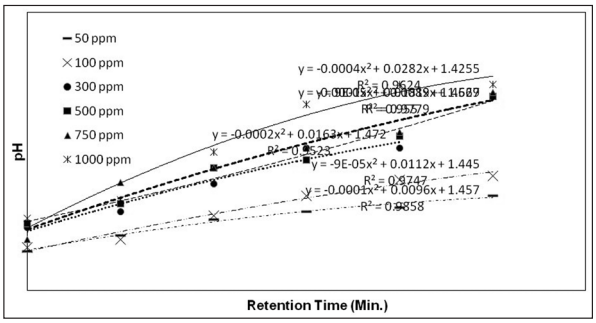

Figure 5. Variation of solution pH with time (initial pH 1.5, radius of RD 4.75 cm, rotation rate 600rpm).

In the current study, the minimum retention time to achieve approximate complete removal of Cr(VI) was much shorter than that reported in the literature. For example, Junyapoon and Weerapong (2006), who used scrap iron filings as the reductant metal, obtained a complete reduction of Cr(VI) in a retention time of 180 minutes. These results may, therefore, confirm the advantages of the rotating disc over other forms of iron used for the reduction of Cr(VI). As mentioned earlier, the rotating disc may have caused some sort of mixing due to the laminar flow developed by its rotation, which may have enhanced the diffusion of fresh reactants to the iron surface. The streamlines generated under laminar flow conditions may also have resulted in unfavorable conditions for the precipitation of the reaction products on the metal surface. Accordingly, better accessibility of the reactants to the iron metal surface was warranted.

3.3. Effect of Initial pH

Generally speaking, the pH of the treated solution may affect the reduction of Cr(VI) via influencing what follows,

a. Availability of excess H^+ necessary for the reduction-oxidation reaction to occur;
b. Cr(VI) anions adsorption on the metal surface;
c. The passivity of the rotating disc surface.

To investigate the effect of the initial pH of the treated solution on the elimination of Cr(VI), the variation of the removal efficiency over a range of initial pH was, therefore, examined. As shown in Fig. 6, for the same retention time, the removal efficiency rapidly and progressively improved with decreasing the initial pH until an equilibrium phase and/or a complete removal was reached. This behavior was more noticeable at higher retention times, thus, indicating that an optimum combination of initial pH and retention time could be sought out in order to maximize the removal efficiency of Cr(VI). Moreover, the reduction reaction represented by Eq. (1), which is believed to be the most significant reaction in the process, requires acid and is thus pH dependent. In other words, the removal of Cr(VI) was favored by low pH as has also been confirmed recently by Chen et al (2015) and Zhu et al. (2016). In addition, the low initial pH values may have encouraged the adsorption of dichromate ion on the metal surface, hence, facilitating the occurrence of the redox reaction. As the pH of the solution increases, the metal surface tends to become negatively charged and the adsorption of similar ions (e.g., the dichromate ions) is, therefore, expected to be retarded due to electrostatic repellence (Tokunaga et al., 2001). It is also strongly believed that the heterogeneous process (solid-liquid reaction) of dichromate sorption on the metal surface is an essential step to the commencement of the reduction reaction, which takes place according to Eq. (1). This is supported by the current findings, which may indicate that sorption of hexavalent chromium (as) was strongly pH dependent and was less likely to occur at high pH values. Eary and Rai (1998) proposed that chromate was not adsorbed in biotite at high pH. Similarly, Zachara et al. (1987) reported that chromate was not adsorbed onto iron oxides at pH of11.5 to 12. Later, Swietlik (2002) reported that at pH 6, Cr(VI) was primarily present in an adsorbed form while as pH increased, the concentration of the dissolved chromates rose until it became completely in solution at pH 8.8. Several investigators observed the formation of passive insulating layers of magnetite and green rust on the surface of zero-valent iron (Brown and Chambers., 2002; White and Paterson, 1994; Williams and Scherer, 2001; Brown and Chambers, 2002). The oxidizing surface was also found to be, increasingly, susceptible to passivation at high pH values as suggested by Lee et al. (2003), and Yongtian (2003). Niu et al. (2005) also reported insignificant Cr(VI) reduction efficiencies due to the formation of magnetite and goethite on the iron surface under alkaline conditions. In the current study, the passivation and shielding of the rotating disc surface were less likely to occur due to the low pH values as well as the short retention times used, which may have played an important role in averting products' precipitation. In addition, practically, the rotating disc creates laminar flow conditions, which swirl the solution in the vicinity of the disc hindering deposit formation on the metal surface. Similar findings were reported by Alowitz and Scherer (2002), who found that the reduction rate of Cr(VI) by the iron metal varied significantly depending on the pH of the solution, being slower at higher pH values.

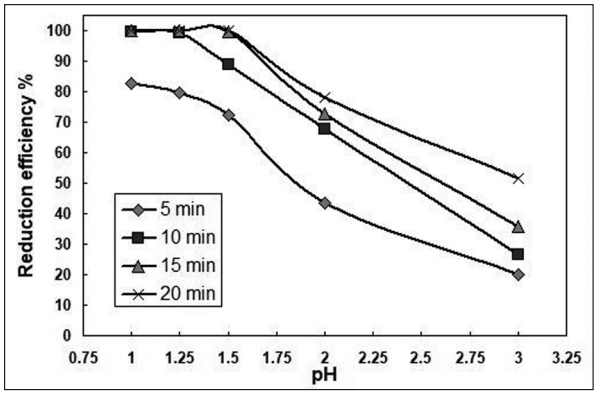

Figure 6. Removal efficiency versus initial pH, (radius of RD 4.75 cm, initial concentration 100 mg/l, rotation rate 600 rpm).

As revealed in the preceding sections, the initial pH of the treated sample highly impacted the time taken to achieve the maximum attainable removal efficiency and/or to reach equilibrium conditions. Fig. 7, which shows the variation of equilibrium time versus the starting pH, clearly indicates that the time taken to reach equilibrium was directly proportional to the initial pH of the sample. For instance, the equilibrium stage (i.e., the maximum attainable removal efficiency of Cr(VI)) for the same treated sample was achieved in a ten-minute time at the starting pH 1 compared to fifteen and forty minutes at an initial pH of 1.5 and 3 respectively. The relatively high removals noted for low initial pH samples could be mainly attributed to the enhanced availability of excess hydrogen ions; H^+ concentration is inversely proportional to pH. Consequently, to comply with regulatory requirements and effluent standards, the use of an optimum combination of pH and retention time is, therefore, vitally important.

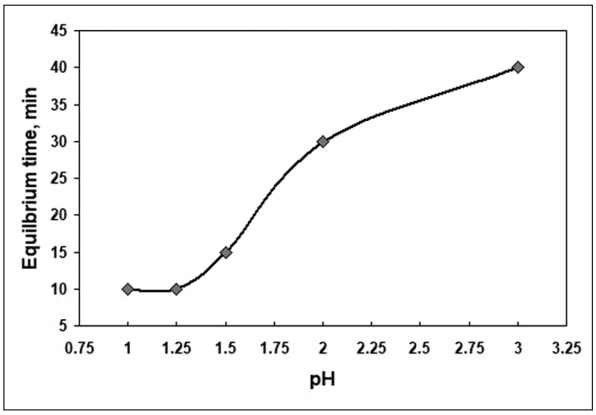

Figure 7. Variation of equilibrium time with initial pH (initial concentration 100 mg/l, radius of RD 4.75 cm, rotation rate 600 rpm).

3.4. The Effect of the Surface Area of the Disc

The effect of the surface area of the rotating disc on the removal efficiency of Cr(VI) was investigated using discs of radii of 3.45 cm, 4.00 cm, and 4.75 cm. The achieved results, displayed in Fig. 8, reveal that the removal efficiency of hexavalent chromium significantly increased as the rotating disc radius increased, but this rise was more pronounced at higher surface areas and longer retention times. Likewise, the utilization of a disc of a relatively higher area resulted in a shorter retention time for the achievement of approximate complete elimination of Cr(VI). For instance, at the retention time of four minutes, increasing the radius of the rotating disc from 3.45 cm to 4.00 cm, improved the removal of Cr(VI) from 31% to 43% in comparison with 42% to 51% when the radius increased from 4.00 cm to 4.75 cm. But at a retention time of fourteen minutes, the removal efficiency improved from 42% to 98% compared to 38% to 75% at a retention time of eight minutes when the radius increased from 3.45 cm to 4.00 cm. The results would have been more revealing if a wider range of surface areas were investigated. The observed sharp increase in the removal efficiency as the disc surface area increased may be attributed to the accompanying augmentation of the disc Re Nos., which increased from 83,704 in case of the 3.45 cm RD to 158,670 for the 4.75 cm RD. The Re No. 158,570 falls within the transitional flow region while the Re No. 83,704 is within the laminar flow regime. Higher Reynolds numbers enhance the transportation of the reacting species to the disc surface, hence, improving Cr(V) removal. In addition, the greater availability of reactive sites as the radius increased may have contributed into the enhancement of the removal efficiency at the higher surface area of RD. Accessibility and availability of reactive sites allow for continuing the reduction of hexavalent chromium especially at higher retention times. It is believed that $Cr_2O_7^{2-}$ anions were adsorbed onto the surface prior to the commencement of the heterogeneous reduction reaction of Cr(VI) by Fe^0 (El-Shazly et al., 2005). The reduction of Cr(VI) in solution by Fe^{2+} (i.e., Equation (3)) is expected to have a less significant impact on Cr(VI) removal due to the competing spontaneous oxidation of ferrous to ferric ions as in Equation (4).

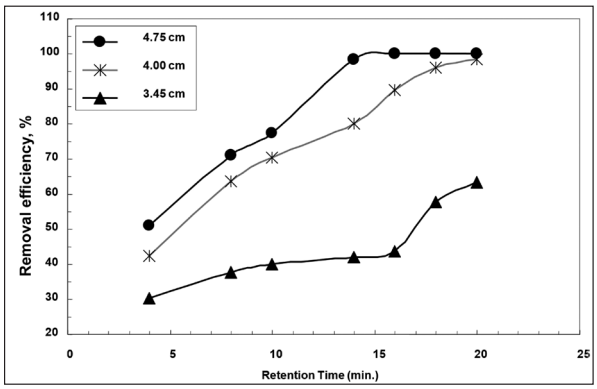

Figure 8. Effect of surface area of RD on the removal efficiency of Cr(VI) (initial concentration 100 mg/l, initial pH 1.5,600 rpm).

However, other forms of the iron metal used for the reduction of Cr(VI)(e.g., fillings, chips, wool, shots and spheres) may experience some shielding effect and formation of agglomerates as well as the development of channeling especially in the case of fixed beds (Prasad et al., 2011; Lee et al., 2003). This necessarily reduces the effective area available for the reduction reaction. Meanwhile, the rotating disc provides higher percentage of the effective area of the iron, in addition to granting almost equal accessibility of the metal surface by the reactants. Accordingly, the minimum surface area of the rotating disc as well as the optimum retention time required for a complete removal of Cr(VI) may be determined easily.

The findings of the current study are consistent with the results reported by Niu et al. (2005) and Junyapoon and Weerpong (2006), who used nanoparticles and fillings of scrap iron respectively to remove Cr(VI) from aqueous solutions. They found that the removal efficiency was directly proportional to the available iron surface area.

3.5. The Effect of the Rotation Rate

To examine the effect of the rotation rate of the iron disc on the reduction of hexavalent chromium, the variation of the removal efficiency of Cr(VI) with the rotation speed was studied. The investigated speeds were 50, 100, 300, 500 and 600 rpm of Reynolds numbers falling within the transitional and laminar flow regions. Fig. 9 shows that that the removal efficiency increased (e.g., segment AB) with the rotation rate until the equilibrium(i.e., a constant removal) (e.g., segment BC) stage was reached. The initial rapid augmentation in the removal of Cr(VI) with increased rpm may indicate that the reduction reaction of Cr(VI) by iron

metal was diffusion (i.e., mass transfer) controlled, which is in agreement with earlier findings (El-Shazly et al., 2005). The increasing rotation rate expectedly increases the diffusion rate of the dichromate anions from the solution bulk to the disc across the boundary layer adjacent to the solid surface. The thickness of the solid surface is inversely proportional to the angular velocity (Levich, 1962) facilitating the mass transfer of the reacting types. On the other hand, increasing the rotation rate is mutually expected to enhance the diffusion of the reaction products away from the surface due to laminar flow conditions developed by the disc movement, thereby, minimizing the tendency of the formation of precipitates on the disc surface, which may inhibit electron transfer resulting in retardation of the reduction reaction. The equilibrium phase (e.g., BC segment) may imply that the removal efficiency of Cr(VI) became less dependent on the rotation rate, therefore, suggesting that at higher speeds the rate-determining step of the reduction process was the reaction kinetics rather than the diffusion of the reacting species through the bulk solution and the boundary layer. Junyapoon and Weerapong (2006) found that the reduction of Cr(VI) was directly proportional to the agitating rate and they similarly attributed this relationship to the enhancement of the diffusion rate of Cr(VI) from the solution bulk to the iron surface as the agitation rate increased; no constant removal efficiency zone was observed. In their study, the maximum rate investigated was 250 rpm due to limitations in agitator's capacity compared to the maximum rotation rate of 600 rpm of the current study, which may explain the inconsistency of the present results with theirs at rotation rates above 400 rpm. Earlier, it was found that the mass transfer coefficient rate and the rate of reduction of hexavalent chromium, using a fixed bed of scrap iron spheres, increased upon increasing the solution velocity (El-Shazly et al., 2005).

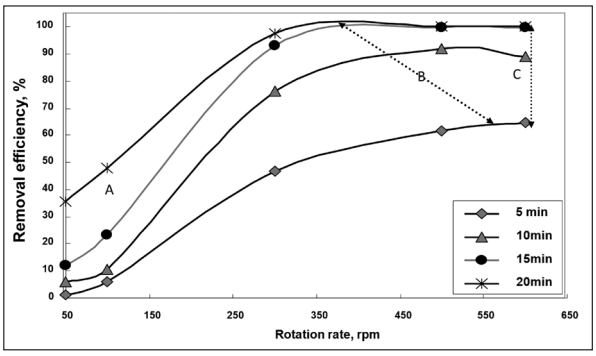

Figure 9. Effect of rotation rate on the removal efficiency of Cr(VI) (initial concentration 100 mg/l, initial pH 1.5, radius of RD 4.75 cm).

3.6. The Effect of the Shape of the Iron Piece

An attempt was made to enhance the removal efficiency of Cr(VI) by employing a fan-shaped rotating iron piece instead of the regular rotating disc as the reductant metal. Fig. 10 shows the variation of the removal efficiency with the retention time for both shapes of the same surface area. As shown, in the first eight minutes of the treatment, the fan-shaped piece resulted in a significant improvement in the removal of Cr(VI) over the regular disc. This advantage was diminished with increasing the retention time, until a stage, at which the performance of both shapes was nearly equal, was reached. It was also important to note that complete reduction could be achieved at a retention time of about fifteen minutes by the rotating disc compared to nearly eighteen minutes in case of the fan-shaped piece. The experimental setup used in the present study can be considered as a stirred or a mechanically agitated tank, which is characterized by a very large spatial variation in the local energy dissipation rates. Two regions of low and high-energy dissipation rates, therefore, coexisted, which in turn resulted in two regions in relation to the flow. In the vicinity of the impeller (i.e., the rotating iron) fluid circulates (i.e., flows); whereas in the rest of the tank, or in the low energy prevailing region, the fluid relatively remains stagnant. The features of these two regions may substantially change depending upon the shape of the impeller used. On the other hand, fan-shaped impellers lead to higher energy dissipation rates in the close zone, so better mixing may be initiated due to the resultant vigorous fluid circulation (El-Ali, 2001). Accordingly, the higher removal efficiency of Cr(VI), initially observed by using the fan-shaped piece may be attributed to local turbulence created via the obstruction of solution circulation by the fan blades and thus positively influencing the mass transfer of the reactants from the solution bulk to the iron surface, which may lead to higher reductions of Cr(VI). As time elapsed, the fluid movement within the inclinations of the fan may have been hindered and hence adversely affected the diffusion of reaction products away from the reductant metal that tended to concentrate with time forming some sort of precipitates on metal surface. This situation may have led to the progressive decline in the performance of the fan compared to the rotating disc at longer retention times. Furthermore, the fan-shaped piece may have hampered the accessibility of the reactants to the iron surface unlike the rotating disc which offered easier access to the reducing metal.

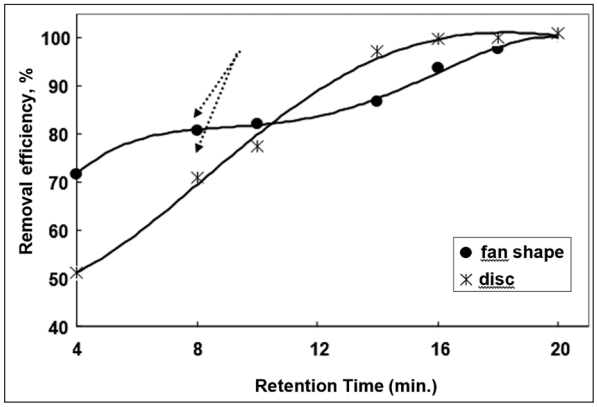

Figure 10. Effect of the shape of the rotating iron piece on the removal efficiency of Cr(VI) (initial concentration100 mg/l, initial pH 1.5, radius of RD 4.75 cm, 600 rpm).

Conclusion

A complete reduction of Cr(VI) was achievable in a relatively short time by using an iron rotating disc.

The reduction rate of Cr(VI) increased with decreasing the initial pH. The optimum pH value (for removing Cr(VI) effectively from wastewaters having initial Cr(VI) concentration of less than 100 mg/l) was 1.5 at which almost a 100% efficiency was achieved in about fifteen minutes. For higher initial concentrations of Cr(VI) more time was required.

The removal of Cr(VI) increased with the increase in the

surface area of the rotating disc.

The removal efficiency of Cr(VI) was found to be, initially, directly proportional to the rotation rate of the rotating disc; the maximum removal was attained at about 600 rpm.

In practice, an optimum combination of the different parameters affecting the elimination of Cr(VI) should be sought out in order to achieve the minimum concentration of remaining Cr(VI).

The use of an iron rotating disc as a reductant metal for Cr(VI) may constitute a viable, easy, and potentially a cost-effective option to small industrial firms experiencing difficulties in the disposal of Cr(VI) –containing liquid effluents.

Abstract

A novel technique for the reduction of hexavalent chromium to trivalent chromium in acidic medium was studied. This technique is a batch treatment utilizing an iron rotating disc as the reductant metal. The elimination of Cr(VI) under different conditions of retention time, rotation rate, ion initial concentration and initial pH of the solution was investigated. The effect of the shape of the rotating iron piece on the Cr(VI) reduction was also examined. It was found that the removal efficiency of Cr(VI), initially, increases with increasing the rotation rate, retention time and the surface area of the disc until the dichromate ions are totally consumed or a state of equilibrium is reached. Conversely, the removal efficiency of Cr(VI) was found to decrease with increasing the solution pH and the initial concentration of Cr(VI). Almost complete removal of Cr(VI) was achievable in a retention time of about fifteen minutes at pH values less than 1.5 and an initial concentration of 100 ppm. The removal of Cr(VI) practically becomes independent of rotation rates above 400 rpm and with the retention time being higher than fifteen minutes. The use of fan-shaped iron piece, unexpectedly, showed insignificant advantages over the rotating disc as the retention time increased.

References

[1] Abdo, M. S. and Sedahmed,G. H., 1998. A New Technique for Removing Hexavalent Chromium from Wastewater and Energy Generation via Galvanic Reduction with Scrap Iron, Energy Convers. Mgmt., 39: 943-951.

[2] Alowitz,M. J.,and SchererM. M., 2002.Kinetics of Nitrate, Nitrite, and Cr(VI) Reduction by Iron Metal,Environ. Sci. and Technol., 36: 299–306.

[3] Beukes, J. P., Pienaar,J. J., LachmanN. G., and GiesekkeE. W.,1999. The Reduction of Hexavalent Chromium by Sulphite in wastewater, Water SA 25: 363-370.

[4] Blowes,D. W., Ptacek,C. J., and Jambor,J. L ., 1997. In-situ Remediation of Chromate Contaminated Groundwater Using Permeable Reactive Walls, Environ. Sci. Technol.,31: 3348-3357.

[5] Brown, G. E. and Chambers,S. A., 2002. Molecular Level Processes Governing the Interaction Contaminants with Iron and Manganese Oxides, Government reports announcements and index, Pacific Northwest National Laboratory, Richland, WA, 1999.

[6] Buerge, I. J. and Hug,S. J., 1997 a. Kinetics and pH Dependence of Chromium(VI) Reduction by Iron(II), Environ. Sci. Technol.,31: 1426-1432.

[7] Buerge, I. J. and Hug,S. J., 1999 b. Influence of Mineral Surfaces on Chromium Reduction by Iron(II), Environ. Sci. Technol., 33(23): 4285-4291.

[8] Cantrell,K. J., Kaplan, D. I., and Wietzma,T. W.,1995. Zero-Valent Iron for the in Situ Remediation of Selected Metals in Groundwater,J. Haz. Mat., 42: 201-212.

[9] Chen, J., Chen, R., and Hong, M., 2015. Influence of pH on Hexavalent Chromium Reduction by Fe(II) and Sufide Compounds, Water Sci. Technol., 72 (11): 22-28.

[10] Demirbas,E., Kobya,M., Senturk, E., and Ozkan,T.,2004. Adsorption Kinetics for the Removal of Chromium(VI) from Aqueous Solutions on the Activated Carbons Prepared from Agricultural Wastes, Water SA 30 (4): 533-539.

[11] Eary, L. E. and Rai,D., 1988. Kinetics of Chromium(III) Oxidation to Chromium(VI) by Reaction with Manganese dioxide, Environ. Sci. Technol.,21: 1187-1193.

[12] El-Ali,M. S., 2001.Performance Characteristics of a Novel Liquid-Liquid Contactor, Ph.D. Thesis, Dalhousie University, Halifax, Canada.

[13] El-Shazly,A. H., Mubarak,A. A., and KonsowaA. H.,2005. Hexavalent Chromium Reduction Using a Fixed Bed of Scrap Bearing Iron Spheres,Desalination, 185: 307-316.

[14] Gilmore,T. J., Holdren,G. R., and KaplanD. I.,1998. Groundwater Well with Reactive Filter Pack,U.S. Patent 5,803,174, U.S. Patent Office, Washington, D.C.

[15] Gould,J. P., 1982. The Kinetics of Hexavalent Chromium Reduction by Metallic Iron, Water Res., 16: 871-877.

[16] Huang,Y., Chen,T., Huang, J., and ChenY., 2008. Effects of Size and Surface Area of Iron on Reduction of Hexavalent Chromium, Journal of University of Science and Technology, Beijing, 30:53-57.

[17] Junyapoon, S. and Weerapong,S.,2006. Removal of Hexavalent Chromium from Aqueous Solutions by Scrap Fillings, KMITL Sci. Tech. J., 6 (1): 1-12.

[18] Igcalinos,J, D. and Besagas, R. L., 2016.Electrochemical Reduction of Hexavalent Chromium from Chemical Oxygen Demand Hazardous Waste Chemicals using Graphite Electrode, 6 (4): 1356-1362.

[19] Kendelewicz,T., Liu,P., Doyle, C. S., and BrownG. E.,2000. Spectroscopic Study of the Reaction of Aqueous Cr(VI) with Fe3O4(III) Surfaces, Surface Sci.,469: 144-163.

[20] Lee,T., LimH., Lee, Y., and Park,J. W.,2003. Use of Waste Iron Metal for Removal of Cr (VI) from Water, Chemosphere, 53:479-485.

[21] Levich,V. G., 1962. Physiochemical Hydrodynamics, 2nd Ed., Prentice Hall, New Jersey, U.S.A.

[22] Mackenzie,P. D., Horney, D. P., and Sivavec,T. M.,1999. Mineral Precipitation and Porosity Losses in Granular Iron Columns, J. Hazard. Mater.,68: 1-17.

[23] Moore,J. W., and Ramamoorthy,S., 1984. Heavy Metals in Natural Waters, Springer Series on Environmental Management, Springer New York.

[24] Niu,S., LiuY., Xu, X.,andLouZ.,2005. Removal of Hexavalent Chromium from Aqueous Solution by Iron Nanoparticles,Journal of Zhejiang Univ. Sci., 6B(10): 1022-1027.

[25] Patterson,J.W., 1985. Industrial Wastewater Treatment Technology, 2nd Edition, Butterworth, Boston, USA.

[26] Ponder,S. M., Darab, J. G. and Mallouk,T. E., 2000. Remediation of Cr(VI) and Pb(II) Aqueous Solutions Using Supported Nanoscale Iron, Environ. Sci. Technol.,34(12): 2564-2569.

[27] Powell,R. M., Puls,R. W.,1995. Hightower, S. K. and SabatiniD. A., Coupled Iron Corrosion and Chromate Reduction: Mechanisms for Subsurface Remediation, Environ. Sci. Technol., 29: 1913-1922.

[28] Prasad,P. V., Chandan, D., and Golder,A. K., 2011. Reduction of Cr(VI) to Cr(III) and Removal of Total Chromium from Wastewater Using Scrap Iron in the Form of Zerovalent Iron (ZVI): Batch and Columns Studies, The Canadian Journal of Chemical Engineering, 31 (6): 1575-1582.

[29] Pratt,A. R., Blowes, D. W., and PtacekC. J., 1997. Products of Chromate Reduction on Proposed Remediation Materials, Environ. Sci. Technol., 31: 2492-2498.

[30] Richard,F. C., and M Bourg,A. C., 1991. Aqueous Geochemistry: A Review, Water Res., 25(7): 807-816.

[31] Scherer,M. M., Balko, B. A., and TratnyekP. G., 1998. The Role of Oxides in Reduction Reactions at the Metal-Water Interface, Mineral water interfacial reactions: kinetics and mechanisms, ACS Symposium Series 715, Sparks D. and GrundlT. (Eds.), American Chemical Society, Washington, D.C., pp. 301-322.

[32] Sedlak,D. L.and Chan,P. G.,1997. Reduction of Hexavalent Chromium by Ferrous Iron, Geochim,Cosmochim., Acta61: 2185-2192.

[33] Shamra,Y. C., Singh,B., Agrawal, A., and Weng,C. H.,2008. Chromium Removal of Chromium by Riverbed Sand from Water and Wastewater: Effect of Important Parameters, J. Hazard. Mater., 151: 789-793.

[34] Swietlik,R., 2002. Kinetic Study of Redox Processes of Chromium in Natural River Water, Polish Journal of Environmental Studies, 11 (4): 441-447.

[35] Tokunaga,T.K., WanJ., Firestone,M.K., Hazen,T.C., Schwartz,E., Sutton S.R. and Newville,M., 2001. Chromium Diffusion and Reduction in Soil Aggregates, Environ. Sci. Technol., 35: 3169–3174.

[36] White, A. F. and Patersson,M. L., Electrochemistry and Dissolution Kinetics of Magnetite and Ilmenite, Geochim. Cosmochim. Acta,58 (8)(1994) 1859-1875.

[37] Williams, A. G. B., and Scherer,M. M., 2001. Kinetics of Cr(VI) Reduction by Carbonate Green Rust,Environ. Sci. Technol.,35: 3488-3494.

[38] Yang,H. F., Fu, P. F. and Zhou,F., 2008. Adsorption and Reduction of Cr(VI) in Aqueous Solution Using Steel Slag Particles, The Chinese Journal of Process Engineering, 8 (3): 499-503.

[39] Yongtian,H., 2003.Chromate Reduction and Immobilization Under High pH and High Ionic Strength Conditions, Ph.D. Dissertation, School of the Ohio State University, U.S.A.

[40] Zachara,J.M., Girvin,D.C., Schmidt, R.L., and Resch,C.T., 1987. Chromate Adsorption on Amorphous Iron Oxyhydroxide in the Presence of Major groundwater Ions, Environ. Sci. Technol., 21(6): 589–594.

[41] Zhu,Y., Wei, L., Xu, J., and Shi,W., 2016. Study on the Effect on the Reduction of Hexavalent Chromium in Soil, International Conference on Environment, Climate Change and Sustainable Development (ECCSD 2016), Beijing, China.

JJEES
Jordan Journal of Earth and Environmental Sciences

Volume 9, (Number 1), April, 2018
ISSN 1995-6681
Pages 21 - 27

X-Ray Fluorescence Spectrometry and Metal Pollution Assessment of Street Dusts Collected From Gasoline Service Stations and Roadsides within Ado Ekiti, Nigeria

Matthew Omoniyi Isinkaye

Department of Physics, Ekiti State University, Ado Ekiti, Nigeria

Received 16 September, 2017; Accepted 11 January , 2018

Abstract

This study is carried out to assess the pollution levels of selected metals in the street dusts collected from gasoline service stations and roadsides within the Ado Ekiti municipality. The concentrations of all the metals in the street dusts were higher than the local background values obtained at a control site except Ni and As. Multivariate statistics such as principal component analysis (PCA), coefficient of variation and Pearson correlation coefficient were used to analyze the results. Evaluation of enrichment factor, contamination factor and pollution index show that the street dusts of Ado Ekiti were contaminated with Ni, Zn, and Pb. Comparison with metal concentrations in other locations around the world shows that Pb concentration in the roadside dust of the study area is higher than the rates presented in the literature about China, Iran, Saudi Arabia and Thailand and is almost five times higher than the average concentration in the soil around the world.

Keywords: Heavy metals; pollution hazards; roadside dust; gasoline; contamination factor; X-ray fluorescence

1. Introduction

Metals are natural components of the earth's environment. They constitute the majority of the elements found in nature. Metals include, alkali, rare earth, heavy and trace metals. Human activities have introduced several pollutants such as heavy and trace metals to the urban settlements. The natural source of metals is generally referred to as geogenic, while those introduced as a result of human activities are known as anthropogenic sources. The background concentrations of heavy and trace metals vary from place to place depending on the composition of parent materials and pedogenic processes associated with different environments. Metals from natural and anthropogenic sources are ubiquitous in the environment and can contaminate urban soil with the associated risks to human health. Exposure to heavy and trace metals can be through dermal contact, ingestion of dust in playing grounds and inhalation of dust particles in streets and roadsides (Abrahams, 2002; Gurung and Bell, 2013; Lu et al., 2014).

Vehicular emission is one of the major sources of metal pollution in the urban environment. The mechanisms of metals emission from vehicles include fuel consumption, engine oil consumption, tire wear and road abrasion (Markus and McBratney, 1996; Wilcke et al., 1998; Zhang et al., 2012). All these processes release heavy metals into the roadside soil. Street dust such as roadside soil serves as reservoir for pollutants, including heavy and trace metals, which are toxic to human health. Street and roadside soil can generate airborne particles and dusts, which may affect the air quality in urban environment (Gray et al., 2003, Abech et al., 2010). These airborne particulate matters may consequently settle on agricultural soil through dry and wet deposition leading to plant uptake of heavy and trace metals. Through this mechanism, heavy and trace metals enter the food chain thereby affecting human health. Almost fifty-three out of the ninety naturally occurring elements belong to the class of heavy and trace metals (Weast, 1984, Aslam et al., 2013). Of these numbers, Fe, K, Ca, Mn, Mo and Mg are essential as micronutrients, while others such as Zn, Ni, Cu, As, Cr and Pb are toxic even at low concentrations. When absorbed, ingested or inhaled, heavy and trace metals can impair important biochemical processes posing threats to plant growth, animal life and human health (Aslam et al., 2013). The consequences of metal contamination in urban environments on the human health include reduced intelligence, renal failure, cardiovascular diseases, and the risk of cancer (Jarup, 2003).

The pollution of urban soil by heavy and trace metals from vehicular emission and petroleum products is a serious worldwide environmental issue. Studies have shown that Pb, Cd, Cu and Zn are the major pollutants in roadside environments due to vehicular activities (Akbar et al., 2006; Chen et al., 2010; Abechi et al., 2010; Zhang et al., 2012; Aslam et al., 2013). In recent years, many researchers have considered the concentration and distribution of heavy metals in street and roadside dusts (Lu et al., 2009; Al-Khashman, 2007; Shi et al., 2008; Aslam et al., 2013). Many of these researches show that a strong correlation exists between heavy metal concentration and human activities such as transportation and industrialization. However, little or no research have been conducted on metal concentrations in the street dust in Ado Ekiti metropolis. Therefore, the objective of this study is to determine the metal concentrations in street dusts collected from gasoline filling stations and roadsides in Ado Ekiti and to assess the pollution hazards resulting from toxic metals.

* Corresponding author. e-mail: matthewisinkaye@eksu.edu.ng

2. Materials and Methods

2.1. Study area

Ado-Ekiti is a city located on latitude 7^0 3' and longitude 5^0 5' in the southwest Nigeria. It is the administrative capital of Ekiti State with a population of about 3.2 million people according to the Nigeria national population census of 2006. The geology of the area consists of Pre-Cambrian basement complex rock with granitic rocks outcropping at several locations within and around the city. The granitic rocks found in the study area are of the charnokite series, mainly referred to as older granites (Okwoli et al., 2014). The climate consists of wet and dry seasons over the year. The wet season occurs between May and October, while the dry season lasts from November to April.

2.2. Sample collection and preparation

Street dust samples were collected from sixteen gasoline service stations spread across various parts of the city and five major roads within Ado Ekiti metropolis. The sampling sites were selected based on spread and the volume of activities and on vehicular density. Fig. 1 shows the Google map of Ado Ekiti indicating the major road networks where samples were collected. Fig. 2 shows the coordinates and spread of the sampling points along the major roads within Ado Ekiti. At each service station, five dust samples were collected at different locations and composited to one. For the roadside, one sample was collected from both sides of the road to make a single composite sample. Samples were collected with a soft touch hand brush and a plastic dust pan. Debris and other unwanted materials were removed immediately after the collection of the sample. In all, 104 sub-samples were collected and formed to twenty-eight composite samples consisting of sixteen street dust and twelve roadside dust samples for x-ray fluorescence (xrf) analysis. For comparison with local background values, a site that is free from traffic, agricultural practices and other human activities was selected from which a composite sample of five replicates was collected to serve as control values for the metal concentrations. The composite samples were taken to the laboratory for further preparations. At the laboratory, the composite samples were dried at the laboratory temperature to eliminate moisture. The dried samples were then sieved using a 100 µm mesh. To avoid the cross contamination of samples, acetone was used to clean the sieve between samples. The sieved samples were then formed into pellets using steel moulds and hydraulic press. Aluminum foil was used as a binder to hold the sample particles together after removal from the moulds.

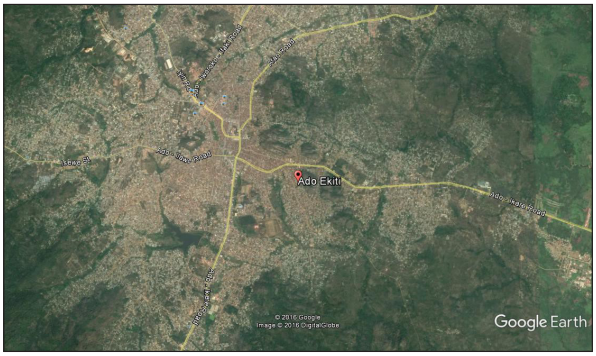

Figure 1. Google map of Ado Ekiti Showing the major roads where samples were collected.

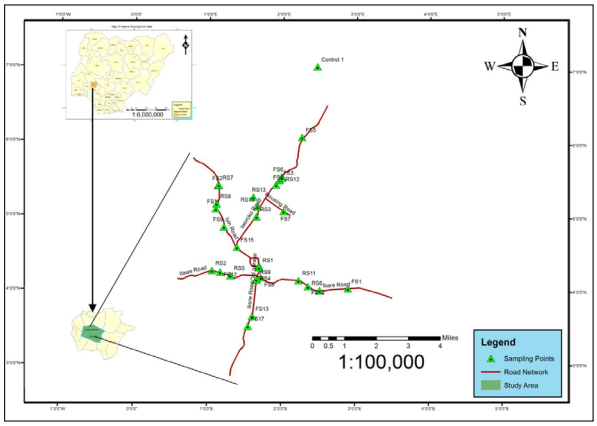

Figure 2. Major road network of Ado Ekiti showing the sampling locations

2.3. Sample irradiation and measurement

The elemental analyses of the samples were performed using energy dispersive X-ray fluorescence (EDXRF) spectrometry. All the analyses were carried out at the XRF laboratory, Centre for Energy Research and Development (CERD), Obafemi Awolowo University, Ile Ife. To analyze the elemental concentrations in the samples, 0.1 g of dust samples were formed into pellets and each pellet was placed in the sample chamber for irradiation. The spectrometer is an ECLIPSE III, self-contained miniature X-ray tube supplied by AMTEK Inc., USA. The detector is a high performance thermoelectrically cooled Si-PIN photodiode (XR-100CR model). The source X-ray tube is maintained at a voltage of 25 kV and a current of 50 µA and each sample was irradiated for 1000 sec. The detector is coupled to a 8000A multichannel analyzer. The resolution of the detector at FWHM peak of 55Fe is 220 eV. Quantitative analysis of the metal concentrations in the irradiated samples was carried out with XRF-FR software package using fundamental parameter approach.

2.4. Pollution index assessment

The pollution levels of Mn, Ni, Cu, Zn, As, and Pb in the street dust samples were determined to assess the extent of potentially toxic metal contamination and to detect the source of metals in the street dusts. In this study, four different pollution indices were used, which are; enrichment factor (EF), contamination factor (CF) and pollution index (P_i). The enrichment factor is one of the most widely used indices to estimate the degree of anthropogenic pollution in the environment (Zakir et al., 2008, Goher et al., 2014). It is used to differentiate between metals originating from human activities or those originating from natural sources (Lu et al., 2014). The enrichment factor was calculated using the following mathematical equation:

$$EF = \frac{C_n / C_{n(ref)}}{B_n / B_{n(ref)}} \quad \text{.....(1)}$$

where, C_n and $C_{n\,(ref)}$ are the measured concentrations of trace and reference metals in the dust samples, respectively. B_n and $B_{n\,(ref)}$ are the background values of the trace and reference metals, respectively. Three classes of enrichment factor exist, which are; EF lower than 0.5 indicating that trace metal is purely geogenic in origin, EF between 0.5 and 1.5 implying that the trace metal could either be geogenic or anthropogenic

in origin, and EF greater than 1.5 showing that the trace metal is purely anthropogenic in origin (Zhang et al., 2007, Hiller et al., 2016). Researchers usually adopt Fe, Al, K, Mn and Ti as reference metals due to their abundance and low occurrence variability in most soil (Liu et al., 2005, Yongming et al., 2006, Turner and Simmonds, 2006, Zhang et al., 2007, Iqbal and Shah, 2011, Lu et al., 2014, Hiller et al., 2016).

The contamination factor (CF) was calculated to assess the degree of contamination in the dust samples by heavy and trace metals. The calculation was carried out using the following mathematical formula:

$$CF = \frac{C_n}{B_n} \quad \text{.....(2)}$$

Where C_n is the measured concentration of metal in the dust sample and B_n is the background values of the same metal. Since data on regional or national heavy and trace metal concentrations are not available in Nigeria, values reported in Taylor (1964) were used as pre-industrial background concentrations (Table 7). The contamination factor is generally classified into four groups: CF lower than 1 shows low contamination, CF between 1 and 3 indicates a moderate contamination, CF greater than 3 up to 6 implies considerable contamination, while CF greater than 6 represents very high contamination (Hiller et al., 2016).

To further assess the quality of the dust samples for trace metal, pollution index (index), as suggested by Huang (1987), was used. It is defined as:

$$P_i = \frac{C_n}{X_a} \quad (C_n \le X_a) \quad \text{.....(3)}$$

$$P_i = 2 + \frac{C_n - X_b}{X_c - X_b} \quad (X_b < C_n \le X_b) \quad \text{.....(4)}$$

$$P_i = 3 + (C_n - X_c)/(X_c - X_b) \quad (C_n > X_c \quad \text{.....(5)}$$

Where C_n is the measured concentration of metal n in the dust samples, X_a is the threshold value for no-pollution, X_b is the threshold value for lowly polluted site and X_c is the threshold value for highly polluted site. X_a, X_b and X_c are given as 40, 50 and 200 mg/kg for Ni, 35, 100 and 400 mg/kg for Cu, 100, 250 and 500 mg/kg for Zn, 35, 300 and 500 mg/kg for Pb 15, 30 and 40 mg/kg for As, respectively (Chen et al., 2010). P_i is generally classified as no contamination, low contamination, moderate contamination, and high contamination.

3. Results and discussion

The basic statistical descriptions of major elements and trace metal concentrations in street dusts collected from gasoline service stations and roadsides are presented in Tables 1 and 2. The mean values for the major elements in the gasoline station samples were 9,727 mg/kg for K, 20,657 mg/kg for Ca, 9,290 mg/kg for Ti, 701 mg/kg for Mn and 31,500 mg/kg for Fe. For the trace metals, the mean values were 140.6 mg/kg for Ni, 23.9 mg/kg for Cu, 182.8 mg/kg for Zn, 124.8 mg/kg for Pb and 16.7 mg/kg for As. The statistical mean concentrations for the major elements in roadside samples were 9,909 mg/kg for K, 14,949 mg/kg for Ca, 9,370 mg/kg for Ti, 765 mg/kg for Mn and 36,269 mg/kg for Fe. For the trace metals, the mean concentrations obtained were 143.3 mg/kg for Ni, 22.5 mg/kg for Cu, 156.0 mg/kg for Zn, 180.3 mg/kg for Pb and 10.4 mg/kg for As. The concentrations of the major elements and trace metals in the street and roadside dusts were highly variable as indicated in the high standard variations shown for each metal in Tables 1 and 2. The variability in metal concentrations was further confirmed by the calculation of coefficient of variation (CV) values. All the major elements (Ca, Ti, Mn and Fe) except K present higher CV in roadside dusts than in street dusts collected from gasoline stations. The same is true for Cu and Zn. This proves that Ca, Ti, Mn, Fe, Cu and Zn show more variability at the roadsides than at the gasoline service stations. Whereas, K, Ni, Pb, and As show more variability at the gasoline stations than at roadsides. For the heavy metals, the concentrations obtained at the sampling locations are higher than those obtained at the control site implying that there is enhanced concentration of metals due to traffic and other human activities. Cu, Zn, and Pb are also higher at the sampling locations compared to the control site. Ni and As are lower at the sampling site compared to the control site. Possible sources of major elements and trace metals in urban soils can be determined by comparing their concentrations in street dust with background values (Atapour, 2015; Lu et al., 2016; Hiller et al., 2016). As seen from Tables 1 and 2, the median concentrations of all the major elements (K, Ca, Ti, Mn and Fe) were higher than their corresponding background values. This suggests that at least half of the street dust samples have their metal origin possibly from anthropogenic sources. For the trace metals (Ni, Cu, Zn, As, and Pb), the median concentrations were either lower or slightly above the background values showing that most of the trace metals originated from the parent rocks. Table 3 shows the Pearson's correlation matrix for the interactions among the metals in street dust samples collected from gasoline service stations. As seen from the table, strong positive interactions existed between K and Ca , Ti , and Mn, Ti and Fe, Mn, and Zn, Fe and Mn, and Zn, Mn and Zn, Cu and Pb and As. All the trace metals (Cu, Zn, Pb and As) except Ni show positive correlation with the heavy metals with the exception of Ca which shows negative correlation with Pb. Table 4 presents the results of Pearson correlation analysis for metals interactions in the roadsides dust samples. The results show that only K and Ca, Ti and Mn, Ti and Ni, Fe and Mn and Cu and Pb exhibited strong relationships. All the trace metals in roadside soil were positively correlated, while Ti shows negative correlation with all the trace metals. Positive correlation among metals indicated a strong possibility for the metals to have originated from the same source, such as anthropogenic or geogenic in origin. Table 5 shows the result of principal component analysis (PCA), which was based on the correlation coefficient matrix for the major and trace metals in street dusts from gasoline service stations. The coefficient is assumed significant only if the value is greater than 0.30 (Gbadebo and Ekwue, 2014). Therefore, metals having PCA coefficient values lower than 0.30 were considered to have no significant contribution to the overall variation observed in the dust samples. From Table 5, four principal components were identified with Eigen values greater than 1.0. The Eigen values for the respective components were 4.172, 2.136, 1.246, and 1.105. The four components jointly account for 86.588 % of the total variation observed in the analyzed samples. PC1 accounted for 41.715 % of the variability K (0.814), Ca (0.454), Ti (0.888), Mn (0.853), Fe (0.877), Cu (0.501),

Zn (0.617), and As (0.585), PC2 accounted for 21.362 % of the total variation and was related to Ti (0.303), Ni (0.624), Cu (0.827), Zn (0.400), Pb (0.609), and As (0.560), PC3 accounted for 12.461 % of the total variation mainly from Ca (0.775), Ni (0.331), Zn (0.337) and Pb (0.433), while PC4 accounted for 11.050 % of the variations from Ni (0.603), Zn (0.397) and Pb (0.608). PCA results for the roadsides samples revealed that four of the principal components also have Eigen values higher than 1.0 (Table 6). The four principal components recorded Eigen values of 3.136, 2.853, 1.706 and 1.084, respectively, all accounting for 87.778 % of the overall variation among the roadsides samples. PC1 accounted for 31.359 % of the variation mainly from K (0.622), Ca (0.672), Ti (0.485), Ni (0.709), Cu (0.726), Zn (0.594), Pb (0.646), and As (0.470), PC2 accounted for 28.525 % with Ti (0.622), Mn (0.982), Fe (0.944), Ni (0.308) Cu (0.0.489), and Zn (0.376), PC3 accounted for 17.059 % with K (0.715), Ca (0.616), Ti (0.400), Ni (0.565) and Zn (0.403), while PC4 accounted for 10.835 % of the total variation and was related to only Pb (0.609) and As (0.751).

Table 1. Statistics of metal concentration in dust samples from gasoline service stations in Ado Ekiti

Statistics	Major elements (mg/kg)					Trace metals (mg/kg)				
	K	Ca	Ti	Mn	Fe	Ni	Cu	Zn	Pb	As
Mean	9,727	20,657	9,290	701	31,501	140.6	23.9	182.8	124.8	16.7
Median	9,234	17,995	8,331	707	29,153	144.0	17.5	169.0	81.50	14.0
SD	3,220	13,367	5,546	248	12,332	80.1	14.2	47.3	96.2	11.8
Minimum	4,304	3,994	2,866	363	16,806	18.0	9.0	126.0	ND	ND
Maximum	14,397	48,921	25,337	1296	54929	348.0	48.0	269.0	294	44
Background values in soil	8,929	3,400	5,611	382.5	17,832	258.5	18.0	128.5	95.5	12.5

Table 2. Statistics of metal concentration in dust samples from roadsides in Ado Ekiti

Statistics	Major elements (mg/kg)					Trace metals (mg/kg)				
	K	Ca	Ti	Mn	Fe	Ni	Cu	Zn	Pb	As
Mean	9,909	14,950	9,380	765	36,268	143.3	22.6	156.0	171.4	10.4
Median	9,959	8,722	6,702	699	32,161	150.5	16.5	128.0	133.0	10.5
SD	3,161	14,258	8,025	379	18,134	66.6	14.5	71.0	107.5	5.1
Minimum	5,221	2,246	3,002	431	21,084	7.0	6.0	91.0	ND	ND
Maximum	16,246	46,875	33,362	1,726	86,596	241.0	43.0	349.0	332.0	19.0
Background values in soil	8,929	3,400	5,611	382.5	17,832	258.5	18.0	128.5	95.5	12.5

Table 3. Pearson's correlation matrix for metal in street dust samples collected from gasoline service stations

	K	Ca	Ti	Fe	Mn	Ni	Cu	Zn	Pb	As
K	1.000									
Ca	**0.621**	1.000								
Ti	**0.739**	0.382	1.000							
Fe	0.476	**0.192**	0.737	1.000						
Mn	**0.668**	**0.292**	**0.888**	0.838	1.000					
Ni	0.071	-0.027	-0.188	-0.064	-0.214	1.000				
Cu	0.470	0.108	0.197	0.309	0.196	0.491	1.000			
Zn	0.269	**0.031**	**0.584**	**0.656**	0.544	-0.209	0.036	1.000		
Pb	0.383	-0.057	0.223	0.302	**0.307**	0.126	0.751	-0.226	1.000	
As	0.359	0.075	0.194	0.260	**0.166**	0.337	0.738	0.243	0.453	1.000

Bolded values are significant at p<0.05

Table 4. Pearson's correlation matrix for metal in street dust samples collected from roadsides

	K	Ca	Ti	Fe	Mn	Ni	Cu	Zn	Pb	As
K	1.000									
Ca	**0.826**	1.000								
Ti	-0.068	-0.153	1.000							
Fe	-0.160	-0.117	**0.617**	1.000						
Mn	-0.214	-0.182	0.510	**0.978**	1.000					
Ni	0.030	0.103	**-0.689**	-0.374	-0.363	1.000				
Cu	0.310	0.324	-0.155	0.385	0.391	0.466	1.000			
Zn	0.003	0.213	-0.094	0.294	0.226	0.529	0.464	1.000		
Pb	-0.114	-0.141	-0.074	0.302	0.270	0.309	0.360	0.490	1.000	
As	0.417	0.401	-0.151	0.220	0.210	0.515	**0.871**	0.559	0.058	1.000

Bolded values are significant at p<0.05

Trace metal concentrations in roadside dusts in Ado Ekiti were compared with those in other cities around the world as obtained by other researchers. The comparison is shown in Table 8 with the world average background concentrations in soil used as reference values. Ni concentration in the roadside dust of the study area is higher than the values presented in the literature about other countries. It is almost three times higher than the mean concentration in the soil around the world. This is due to the high concentration of Ni (258.5 mg/kg) in the local background soil (Table 2). Cu is lower in this study than the values obtained in other locations. The mean value of Zn in Ado Ekiti is higher than the values obtained in Angola (Luanda), Iran (Iran), and China (Beijing). The level of Pb in the roadside dust within Ado Ekiti is considered to be in the median range of values reported about other locations, but it is almost five times higher than the world mean value in the soil as reported in Martins and Whitfield (1983). Arsenic concentration in Ado Ekiti is comparable to values from China (Beijing and Xian) and Saudi Arabia (Jeddah). The concentrations of the potentially toxic metals (Ni, Cu, Zn, Pb and As) were compared with threshold levels for toxic metal in the soil used in Finland, Australia, USA, and Canada because such standards are not available for Nigeria (Table 9). As seen from the table, the concentration of Ni is greater than the threshold levels set for all countries. Cu is lower than the standards except for USEPA (US Environmental Protection Agency). Zn and Pb concentrations at the gasoline service stations and roadsides are higher than USDOE (US Department of Energy), USEPA and C-EQG (Canadian Environmental Quality Guidelines) standards. The concentrations of As in street dusts are lower than the ecological investigation level set for the Australian soil.

Table 5. Principal Component Analysis (PCA) of metals in street dusts from gasoline stations

	PC1	PC2	PC3	PC4
Eigen value	4.172	2.136	1.246	1.105
Total variance (%)	41.715	21.362	12.461	11.050
Cumulative variance (%)	41.715	63.077	75.538	86.588
K	**-0.814**	0.116	0.382	-0.248
Ca	**-0.454**	-0.059	**0.775**	-0.207
Ti	**-0.888**	**-0.303**	0.045	-0.052
Mn	**-0.853**	-0.161	-0.239	0.213
Fe	**-0.877**	-0.293	-0.093	-0.101
Ni	0.037	**0.624**	**0.331**	**0.603**
Cu	**-0.501**	**0.827**	-0.072	0.041
Zn	**-0.617**	**-0.400**	**-0.337**	**0.397**
As	**-0.585**	**0.560**	-0.124	0.222
Pb	-0.204	**0.609**	**-0.433**	**-0.608**

Table 6. Principal Component Analysis (PCA) of metals in roadside dusts

	PC1	PC2	PC3	PC4
Eigen value	3.136	2.853	1.706	1.084
Total variance (%)	31.359	28.525	17.059	10.835
Cumulative variance (%)	31.359	59.883	76.942	87.778
K	**0.622**	-0.055	**-0.715**	0.228
Ca	**0.672**	-0.038	**-0.616**	0.123
Ti	**-0.485**	**0.622**	**-0.400**	-0.125
Mn	-0.127	**0.982**	0.031	-0.001
Fe	-0.161	**0.944**	0.103	0.044
Ni	**0.709**	**-0.308**	**0.565**	-0.174
Cu	**0.726**	**0.489**	0.151	-0.009
Zn	**0.594**	**0.376**	**0.403**	-0.181
As	**0.470**	0.280	0.248	**0.751**
Pb	**0.646**	0.226	-0.279	**-0.609**

Table 7. Mean values of enrichment factor (EF), contamination factor (CF) and pollution index (PI) obtained for streets dusts in Ado Ekiti

		Gasoline service stations			Roadsides		
Trace metal	Geochemical background (Earth crust)[a] (mg/kg)	Enrichment factor	Contamination factor	Pollution index	Enrichment factor	Contamination factor	Pollution index
Ni	75	2.64	1.87	2.54	2.59	1.91	2.58
Cu	55	0.55	0.43	0.68	0.48	0.41	0.64
Zn	70	3.40	2.61	1.55	2.92	2.16	1.35
Pb	12.5	8.92	7.49	1.05	10.5	9.61	1.01
As	13	1.43	1.13	0.98	0.91	0.67	0.60

aTaylor (1964)

Table 8**.** Comparison of trace metal concentrations in roadside dusts in Ado Ekiti with values from other countries

Country (City)	Trace metal concentration (mg/kg)					Reference
	Ni	Cu	Zn	Pb	As	
Angola (Luanda)	10	38	98	266	-	Ferreira-Baptista and De Miguel, 2005
China (Beijing)	26.7	29.7	92.1	35.4	8.1	Chen et al., 2010
China (Xian)	36.2	74.2	462.6	176.2	14.2	Lu et al., 2014
China (Xuzhou)	55	38	224	40	-	Wang and Fu, 2014
Greece (Kavala)	58	124	272	301	-	Christoforidis and Stamatis, 2009*
Iran (Tehran)	14.9	22.8	49.8	50.2	-	Sayadi and Sayyed, 2011**
Jordan (Amman)	88	177	258	236	-	Al-Khashman, 2007
Saudi Arabia (Jeddah)	46.7	-	222.2	47.5	13.9	Kadi, 2009
Thailand (Maha Sarakham)	-	11.23	35.96	14.35		Ma and Singhirunnusorn, 2012
Nigeria (Ado Ekiti)	143.3	22.6	156.0	171.4	10.4	Present study
World background value	50	30	90	35	6	Martin and Whitfield, 1983

**Industrial area soil* ***Nursery school dust*

Table 9**.** Comparison of potentially toxic metals in street dusts with toxicological reference levels for some countries

Metal	Gasoline service station (mg/kg)	Roadside (mg/kg)	Finland threshold level[b] (mg/kg)	Australia ecological investigation level[c] (mg/kg)	USDOE threshold effect concentration[c] (mg/kg)	USEPA[e] (mg/kg)	C-EQG Probable Effect level[f] (mg/kg)
Ni	140.6	143.3	50	60	39.6	16	-
Cu	23.9	22.6	100	100	28	16	35.7
Zn	182.8	156.0	200	200	159	110	123
Pb	124.8	171.4	60	600	34.2	31	35
As	16.7	10.4	5	20	-	-	12

[b]MEF (2007), [c]DEC (2010), [d]Jones et al. (1997), [e]USEPA (1999), [f]Environment Canada (2002)

Conclusion

Major element and trace metal concentrations in the street dust samples collected from gasoline service stations and roadsides in Ado Ekiti have been evaluated in order to estimate the pollution risks to the population. Results show that the concentrations of the analyzed metals in the street dusts were a little enhanced compared to local background concentrations except Ni and As. Though vehicular and human activities have increased the metal concentrations in the street dusts of Ado Ekiti, pollution indices assessments indicate that the street dusts are not highly contaminated with potentially toxic metals except for Pb, which exhibits a high degree of contamination.

References

[1] Abechi, E.S., Okunola, O.J., Zubairu, S.M.J., Usman, A.A. and Apene, E., 2010. Evaluation of heavy metals in roadside soils of major streets in Jos metropolis, Nigeria. Journal of Environmental Chemistry and Ecotoxicology, 2 (6): 98-102.

[2] Abrahams, P.W., 2002 Soils: their implications to human health. Science of the Total Environment, 291(1): 1-32.

[3] Akbar, K.F., Hale, W.H., Headley, A.D., and Athar, M., 2006. Heavy metal contamination of roadside soils of Northern England. Soil and Water Research, 1(4): 158-163.

[4] Al-Khashman, O. A., 2007. The investigation of metal concentrations in street dust samples in Aqaba city, Jordan. Environmental Geochemistry and Health, 29: 197–207.

[5] Aslam, J., Khan, S.A. and Khan, S.H., 2013. Heavy metals contamination in roadside soil near different traffic signals in Dubai, United Arab Emirates. Journal of Saudi Chemical Society, 17(3): 315-319.

[6] Atapour, H., 2015. Geochemistry of potentially harmful elements in topsoils around Kerman city, southeastern Iran. Environmental Earth Sciences, 74(7): 5605-5624.

[7] Chen, X., Xia, X., Zhao, Y., and Zhang, P., 2010. Heavy metal concentrations in roadside soils and correlation with urban traffic in Beijing, China. Journal of Hazardous Materials. 181: 640-646.

[8] Christoforidis, A. and Stamatis, N., 2009. Heavy metal contamination in street dust and roadside soil along the major national road in Kavala's region, Greece. Geoderma, 151(3): 257-263.

[9] DEC (Department of Environment and Conservation, Western Australia), 2006. The Use of Risk Assessment in Contaminated Site Assessment and Management: Guidance onthe Overall Approach. Contaminated Sites Management Series. Available at: Error! Hyperlink reference not valid..

[10] Environment Canada, 2002. Canadian sediment quality guidelines for the protection of aquatic life: Summary table. <http://www.doeal.gov/SWEIS/OtherDocuments/328%20envi%20 canada%202002.pdf>.

[11] Ferreira-Baptista, L. and De Miguel, E., 2005. Geochemistry and risk assessment of street dust in Luanda, Angola: a tropical urban environment. Atmospheric Environment, 39: 4501-4512.

[12] Gbadebo, A.M. and Ekwue, Y.A., 2014. Heavy metal contamination in tailings and rocksamples from an abandoned goldminein southwestern Nigeria. Environmental Monitoring and Assessment, 186: 165-174

[13] Goher, M.E., Farhat, H.I., Abdo, M.H. and Salem, S.G., 2014. Metal pollution assessment in the surface sediment of Lake Nasser, Egypt. The Egyptian Journal of Aquatic Research, 40(3): 213-224

[14] Gray, C.W., McLaren, R.G. and Roberts, A.H., 2003. Atmospheric accessions of heavy metals to some New Zealand pastoral soils. Science of the Total Environment, 305(1): 105-115.

[15] Gurung, A. and Bell, M.L., 2013. The state of scientific evidence on air pollution and human health in Nepal. Environmental Research, 124: 54-64

[16] Hiller, E., Lachká, L., Jurkovič, Ľ., Ďurža, O., Fajčíková, K. and Vozár, J., 2016. Occurrence and distribution of selected potentially toxic elements in soils of playing sites: a case study from Bratislava, the capital of Slovakia. Environmental Earth Sciences, 75(20): 1390-

[17] Huang, R., 1987. Environment Peadology. Higher Education Press.

[18] Iqbal, J. and Shah, M.H., 2011. Distribution, correlation and risk assessment of selected metals in urban soils from Islamabad, Pakistan. Journal of Hazardous Materials, 192(2): 887-898.

[19] Järup, L., 2003. Hazards of heavy metal contamination. British Medical Bulletin, 68(1): 167-182.

[20] Jones, D.S., Sutter II, G.W. and Hull, R. N., 1997. Toxicological benchmarks for screening contaminants of potential concern for effects on sediment-associated biota: 1997 Revision, ES/ER/TM-95/R4. Oak Ridge National Laboratory, prepared for the US Department of Energy. 48 p.

[21] Kadi, M.W., 2009. Soil Pollution Hazardous to Environment: A case study on the chemical composition and correlation to automobile traffic of the roadside soil of Jeddah city, Saudi Arabia. Journal of Hazardous Materials, 168(2): 1280-1283.

[22] Liu, W.H., Zhao, J.Z., Ouyang, Z.Y., Söderlund, L. and Liu, G.H., 2005. Impacts of sewage irrigation on heavy metal distribution and contamination in Beijing, China. Environment International, 31(6): 805-812.

[23] Lu X., Zhang X., Li Y.L. and Chen H., 2014. Assessment of metals pollution and health risk in dust from nursery schools in Xian, China. Environmental Research, 128: 27-34.

[24] Lu, Y., Jia, C., Zhang, G., Zhao, Y. and Wilson, M.A., 2016. Spatial distribution and source of potential toxic elements (PTEs) in urban soils of Guangzhou, China. Environmental Earth Sciences, 75(4): 1-15.

[25] Ma, J. and Singhirunnusorn, W., 2012. Distribution and health risk assessment of heavy metals in surface dusts of Maha Sarakham municipality. Procedia-Social and Behavioral Sciences, 50: 280-293.

[26] Markus, J.A. and McBratney, A.B., 1996. An urban soil study: heavy metals in Glebe, Australia. Journal of Soil Research, 34(3): 453-465.

[27] Martin, J. M. and Whitfield, M., 1983. The significance of the river input of chemical elements to the ocean, In: Trace Metals in Sea Water, Springer US, pp. 265-296.

[28] MEF (Ministry of the Environment, Finland), 2007. Government Decree on the Assessment of Soil Contamination and Remediation Needs. 214/2007 (March 1, 2007). Available at: http://www.finlex.fi/en/laki/kaannokset/2007/en20070214.

[29] Okwoli, E., Onoja, O.S. and Udoeyop, U.E., 2014. Ground Magnetic and Electrical Resistivity Mapping for Basement Structures Over Charnokitic Terrain in Ado Ekiti Area, Southwestern Nigeria. International Journal of Science and Technology, 3(10): 683-689.

[30] Sayadi, M.H. and Sayyed, M.R.G., 2011. Comparative assessment of baseline concentration of the heavy metals in the soils of Tehran (Iran) with the comprisable reference data. Environmental Earth Sciences, 63(6): 1179-1188.

[31] Shi, G., Chen, Z., Xu, S., Zhang, J., Wang, L., Bi, C. and Teng, J., 2008. Potentially toxic metal contamination of urban soils and roadside dust in Shanghai, China. Environmental Pollution, 156(2): 251-260.

[32] US EPA., 1999. U.S. Environmental Protection Agency. Screening level ecological risk assessment protocol for hazardous waste combustion facilities, vol. 3, Appendix E: Toxicity reference values. EPA530-D99-001C.

[33] Wang, X.S., and Fu, J., 2014. Heavy metals in Xuzhou urban roadside topsoils (China): magnetic characterization and enrichment mechanism. Environmental Earth Sciences, 72(9): 3307-3316.

[34] Weast, R.C., 1984. CRC Handbook of Chemistry and Physics, 64th Edn (CRC Press, Boca Raton

[35] Wilcke, W., Müller, S., Kanchanakool, N. and Zech, W., 1998. Urban soil contamination in Bangkok: heavy metal and aluminium partitioning in topsoils. Geoderma, 86(3): 211-228

[36] Yongming, H., Peixuan, D., Junji, C. and Posmentier, E.S., 2006. Multivariate analysis of heavy metal contamination in urban dusts of Xi'an, Central China. Science of the Total Environment, 355: 176-186

[37] Zakir, H. M., Shikazono, N. and Otomo, K., 2008. Geochemical distribution of trace metals and assessment of anthropogenic pollution in sediments of Old Nakagawa River, Tokyo, Japan. American Journal of Environmental Sciences, 4(6): 654

[38] Zhang, F., Yan, X., Zeng, C., Zhang, M., Shrestha, S., Devkota, L.P. and Yao, T., 2012. Influence of traffic activity on heavy metal concentrations of roadside farmland soil in mountainous areas. International Journal of Environmental Research and Public Health, 9(5): 1715-1731.

[39] Zhang, J. and Liu, C.L., 2002. Riverine composition and estuarine geochemistry of particulate metals in China—weathering features, anthropogenic impact and chemical fluxes. Estuarine, Coastal and Shelf Science, 54(6): 1051-1070

JJEES
Jordan Journal of Earth and Environmental Sciences

Volume 9, (Number 1), April, 2018
ISSN 1995-6681
Pages 29 - 38

Prevalence of Urolithiasis in Adults due to Environmental Influences: A Case Study from Northern and Central Jordan

Iyad Ahmed Abboud

Department of Geology/Biology, Faculty of Science, Taibah University, Yanbu, Saudi Arabia

Received 31 October, 2017; Accepted 1 January , 2018

Abstract

The Urinary stone disease, known as urolithiasis, is one of the most prevalent health problems around the world. It is considered as one of the most serious disease in humans in terms of continuity, repetitions, and symptoms. This study aims to determine the prevalence of urolithiasis , the incidences, and the risk factors of this disease among the population of northern Jordan. Moreover, it studies the effects of environmental, geographical, and biological factors that contribute to the occurrence of urolithiasis. More than 250 samples of urinary stones were collected from five hospitals in Jordan over the course of five years. They were used to assess the logistical and polynomial regression for each potential risk factor in order to determine the prevalence of urolithiasis through the demographic features. The processing of the climatic, geographic, and geochemical data revealed that there is a relationship between the environmental factors and the urolithiasis prevalence. Strong relationships were observed between the prevalence of urinary stones and the population distribution, gender, and age of the individuals in the study area. The local climatic condition is characterized by high temperatures in summer, excessive exposure to sunlight, and semiarid to arid conditions as well as a high concentration of bicarbonates and fluoride in water. These factors were observed to affect human health by their contribution to the formation and growth of urinary stones. It was noted that the urolithiasis disease prevails increasingly at the age >40 years and is found more significant in males than in females. This study investigates the impact of environmental factors on the formation and composition of stones through diet in addition of the effect of water hardness on the formation of oxalate stones which optimize their impact in bicarbonate concentration >300 gm/L. Moreover, geographical factors play a big role in the formation, prevalence, and composition of urinary stones. As will be observed in this study, the factors contributing to the high rate of the disease and its prevalence in regions with high temperature >20 ºC, feature increased exposure to sunlight, altitude >500 m, and soil of the Vertisols type.

Keywords: Urinary calculi, Urolithiasis, Environmental effects, Epidemiology, Jordan.

1. Introduction

The Urinary stone disease (urolithiasis) is one of the most prevalent medical problems occurring worldwide (Abboud, 2008a; Abboud, 2008b; Abboud, 2008c; Scales et al., 2012; Giannossi and Summa, 2013). Identifying the mineral composition of urinary stones helps in elucidating the impact of geo-environmental factors (Tasian et al., 2014; Fukuhara et al., 2016) and the nutrition behavior on the formation and growth of urinary stones (Alsheyab et al., 2007; Abboud, 2008a; Marickar and Vijay, 2009; Robertson, 2012).

Geological characteristics and climatic features seem to play an important role in the development of urolithiasis, its prevalence, recurrence, and the stone type (Basiri et al., 2010). Several environmental and geographical factors, such as temperature, height above mean sea level, daily and seasonal climate variability are known to have a direct or indirect impact on human health (Safarinejad, 2007; Tasian et al., 2014). Moreover, poor water quality due to the geological factors and/or anthropogenic pollutants is frequently concomitant with health problems (Abboud, 2014). These hazards may range from simple threats to harmful risks that may lead to the loss of life or damage in certain organs as is the case in the kidney stones which may lead to disruption in the daily work of the kidneys, among many other effects on human health.

In addition, the nutrition and lifestyle of many individuals may be a direct cause of the emergence of many hazards and diseases associated with the environmental, geographical, and geological factors (Marickar and Vijay, 2009), which make certain nutrients react with certain genetic factors in individuals thereby stimulating the emergence of some of these genetic diseases in some people. Scales et al. (2012) concluded in their study conducted on some population in the USA that diet and lifestyle are two of the most important factors that play an important role in the pathogenesis of kidney stones. However one can never rule out the impact of environmental and geographical factors on the prevalence of many diseases in some hot geographic regions in which people are totally dependent on aquifers (Chandrajith et al., 2006; Abboud, 2017).

The risk assessment of the environmental and geographical factors and their impact on human health are important to arrive at through disease maps that show where these diseases are prevalent and explore patterns and changes and their relationship with the environmental and geographical factors. The assessment of environmental and geographical health risks are part of the environmental epidemiology which plays

* Corresponding author. e-mail: iabboud@Taibahu.edu.sa

an important role in the effectiveness of the environmental remediation programs (Nielsen and Jensen, 2005). In order to determine the consequences of the urinary stone disease at the level of the population and community, and to identify its risk factors on individuals and the possibility of the recurrence of the disease in many people, it is necessary to understand the epidemiology of the urinary stone disease accurately.

There are quite a number of epidemiological studies of urolithiasis conducted in several countries around the world, including Middle Eastern countries with the exception of Jordan. The current study is though to be be the first epidemiological study on urolithiasis in Jordan. The aim of this study is to highlight the environmental epidemiology in the Mediterranean region especially in Jordan. Moreover, it also aims at identifying the most pivotal factors that play an important role in the prevalence of environmental health risks in the region. Hopefully, this study will try to identify the main environmental and geographical factors that play an essential role in the prevalence of the urinary stone disease in Jordan and will provide and display additional information on this disease and how to prevent it and rehabilitate the infected population.

2. Materials and Methods

2.1. Urinary Stone Data

Over a five-year span (from 2007 to 2012) more than 250 samples of urinary stones extracted surgically from patients with urolithiasis were collected at five hospitals. (Namely: The Hussein Medical City, Hospital of Princess Basma, Al-Eman Hospital, Al-Mafraq Governmental Hospital, and Jerash Governmental Hospital) to study and determine the temporal changes in urolithiasis and link these factors to the gender and age groups of the infected individuals. The method of logistical and polynomial regression for each potential risk factor was used in order to assess the prevalence of urolithiasis through the demographic features. This method resulted from odds ratios (ORs), P-values, and 95 % of the members of a particular social group will submit a urolithiasis report for the reference group in the same region. This pattern of the variables which related a univariate association with urolithiasis through the p-value ($P < 0.05$) is statistically significant.

The urinary stone samples extracted from the patients were washed in H_2O_2 to get rid of any organic matter stuck on the outer surface and were dried for a month at the laboratory temperature for photographing. Visual observations of the urinary stone samples extracted from patients were listed; they include: size, color, shape, topography, and surface features. To determine the mineralogical composition of urinary stone samples , some samples were ground in an agate mortar to study the powder by X-ray diffraction (XRD: Philips type with X-Pert Pro XRD systems) at Al al-Bayt University labs.

2.2. Epidemiological Data

All epidemiological data in this study were collected from hospitals of the Jordanian Ministry of Health (JMH) for patients from northern and central Jordan. This study included residents of the territory of the governorates of Amman, Irbid, Mafraq, Ajloun, and Jerash. The current total population of Jordan amounted to 9.5 million people including 2.9 million inhabitants being non-Jordanians (DS, 2015; Ghazal, 2016). The population is distributed in the study area as follows: more than four million people or (42.05 %) live in Amman, 1,770,158 (18.8 %) in Irbid, 549,948 (5.8 %) in Mafraq, 237,059 (2.5 %) in Jerash and 176,080 (1.9 %) in Ajloun province (DS, 2015). These numbers equal 6,739,771 (70.6 %) people out of 9.2 total population of Jordan. Figure 1 shows the distribution of the population in the five governorates of Jordan, and the prevalence rate of the disease in these regions between the years 2007 and 2012. It also shows patients who were admitted to hospitals because they suffer from the urinary stone disease, whether from these provinces or from outside. Generally speaking, about 68 % of the Jordanian people have health insurance (DS, 2015). Therefore, in order to estimate the prevalence of the urinary stone disease and calculate the numbers of people infected accurately, all cases that were checked in to the hospitals in all provinces, were followed up. Also the archival records in the emergency rooms, or at the specialty physicians clinics were alos checked. A total of 525 questionnaires were distributed to urolithiasis patients, of which 285 were answered. The questionnaires included more than fifty questions covering the entire condition of the patient; marital status, the overall physical health, nutrition, and the disease recurrence; in addition to questions that may have a direct or indirect relationship with the prevalence of the urinary stone disease in humans.

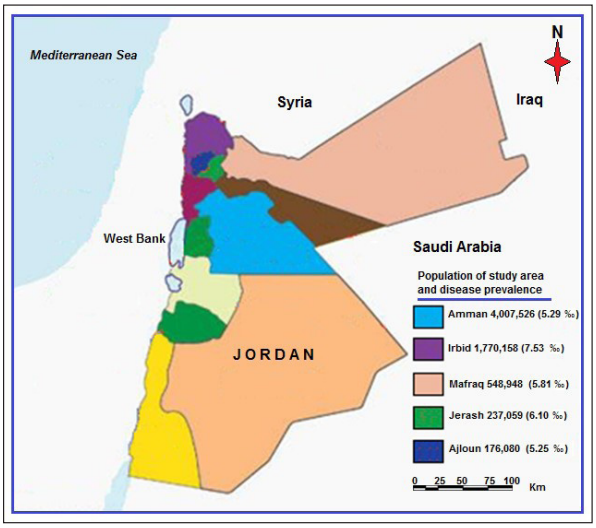

Figure 1. Distribution of population on five governorates of Jordan, and distribution of the specific prevalence rate of disease between 2007 and 2012

All these steps have been taken in order to attempt to verify the numbers of the infected patients and their conditions very accurately and to arrive at a correct diagnosis of the disease on a scientific basis and not by default, and in the end be able to suggest adequate health care by avoiding a wrong diagnosis of the disease usually provided only through some visible symptoms or the medical history without doing the necessary examinations Cases with kidney disease or the gallstone disease were separated from the cases of urolithiasis in order to arrive at an accurate distribution and certain prevalence of the disease. Finally, the personal data obtained from the patients were classified into the specified tables according to address, age, sex, social case, medical history, and diet, in order to compare the population infected with urinary stone disease with the total population and classify them based on

their age and gender.

The data of the urinary stone disease patients were obtained from different hospitals and were processed through standard statistical methods and programs (Mendenhall, 1967), namely the Program of Epidemiological Statistics for Public Health (OPENEPI), version 2.2.1, and the easy-to-use-statistical software, MedCalc Program, version 16.8.4.

2.3. Climate, Water, and Soil Data

The major bulk of information on the annual and cumulative climate conditions such as temperature (Fig. 2), precipitation (Fig. 3), altitude (Fig. 4), sunlight, and the intensity of the brightness was obtained from the Jordan Meteorological Department (JMD) between 1999 and 2016 (Weather online, 2016).

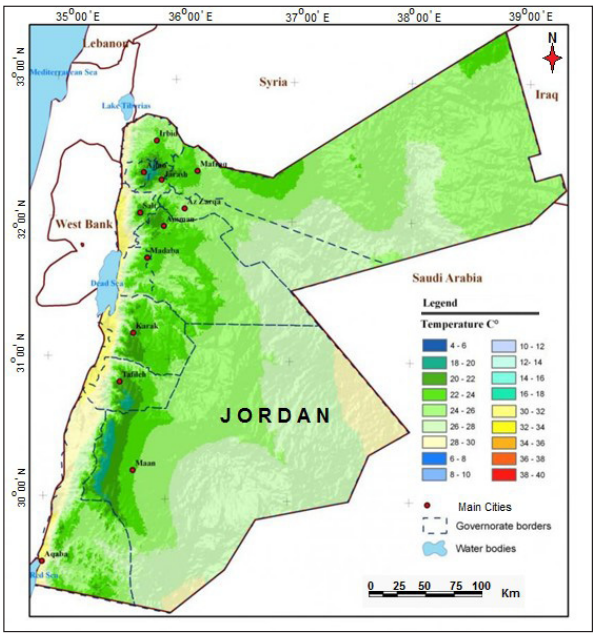

Figure 2. Mean annual maximum temperatures of study area between 1973 and 2012 (Map source: Jordan climate maps (Current climate) (2016). Map prepared by NCARE. Author: M. Saba; E. De Pauw; W. Goebel. Map source: http://www.icarda.org/jordan-climate-maps-current-climate)

It is found that the population in the study area use groundwater for drinking and other domestic uses. To determine the chemical composition of the groundwater in the study area 130 samples from all the provinces were analyzed (Abboud, 2017). Accordingly, ionic data to estimate the relationship between urolithiasis and the groundwater hardness was used in the study area. In order to determine the total hardness (TH) of the groundwater samples the contents of calcium, magnesium, and bicarbonate (Abboud, 2014; Abboud, 2017), were measured and expressed in units of milligrams per liter (mg/L). The classification of groundwater hardness was as follows: soft water (TH <75 mg/L), moderately hard water (75-150 mg/L), hard water (150-300 mg/L), and very hard water (>300 mg/L).

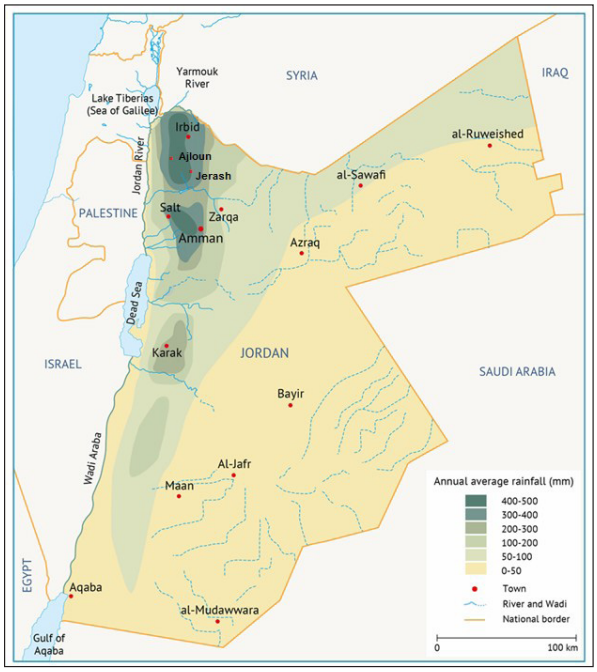

Figure 3. Distribution of the annual average rainfall (mm) in the study area between 1973 and 2012 (Map source: Annual average rainfall (mm) between 1973 and 2012 (2012). See link: https://water.fanack.com/wp-content/uploads/sites/2/2015/11/Jordan-Geography-and-Climate-Figure-5-Annual-average-rainfall-and-precipitation-Fanack-after-MWI.gif)

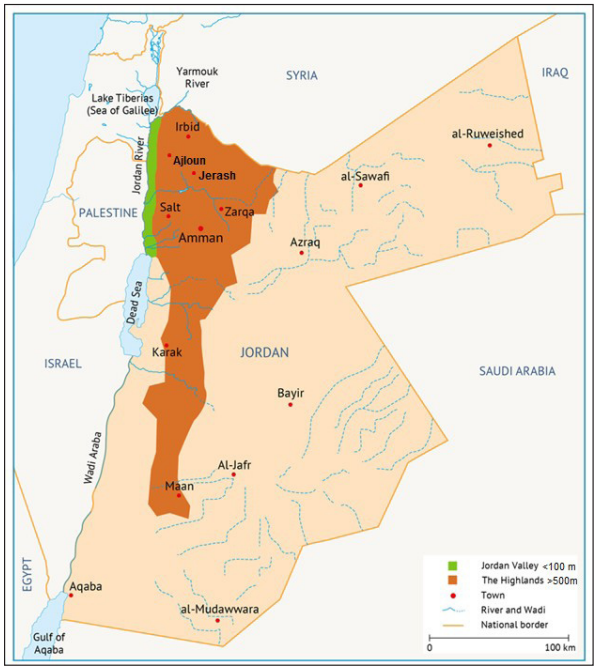

Figure 4. Mean altitude regions of study area (Map source: Fanack after Altz-Stamm, A., 2012. https://water.fanack.com/jordan/water-use/
https://water.fanack.com/wp-content/uploads/sites/2/2015/11/Jordan-Water-Use-Figure-13-Jordan%E2%80%99s-main-agricultural-regions-Fanack-after-Altz-Stamm-2012.gif

The types of soil in the study area have been identified depending on JOSCIS (2012). They are classified into macroscale, according to the the difference in their physical and chemical properties, (Fig. 5). So on the basis of the differences in the geology and lithology of study area rocks (Fig. 6), soil is classified into seven different classes (JOSCIS, 2012).

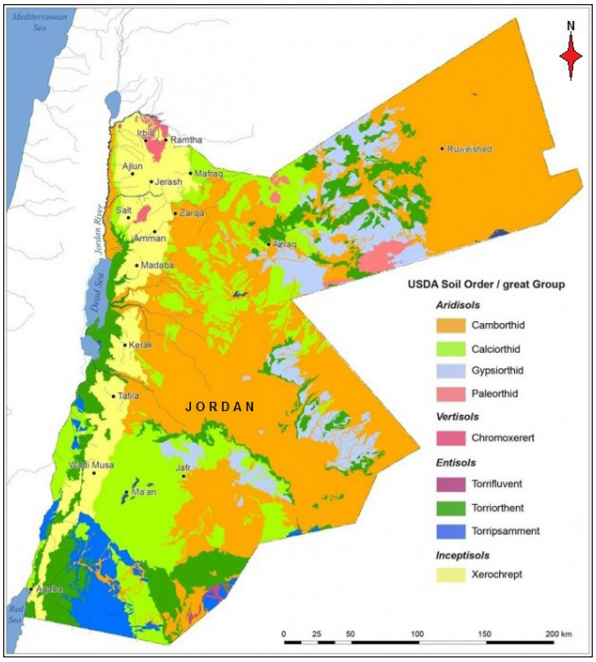

Figure 5. The main pedological regions of study area (Source: JOSCIS Database (2012). Conception: B. Lucke; A. Taimeh; F. Ziadat.. (Map source: Al-Hadidi M. M., Al-Kharabsheh A. A., Ta'any R. A. Impact of Over-Pumping on the Groundwater Quality of the Dead Sea Basin/ Jordan. Curr World Environ 2013; 8(3). doi : http://dx.doi.org/10.12944/CWE.8.3.04)

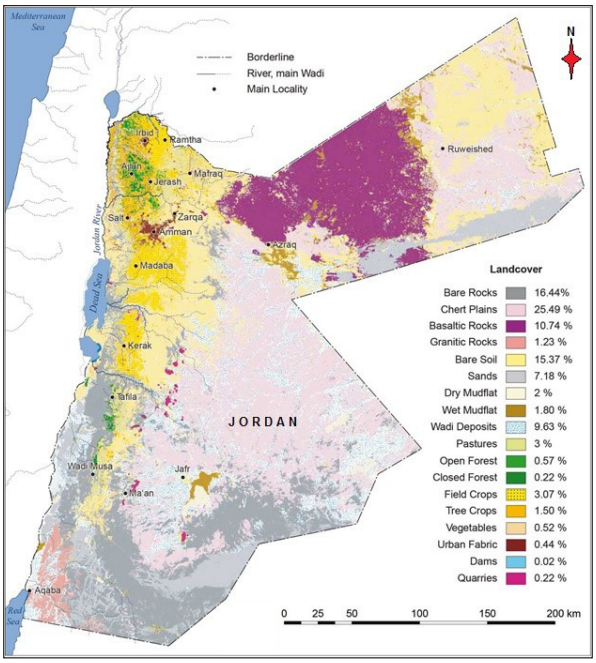

Figure 6. Geologically; the rocks distribution of Jordan land cover (Source: RJGC (2006). land cover map 1/250 000, 2006 and Conception and design: RJGC and M. Ababsa, IFPO 2010). See this link: http://books.openedition.org/ifpo/docannexe/image/4858/img-1.jpg and see; Myriam Ababsa (2014). Jordan's Land Cover. P.485. Chapter: A Land of Contrasts. p. 40-41. Éditeur: Presses de l'Ifpo. ISBN: 9782351593783, ISBN Multi-formats: 978-2-35159-438-4

3. Results and Discussions

Several medical and scientific studies have suggested that the epidemiological analysis research is very significant in order to identify the geoenvironmental factors that cause diseases and be able to control them. The processing of the climatic, geographic, and geochemical data of the study area revealed that there is a relation between the environmental factors and the epidemiology of urolithiasis. In other words, strong relationships were observed between the prevalence of the urinary stone disease and the public distribution, gender, and age of the infected individuals.

Climatic and geographical changes play an important role in the prevalence of urinary stone disease in hot and dry climates (Chen et al., 2000; Al-Eisa et al., 2002; Lee et al., 2002; Hesse et al., 2003; Komatina, 2004; Robertson, 2012; Giannossi and Summa, 2013; Tasian et al., 2014). The local environment in the study area is characterized by high temperatures in summer (30-38 ºC), excessive exposure to sunlight, semiarid to arid conditions (Jordan climate maps, 2016) as well as high concentration of bicarbonates and fluoride in the water of the study area (Abboud, 2014; Abboud, 2017). These factors were observed to affect the human health negatively by helping in the formation and growth of urinary stones and therefore increasing the number of infected cases (Tables 1 and 2). However, such effects were age dependent (>40 years) and were more evident in males than in females (61.03 %; Tables 1, 2). This finding was somehow reflected by Alsheyab et al. study (2007) where the incidence ratio was of 74.9 % in males and the most vulnerable ages were found to be between 30-50 years. Safarinejad (2007) found that the urolithiasis incidence in males was of (6.1 %) which is slightly higher than that in females (5.3%) and that it increases with age. In Abboud (2008c), the incidence of urolithiasis in males was (51.1 %) with the average age being 50 years and (44.3 %) in feamles. Basiri et al. (2010) showed a peak in the incidence of urolithiasis of (58 %) in males ranging in age between 55 and 65 years. Moreover, the prevalence of calculi stone among the Jordanian population is often similar to the global average. Accordingly urolithiasis in Jordan can be described as a prevalent local problem as is the case on a global scale.

As far as diet is concerened, eating green leaves, vegetables, red meat, chicken meat, and eggs all help to increase the concentration of Ca in the human body, which in turn helps in the formation of urinary stones. In addition, some kinds of vegetables, cheese, eggs, and milk increase the concentration of phosphorus in the human body which also contributes to the formation of urinary stones. Therefore, the nutritional factors, especially the non-medical diet system, play an important role in the formation of urinary stones through the lack of dietary fibers, the increased intake of animal protein and calcium (Robertson et al., 1979; Breslau et al., 1988; Holmes et al., 2001; Robertson, 2012), and the increased intake of green leaves and coffee (Abboud, 2008c). The results of the present study demonstrate that the impact of nutritional factors on the formation of urinary stones is age and gender specific. Whereas, these variables were more evident and influential in ages above forty, and were more prevalent in males than in females, 61.03 % (Tables 1 and 2).

Table 1. Urolithiasis prevalence in study area between 2007 and 2012 (Prevalence n and % calculated per year)

Region	Gender	**Population *n***		Population %		**Prevalence *n***		Prevalence %	Prevalence ‰	
Amman	Male	2,059,868	4,007,526	51.4	59.45	12,685	21,213	59.8	6.16	5.29
	Female	1,947,658		48.6		8,528		40.2	4.38	
Irbid	Male	911,631	1,770,158	51.5	26.25	8,165	13,320	61.3	8.96	7.53
	Female	858,527		48.5		5,155		38.7	6.01	
Mafraq	Male	301,921	548,948	55	8.2	2,107	3,188	66.1	6.98	5.81
	Female	247,027		45		1,081		33.9	4.38	
Jerash	Male	122,678	237,059	51.75	3.5	919	1,447	63.5	7.49	6.10
	Female	114,381		48.25		528		36.5	4.62	
Ajloun	Male	91,562	176,080	52	2.6	592	924	64.1	6.47	5.25
	Female	84,518		48		332		35.9	3.93	
Total	Male	3,487,660	6,739,771	51.75	100	24,468	40,092	61.03	7.02	5.95
	Female	3,252,111		48.25		15,624		38.97	4.81	

Table 2. Prevalence of urinary stones for 1,000 inhabitants: age and gender difference

Age	Study area (Amman, Irbid, Mafraq, Jerash, and Ajloun regions)									
	Gender	**Population *n***		Population %	**Prevalence *n***		Prevalence %		Prevalence ‰	
< 20	Male	1,579,758	3,065,334	23.4	1,744	2,847	4.35	0.093	1.104	0.93
	Female	1,485,576		22.0	1,103		2.75		0.74	
20-39	Male	1,129,679	2,175,389	16.8	7,165	12,589	17.87	0.579	6. 34	5.79
	Female	1,045,710		15.4	5,424		13.53		5.19	
40-50	Male	390,008	729,794	5.8	7,060	12,510	17.61	1.577	18.1	15.77
	Female	339,786		5.1	4,450		11.1		13.1	
51-60	Male	208,901	402,926	3.1	5,332	8,660	13.3	2.149	25.52	21.49
	Female	194,025		2.9	3,328		8.3		17.15	
> 60	Male	179,314	366,328	2.7	3,167	4,486	7.9	1.225	17.66	12.25
	Female	187,014		2.8	1,319		3.29		7.05	
Total	Male	3,487,660	6,739,771	51.75	24,468	40,092	61.03	0.595	7.02	5.95
	Female	3,252,111		48.25	15,624		38.97		4.81	

Table 1 shows that 40,092 people of the total population (6,739,771 people) in the study area suffer from the urinary stone disease, with the lifetime prevalence of urolithiasis being of 5.95 ‰ (Table 2). Moreover, most of the patients were males (24,468 (61.03 %) and/or older than forty years (Table 2). The prevalence and appearance of urinary stone disease increases with age.

The prevalence of the urinary stone disease in the average age of the residents of the study area was 5.95 ‰ with an average prevalence of 7.02 ‰ in male; which is higher than that in females (4.81 ‰, Table 2). These results are found to be in accordance with previous studies, and show that the relative risk of urinary stone disease in males is 1.46 times of the relative risk for females. They also reveal that the possibility of the formation and growth of lithiasis in males (being 45 %) is greater than that in females. This finding reflects other results in international studies such as Giannossi and Summa (2013) (1.2), Serio and Fraioli (1999) (1.25), Borghi et al. (1990) (1.5), and Basiri et al. (2010) (1.38) with a 58 % possibility in males.

On the whole the frequency_of urinary stone formation was observed more in males than in females as appeared from the field survey which lasted more than five years in the study area . The overall rate of the infection with the disease reached 5.95 ‰ with 7.02 ‰ of the cases occurring in males and 4.81 ‰ of them in female (Table 2). The data presented in Table 2 show that the lower prevalence of urinary stone disease was observed in the ages <20 years at a rate of 0.93 ‰, while the highest proportion of prevalence was noticed in the age group between 51-60 years with a rate of 21.49 ‰. It was also noted that the rate of prevalence of the disease in males is much higher than that in female ranging from 1.32 times in the ages between 20-39 years to 2.40 times in the age >60 years. These rates are considered high for a population that is characterized by a roughly equal number of males and females in all age groups: (1:1) ratio (Table 2).

It can be inferred that the urinary stone disease is scarce in children or adolescents under the age of twenty years, where the prevalence rate ranged from 0.74 ‰ in females to 1.104 ‰ in the males. This result is inconsistent with findings in several international studies, including Borghi et al. (1990) and Vahlensieck et al. (1982) where the prevalence of the disease among children ranging between 2 ‰ to 2.7 ‰ and in Giannossi and Summa (2013) where it was 1.2 ‰.

Tables 3 to 7 show the odds ratios acquired through the gathering and the prospect as a p-value, which signalizes how possible it is that the gathering visible is sufficient to opportunity. Tables 3 and 4 show a positive correlation between the risk factors and the disease, which become high when combined with many parameters such as age and sex. So these Tables show high and multi declines significant in all the cases that have been assembled, without any chance found or observed in the composition of the stones, leaving it to chance.

Table 3. Relation between potential risk factor of age group and urolithiasis

Risk factors of age group	Total no.	No. of cases	Odds ratio	95% confidence interval (CI)	Significance level (*p* value)
40 - > 60	1,499,048	24,656	19.9324	0.8119	0.0669
51- > 60	769,254	13,146	19.1714	0.7809	0.0705
> 60	366,328	4,486	26.8838	1.095	0.0438

Table 4. Relation between potential risk factor of Age group + Gender and urolithiasis

Risk factors of age group + gender	Total no.	No. of cases	Odds ratio	95% confidence interval (CI)	Significance level (*p* value)
40 - > 60 + male	778,223	15,559	16.3387	0.6655	0.0871
40 - > 60 + female	720,825	9,097	26.0778	1.0622	0.0458
51- > 60 + male	388,215	8,499	14.8917	0.6066	0.0982
51- > 60 + female	381,039	4,647	26.9961	1.0995	0.0436
> 60 + male	179,314	3,167	18.5370	0.755	0.0738
> 60 + female	187,014	1,319	46.9106	1.91	0.0185

Table 5. Relation between potential risk factor of Mean annual temperature (º C) and urolithiasis

Risk factors of mean annual temperature (º C)	Total no.	No. of cases	Odds ratio	95% confidence interval (CI)	Significance level (*p* value)
20 - 24 ºC	1,361,811	23,699	18.8205	0.7666	0.0723
20 - 24 ºC + male	708,008	14,927	15.4766	0.6304	0.0935
20 - 24 ºC + female	653,803	8,772	24.5096	0.9983	0.0501
20 - 24 ºC + 40 – 60 age	1,040,462	18,538	18.3748	0.7485	0.0747
20 - 24 ºC + 40 - 60 + male	550,922	11,419	15.7480	0.6415	0.0914
20 - 24 ºC + 40 - 60 + female	489,540	7,119	22.5869	0.92	0.0563

Table 6. Relation between potential risk factor of High altitude (m.a.s.l.) and urolithiasis

Risk factors of high altitude (m.a.s.l.)	Total no.	No. of cases	Odds ratio	95% confidence interval (CI)	Significance level (*p* value)
550 – 1200	1,167,143	19,197	19.9322	0.8119	0.0669
550 – 1200 + male	606,972	12,128	16.4874	0.6716	0.0861
550 – 1200 + female	560,171	7,069	10.5195	0.4285	0.1496
550 – 1200 + 40 - 60	838,605	15,358	17.8674	0.7278	0.0775
550 – 1200 + 40 - 60 + male	433,847	9,599	14.7316	0.6001	0.0995
550 – 1200 + 40 - 60 + female	404,758	5,759	23.0923	0.9406	0.0545

Table 7. Relation between potential risk factor of Water hardness (mg/L) and urolithiasis

Risk factors of water hardness (mg/L)	Total no.	No. of cases	Odds ratio	95% confidence interval (CI)	Significance level (*p* value)
150 – 300	827,474	13,610	19.9323	0.8119	0.0669
>300	646,089	10,626	20.6403	0.8407	0.0638
>300 + male	1,503,181	6,706	74.3794	3.0296	0.0083
>300 + female	1,401,659	3,921	118.8099	4.839	0.0034
>300 + 40 - 60	488,202	8,693	18.3857	0.7489	0.0746
>300 + 40 - 60 + male	258,129	5,341	15.7751	0.6425	0.0912
>300 + 40 - 60 + female	230,072	3,352	22.5424	0.9181	0.0564

Five governorates in northern Jordan were surveyed in order to determine the average rate of the entry of urinary stone disease in government hospitals (Fig. 1). The combination of the medical and scientific standards in collecting the samples determined the methodology of the study. It was observed that the governorate of Irbid exhibited the highest prevalence of the disease (7.53 ‰) followed by Jerash (6.10 ‰) and then Ajloun (5.25 ‰) (Table 1). Moreover, the prevalence of the disease was noted more in males than in females in all the provinces. It is also found significantly higher than the proportion of the regional prevalence of the disease, being 5.95 ‰ (Table 1). The provinces of the far north, especially Irbid and Jerash exhibited the highest rates of the sickness altitude (Fig. 1). The main reason behind the higher incidence of the urolithiasis disease among the population of the Irbid governorate than other places was water hardness.

There was no direct impact of the population number on the increase or decrease of the prevalence of the urinary stone disease. However there was a significant impact of age on the incidence of disease, especially in males (Table 2). The biggest prevalence of the disease was in the age group 20-39 years at 31.4 % followed by the age group 40-50 years 28.71 % and finally the age group 51-60 years at 21.6 %. The explanation of such an increase and distribution among the age groups is that the formation of urinary stones in humans takes a long period of time for the stones to reach the complete size and begin to affect the human health. Therefore, the emergence of the disease occurs in the later stages of life. In addition, the lifestyle of males in small towns may also help in the growth of urinary stones with the rate being higher than the urban regions.

The population of the study area was split into three

geographic regions based on differences in geological, environmental, and climatic characteristics. The first zone consisted of the Amman, Irbid, and Jerash Governorates; the second zone included the Ajloun Governorate, and third zone included the (Mafraq Governorate. It was found that there is a significant correlation between the prevalence of the urolithiasis disease and the differences in some geographical, geological, environmental, and climatic features. The highest prevalence rate of the urolithiasis disease was in the first zone, followed by the third zone. The lowest prevalence rate was in the second zone (Table 1). The most important geological, environmental, and climatic differences that have affected the different proportions of the urolithiasis disease in the study area were summarized on the basis of the rock type (Fig. 6), soil type (Fig. 5), water hardness, the difference in temperatures (Fig. 2), the difference of annual rain ratio (Fig. 3), altitude (Fig. 4), the proportion of solar radiation, and the lifestyle of the population.

Based on the results of the utilization of X-ray diffraction (XRD) and the scanning electron microscope (SEM) on the samples collected for this study and on the basis of the results of the previous studies of Abboud (2008a, 2008b), 60 % of urinary stones composed of oxalates and are distributed in the following proportions: 26.7 % of pure calcium oxalate, 10 % of oxalate/cholesten, 10 % of oxalate/uric acid, 10 % of oxalate/cholesten/uric acid, and 3.3 % of oxalate/cholesten/cystine. Moreover, 13.3 % of the stones were cholesten stones, 23.4 % were cholesten/urate (uric acid) stones, and 3.3 % were cholesten/cystine stones. It was observed that the urinary stones that were extracted surgically from the male and female patients in the study area are of nine different groups.

The ratio of uric acid stones were more prevalent in males than in females. The reason for the abundance of these stones in males is the presence of a strong acid environment, which is a critical risk factor causing the crystallization of uric acid stones and turning them into precipitated crystals of various forms in the urinary liquid (Ferrari and Bonny, 2004). Struvite stones were more prevalent in females. In this context, Giannossi and Summa (2013) ascribed the presence of this type of stones to the medical history of the family. Then, the whewellite and weddellite stones prevailed semi-symmetrically or about equally in males and females. According to Giannossi and Summa (2013) cystine stone formation is caused primarily by the hyper cystinuria and is a genetic factor. Moreover, calcium oxalate stones may be produced directly from the body (Giannossi and Summa, 2013), or are diet-related (Abboud, 2008c) or hyperoxaluria-related (Brinkley et al., 1990; De Mendonca et al., 2003). The high temperature stimulates an increased urinary excretion of calcium, which causes the supersaturation of calcium oxalate and calcium phosphate increasing the probability of the risk of urinary stone formation (Marston et al., 1992). All the above –mentioned factors which help in the formation of urinary stones are linked strongly to the dietary habits and lifestyle of the people in addition to the water type and water consumption (< 2 L/d).

Another factor that affects the stone type is the age of patient. Uric acid stones were more evident in people older than fifty years of age, while calcium oxalate stones were prevalent in people aged between 30-50 years. In order to further understand the prevalence mechanisms of the urinary stone disease in the study area and link this distribution with the stone type and place, the surroundings of patients and their place of birth were considered. A concentration of urinary stones prevalence of oxalates was observed in the first zone, while uric acid stones were found to be more prevalent in the third zone.

To determine the most significant environmental risk factors that cause the formation of urinary stones in humans, it is necessary to evaluate the effect of annual average temperatures as it is of great significance. The annual average temperatures in Amman, Irbid, and Jerash range between 20-24 ºC. In the Ajloun region they range between 18-22 ºC, and in the Mafraq region they fall between 22-28 ºC.

Despite the possibility that there might be some climate variations in the region, whether seasonal or annual, the study attempted to determine the average annual temperatures in the study area, On this basis the study attempted to correlate the prevalence of urolithiasis and the temperature. The final results show that the high temperature in summer induces a rise in the dehydration levels in the human body, which helps in the formation of urinary stones. Al-Eisa et al. (2002) proved a strong correlation between the prevalence of urinary calculi in Kuwait and the high temperature. Brikowski et al. (2008) pointed out that generally speaking the increased temperature means an increase in the likelihood of the incidence of the nephrolithiasis risk. Boscolo-Berto et al. (2008) confirmed that the emergence of renal colic resulting from kidney stones has a direct relation with temperatures higher than 27 °C. Likewise, Safarinejad (2007) observed an increase in the prevalence of urinary stones in males and females through the increased average annual temperature and/or sunlight index. According to Akoudad et al. (2010) hydrological and climatic factors are instrumental in the formation and prevalence of urinary stones. Giannossi and Summa (2013) considered the range temperature T >13 ºC the critical line at which there might be the risk for humans to develop the urinary stone disease. Tasian et al. (2014) found that the incidence of nephrolithiasis rose with the increase in the average daily temperature in some USA cities (Atlanta, Georgia; Chicago, Illinois; Dallas, Texas; Los Angeles, California; and Philadelphia, Pennsylvania). Despite the slight difference in the length or short duration of temperature in the regions of the study area, the annual temperature average in all the regions of the study area will more likely to help develop urinary stones. The Mafraq area, located within an arid and semiarid climate zone, showed the longest period of high temperatures. The Ajloun area located within the wet Mediterranean climate showed the shortest period and of low temperatures

Table 5 shows the possibilities of odds ratio calculations. The increase in the chance of an infection with the disease was found to correlate with high temperature, being a male rather than a female, and with a specific age group. The annual average temperatures between 20-24 ºC, being a male and/or from the (40-60) age group make people more vulnerable to the risk of developing urinary stones (Table 5). However the link between the emergence of the disease among females

from a certain age group and temperature was found less influential.

There are many studies in the world that confirmed the existence of a close relationship between urolithiasis and the increasing temperature (Marston et al., 1992; Al-Eisa et al., 2002; Basiri et al., 2004; Boscolo-Berto et al., 2008; Akoudad et al., 2010; Giannossi and Summa, 2013; Tasian et al., 2014), or/and rotate of seasons in the year (Fujita, 1979; Chauhan et al., 2004; Boscolo-Berto et al., 2008; Chen et al., 2008; Basiri et al., 2009; Lo et al., 2010; Tiu et al., 2010; Scales et al., 2012; Fukuhara et al., 2016), or/and temperature and the seasons rotations (Brikowski et al., 2008; Freeg et al., 2012; Fukuhara et al., 2016). The results of the current study concerning the relationship between temperature and the formation of urinary calculi are consistent with the results in the above-mentioned studies.

Like temperature, altitude also has a correlation with the formation and evolution of urinary stones. To elucidate the impact of altitude on urolithiasis, the relationship has been calculated over various periods at altitudes between 550 m to 1,200 m covering all the study regions (Table 6).

The process of the formation of urinary stones in humans is not an instantaneous process, but rather a cumulative process of different materials that increase the degree of saturation in the fluid leading to precipitation into a solid state. Therefore, it is difficult to set clear boundaries between the seasons in which the urinary stones are formed in the bladder or in any other organ of the human body. There is no specific geometric distribution found in the the numbers of patients who suffer from urinary stones seen at hospitals. During summer seasons, when the rise in temperature increases the proportion of water consumption per capita, and/or when there is a lack of hydration and not drinking enough water during the summer, there is more chance for the concentration of the nuclei of atoms to form urinary stones. In the winter seasons, the body does not naturally require the same amount of water for drinking, which also stimulates the formation of urinary stones. Based on the dehydration theory in (Embon et al., 1990; Pin et al., 1992; Borghi et al., 1993; Borghi et al., 1999; Basiri et al., 2004; Boscolo-Berto et al., 2008) who all propose that the increased crystallization of the stone in the urine is relevant to the lower volume of urine and the decrease in the amount of fluids in the body as a result of sweating in hot and dry climates. Also, the too much exposure to the sunlight increases vitamin D intake, which also helps in the formation of urinary stones in the body (Parry and Lister, 1995; Lo et al., 2010). The final results of this study show that the seasons of the year are to be considered indicative or relevant to the formation of urinary stones in all regions. Also, the rise in temperature needs to be taken as an important factor in the composition of urinary stones in certain areas.

Similarly, water hardness was reported as a relevant environmental factor in the formation of urinary stones in the human body (Sierakowski et al., 1979; Kohri et al., 1993; Abboud, 2008c; Abboud, 2017). The quality and quantity of water intake by individuals play an important role also as a risk factor in the formation of urinary stones. In particular, water containing high levels of calcium and magnesium and/or water characterized by water hardness i.e. more than 300 mg/L is another rsik factor for urolithiasis. Given the fact that water hardness in the study area is mostly higher than 300 mg/L, drinking hard water helps in the development of urolithiasis. Table 7 shows the strength of odds ratio values of the correlation between the urinary stone formation and the age group (40-60 year), being male, and also water hardness (>300 mg/L).

Table 1 shows that Irbid region is the highest in the prevalence rates of the urinary stone disease, followed by the Jerash, Mafraq, Amman, and Ajloun.: 7.53 ‰, 6.1 ‰, 5.81 ‰, 5.29 ‰, and 5.25 ‰ respectively. Therefore, the odds ratio of risk factors for people living in pedological of Irbid region was calculated in this study.

Figure 5 shows the most important classifications of soils spreading in the study area. The type of soil spreading in Irbid region is vertisols. It is a clay soil rich in the montmorillonite mineral and also of high thickness formed by the weathering processes of basaltic rocks in the region. The soil spreading in the regions of Amman, Jerash, and Ajloun are of the type xerochrept consisting of unconsolidated alluvium from the limestone source (Fig. 5). Soil in the Mafraq region is of the kind aridisols usually spread in arid and dry areas, and is often poor in organic matter. It was formed originally from carbonate and silicate materials (Fig. 5). It is expected that the different types of soil affect the ions dissolved and the concentration in the groundwater. Those soil types also affect the quality of the ions that are concentrated in the tissues of plants eaten by the people in those regions. All this leads in the end to the development of urinary stones of different types in individuals. In addition, the concentration of many chemical elements in the urinary stones extracted from the patients explains the origin of these elements either as coming from the drinking water or the diet style of individuals.

Magnesium, sodium, and calcium ions are concentrated in the soil of the Irbid region because they are composed of the montmorillonite mineral. Therefore, an increase in the concentration of these ions in the groundwater wells of the region was noticed as a result of the washing and leaching processes that occur in the soil dissolving these ions and transferring them into aquifer. The regions of Amman, Jerash, and Ajloun are rich in limestone. Therefore, we notice an increase in the concentration of Ca ion in the groundwater of the wells of these regions due to its solubility during the flow of water in the soil and its passage to the reservoirs of the groundwater. The Mafraq region is rich in Ca, Mg, Na, and Si ions because it contains mainly carbonate and silicate minerals. This is inevitably reflected on the quality of the groundwater in that region. The concentration of these ions in these soil types explains their increased concentration in the groundwater of these regions. This also shows their increased concentration in the vegetation of the area as a result of the plant absorption of the water directly through the soil or indirectly from the water contained in the soil particles. As a result of the consumption of the groundwater of the wells by the population of those regions or as a result of eating plants growing in those soils, an increase in the concentration of those elements in the tissues of the body occurs increasing the chances for the formation of urine stones.

The relationship between the prevalence of urolithiasis

and altitude, soil type, and climatic features prevailing at Irbid region has been exmained in this study. Odds ratios showed a strong and absolute correlation between the prevalence of urolithiasis and the type of soil in Irbid region. The reason for this strong corrleation is the direct effect of some environmental and geological factors which play an important role in the formation of the soil and its minerals such as morphology, rock type and lithology, precipitation, drainage system, altitude, and temperature. The rock type and soil thickness profiles in the Irbid region play an essential role in the mineral type concentrated in the soil which has an impact on the quality of the chemical elements that are absorbed by crops. The population of this region depend on those crops in their diets which increases the likelihood and exposure to the urinary stone disease.

Conclusion

The epidemiological survey was carried out in this study to examine the prevalence of urolithiasis in five governorates in northern and central Jordan.The average prevalence rate found was 5.95 ‰. This study attempted to link the risk of developing urolithiasis and its prevalence to some geographic variables and several demographic, geological, and environmental factors in addition to some human habits. The highest prevalence of the urinary stone disease was found in the governorate of Irbid. Climatic conditions, relatively high temperatures, or high solar radiation, precipitation, as well as some environmental, geographical, and geological factors including water hardness being (>300 mg/L), relative altitude being higher than (500 m), rock type, and the mineral components of the soil, along with some human characteristics, such as gender and age being (>40) years, can all be very siginificant risk factors to the human health and provide sufficient explanation for the increased prevalence of the urinary stone disease among the population of the study area.

The epidemiological survey carried out in this study is considered the first of its kind in the region. It is the starting point in the expansion of knowledge about the mechanism of the disease distribution in the region among the population, their sexes and ages. It also provides sufficient details to help draw a clear picture about the impact of the disease on the community and its causes. Hopefully, the results of the current study will contribute to the design and implementation of comprehensive prevention projects to reduce the extent and prevalence of the disease as much as possible.

الملخص

أمراض الحصى البولية هي الأكثر انتشارا في جميع أنحاء العالم، وتعتبر واحدة من الأمراض الأكثر تأثيرا في الإنسان، من حيث استمرارية المرض، والتكرار، أو الأعراض. يتم التحكم في تشكيل ونمو الحصيّات البولية من قبل العديد من العوامل البيولوجية والبيئية والجغرافية. في هذه الدراسة، تم تحديد انتشار المرض، وحدوثه، وعوامل الخطر الناتجه عن التّحصّي البولي في سكان شمال الأردن. لذلك دُرس تأثير العوامل البيئية والجغرافية والبيولوجية التي قد تساهم في حدوث المرض. ولوحظ أن الانتشار المتزايد لمرض التّحصّي البولي يكون في عمر ٤٠ سنة، والذكور أكثر عرضة للإصابة بالمرض من الإناث. ولخص تأثير العوامل البيئية على تكوين الحصيّات البولية من خلال النظام الغذائي للأفراد، نمط الحياة، وكذلك تأثير عسر الماء بالذات في تكوين حصى الأوكسالات بسبب تركيز البايكربونات >٣٠٠ غم/لتر. وأخيرا، لعبت العوامل الجغرافية دوراً هاماً في تكوين وانتشار وتكوين الحصيّات البولية. كما لوحظ في هذه الدراسة ارتفاع معدل المرض وانتشاره في المناطق ذات درجة الحرارة العالية >٢٠ درجة مئوية، وزيادة التعرض لأشعة الشمس، والارتفاع >٥٠٠ م، والتربة من نوع فيرتي سويلس.

Acknowledgments

I'm grateful to the laboratory of the Water Authority in the Ministry of Water and Irrigation in Amman, Jordan, and the Institute of Earth and Environmental Sciences at Al al-Bayt University, Jordan, for helping in the analyses of the water and stone samples. I'm thankful to Mr. Sa'ed Abu Snineh for helping in the data collection,. I also thank Dr. Naim Ezghoul, and Dr. Ahmed Saleh of Taibah University for their valuable revision of the manuscript.

References

[1] Abboud, I. A. 2008a. Mineralogy and chemistry of urinary stones: patients from North Jordan, Environmental Geochemistry and Health, 30(5): 445-463. doi: 10.1007/s10653-007-9128-7.

[2] Abboud, I. A. 2008b. Concentration effect of trace metals in Jordanian patients of urinary calculi, Environmental Geochemistry and Health, 30(1): 11-20. doi: 10.1007/s10653-007-9103-3.

[3] Abboud, I. A. 2008c. Analyzing Correlation Coefficients of the Concentrations of Trace Elements in Urinary Stones, Jordan Journal of Earth and Environmental Sciences, 1(2): 73- 80.

[4] Abboud, I. A. 2014. Describe and Statistical Evaluation of Hydrochemical Data of Karst Phenomena in Jordan: Al-Dhaher Cave Karst Spring, Researcher, 6(3): 56-76. doi:10.7537/marsrsj060314.11.

[5] Abboud, I. A. 2017. Geoenvironmental factors that play an important role in the formation of human urinary calculi in Jordan, Journal of African Earth Sciences (JAES), Elsevier Ltd, in Press.

[6] Akoudad, S., Szklo, M., McAdams, M. A., Fulop, T., Anderson, C. A. M., Coresh, J., and Kottgen, A., 2010. Correlates of kidney stone disease differ by race in a multiethnic middle-aged population: the ARIC study, Prev. Med., 51: 416–420.

[7] Al-Eisa, A. A., Al-Hunayyan, A., and Gupta, R., 2002. Pediatric urolithiasis in Kuwait, Int. Urol. Nephrol., 33: 3–6.

[8] Alsheyab, F., Bani Hani, A., and Mosameh, Y., 2007. Chemical composition of urinary calculi in north Jordan, Journal of Biological Sciences, 7(7): 1290-1292.

[9] Altz-Stamm, A. 2012. See links: https://water.fanack.com/jordan/water-use/ https://water.fanack.com/wp-content/uploads/sites/2/2015/11/Jordan-Water-Use-Figure-13-Jordan%E2%80%99s-main-agricultural-regions-Fanack-after-Altz-Stamm-2012.gif

[10] Annual average rainfall (mm) between 1973 and 2012, 2012. See link: https://water.fanack.com/wp-content/uploads/sites/2/2015/11/Jordan-Geography-and-Climate-Figure-5-Annual-average-rainfall-and-precipitation-Fanack-after-MWI.gif)

[11] Basiri, A., Moghaddam, S. M., Khoddam, R., Nejad, S. T., and Hakimi, A., 2004. Monthly variations of urinary stone colic in Iran and its relationship to the fasting month of Ramadan, J. Pak. Med. Assoc., 54: 6–8.

[12] Basiri, A., Shakhssalim, N., Khoshdel, A. R., Ghahestani, S. M., and Basiri, H., 2010. The demographic profile of urolithiasis in Iran: a nationwide epidemiologic study, Int. Urol. Nephrol., 42: 119–126. doi: 10.1007/s11255-009-9588-z.

[13] Basiri, A., Shakhssalim, N., Khoshdel, A. R., and Naghavi, M., 2009. Regional and seasonal variation in the incidence of urolithiasis in Iran: a place for obsession in case finding and statistical approach, Urol. Res., 37: 197–204.

[14] Boscolo-Berto, R., Dal Moro, F., Abate, A., Arandjelovic, G., Tosato, F., and Bassi, P., 2008. Do weather conditions influence the onset of renal colic? A novel approach to analysis, Urol. Int., 80: 19–25.

[15] Borghi, L., Meschi, T., Amato, F., et al., 1993. Hot occupation and nephrolithiasis, J. Urol., 150(6): 1757–1760.

[16] Borghi, L., Ferretti, P. P., Elia, G. F., Amato, F., Melloni, E., Trapasi, M. R., and Novarini, A., 1990. Epidemiological study of urinary tract stones in a Northern Italian City, Br. J. Urol., 65: 231–235.

[17] Borghi, L., Guerra, A., Meschi, T., Briganti, A., Schianchi, T., Allegri, F., et al., 1999. Relationship between supersaturation and calcium oxalate crystallization in normals and idiopathic calcium oxalate stone formers, Kidney Int., 55: 1041–1050.

[18] Breslau, N. A., Brinkley, L., Hill, K. D., and Pak, C. Y. C., 1988. Relationship of animal protein-rich diet to kidney stone formation and calcium metabolism, J. Clin. Endocrinol. Metab., 66: 140–6.

[19] Brikowski, T. H., Lotan, Y., and Pearle, M. S., 2008. Climate-related increase in the prevalence of urolithiasis in the United States, The National Academy of Sciences of the USA, PNAS, 105(28): 9841–9846. doi:10.1073/pnas.0709652105.

[20] Brinkley, L. J., Gregory, J., and Pak, C. Y. C., 1990. A further study of oxalate bioavailability in foods, J. Urol., 144: 94–96.

[21] Chandrajith, R., Wijewardana, G., Dissanayake, C. B., and Abeygunasekara, A., 2006. Biomineralogy of human urinary calculi (kidney stones) from some geographic regions of Sri Lanka, Environmental Geochemistry and Health, 28(4): 393–399. doi: 10.1007/s10653-006-9048-y.

[22] Chauhan, V., Eskin, B., Allegra, J. R., and Cochrane, D. G., 2004. Effect of season, age, and gender on renal colic incidence, Am. J. Emerg. Med., 22: 560–563.

[23] Chen, Y. K., Lin, H. C., Chen, C. S., and Yeh, S. D., 2008. Seasonal variations in urinary calculi attacks and their association with climate: a population based study, J. Urol., 179: 564–569.

[24] Chen, Y, Roseman, J. M., Devivo, M. J., and Huang, C., 2000. Geographic variation and environmental risk factors for the incidence of initial kidney stones in patients with spinal cord injury, J. Urol., 164: 21–26.

[25] De Mendonca, O. G. C., Martini, L. A., and Baxmann, A. C., 2003. Effects of an oxalate load on urinary excretion in calcium stone formers, J. Ren. Nutr., 13: 39–46.

[26] DS, Department of Statistics, 2015. See this link: http://census.dos.gov.jo/wp-content/uploads/sites/2/2016/02/Census_results_2016.pdf

[27] Embon, O. M., Rose, G. A., and Rosenbaum, T., 1990. Chronic dehydration stone disease, Br. J. Urol., 66(4): 357–362. doi: 10.1111/j.1464-410X.1990.tb14954.x.

[28] Ferrari, P., and Bonny, O., 2004. Diagnostik und prevention des harnsauresteins, Ther. Umsch., 61: 571–574.

[29] Freeg, M. A., Sreedharan, J., Muttappallymyalil, J., Venkatramana, M., Shaafie, I. A., Mathew, E., et al., 2012. A retrospective study of the seasonal pattern of urolithiasis, Saudi J. Kidney Dis. Transpl., 23: 1232–1237.

[30] Fujita, K. 1979. Weather and the incidence of urinary stone colic, J. Urol., 121: 318–319.

[31] Fukuhara, H., Ichiyanagi, O., Kakizaki, H., Naito, S., and Tsuchiya, N., 2016. Clinical relevance of seasonal changes in the prevalence of ureterolithiasis in the diagnosis of renal colic, Urolithiasis, 44(6): 529–537. doi: 10.1007/s00240-016-0896-3.

[32] Ghazal, M. 2016. Population stands at around 9.5 million, including 2.9 million guests. See this link: http://www.jordantimes.com/news/local/population-stands-around-95-million-including-29-million-guests.

[33] Giannossi, M. L., and Summa, V., 2013. An Observation on the Composition of Urinary Calculi: Environmental Influence, in Medical Geochemistry: Geological Materials and Health, P. Censi et al. (eds.), Springer Science+Business Media Dordrecht. doi: 10.1007/978-94-007-4372-4__5.

[34] Hesse, A., Brandle, E., Wilbert, D., Kohrmann, K. U., and Alken, P., 2003. Study on the prevalence and incidence of urolithiasis in Germany comparing the years 1979 vs. 2000, Eur. Urol., 44(6): 709–713.

[35] Holmes, R. P., Goodman, H. O., and Assimis, D. G., 2001. Contribution of dietary oxalate to urinary oxalate excretion, Kidney Int., 59: 270–276.

[36] Jordan climate maps (Current climate). 2016. Map prepared by NCARE. Author: M. Saba; E. De Pauw; W. Goebel. Map source: http://www.icarda.org/jordan-climate-maps-current-climate).

[37] JOSCIS Database. 2012. Conception: B. Lucke; A. Taimeh; F. Ziadat.. (Map source: Al-Hadidi M.M, Al-Kharabsheh A.A, Ta'any R.A. Impact of Over-Pumping on the Groundwater Quality of the Dead Sea Basin/ Jordan. Curr. World Environ., 2013, 8(3). doi : http://dx.doi.org/10.12944/CWE.8.3.04).

[38] Kohri, K., Ishikawa, Y., Iguchi, M., Kurita, T., Okada, Y., and Yoshida, O., 1993. Relationship between the incidence infection stones and the magnesium–calcium ratio of tap water, Urol. Res., 21: 269–72.

[39] Komatina, M. M. 2004. Medical geology: effects of geological environments on human health. Elsevier, Amsterdam, p. 488.

[40] Lee, Y. H., Huang, W. C., Tsai, J. Y., Lu, C. M., Chen, W. C., Lee, M. H., Hsu, H. S., Huang, J. K., and Chang, L. S., 2002. Epidemiological studies on the prevalence of upper urinary calculi in Taiwan, Urol. Int., 68(3): 172–177.

[41] Lo, S. S., Johnston, R., Al Sameraaii, A., Metcalf, P. A., Rice, M. L., and Masters, J. G., 2010. Seasonal variation in the acute presentation of urinary calculi over 8 years in Auckland, New Zealand, B. J. U. Int., 106: 96–101.

[42] Marickar, Y. M. F., and Vijay, A., 2009. Female stone disease: the changing trend. SYMPOSIUM PAPER. Urol. Res., 37: 337–340. doi: 10.1007/s00240-009-0216-2.

[43] Marston, W. A., Ahlquist, R., Johnson, G. Jr., and Meyer, A. A., 1992. Misdiagnosis of ruptured abdominal aortic aneurysms, J. Vasc. Surg., 16: 17–22.

[44] Mendenhall, W. 1967. Introduction to probability and statistics, 2nd Ed., Wadsworth Publishing Company, Inc., Belmont, Chap. 10.

[45] Nielsen, J. B., and Jensen, T. K., 2005. Environmental epidemiology. In: Selinus, O., Alloway, B., Centeno, J.A., Finkelam, R.B., Fuge, R., Lindh, P., and Smedley, P. (eds) Essential of medical geology, vol. 21. Elsevier Academic Press, Amsterdam, pp 529–540.

[46] Parry, E. S., and Lister, I. S., 1975. Sunlight and hypercalciuria, Lancet, 1(7915): 1063–1065. doi:10.1016/S0140-6736(75)91830-9.

[47] Pin, N. T., Ling, N. Y., and Siang, L. H., 1992. Dehydration from outdoor work and urinary stones in a tropical environment, Occup. Med. (London), 42(1): 30–32. doi:10.1093/occmed/42.1.30.

[48] RJGC. 2006. Land cover map 1/250 000, 2006 and Conception and design: RJGC and M. Ababsa, IFPO 2010. See this link: http://books.openedition.org/ifpo/docannexe/image/4858/img-1.jpg.
and see; Myriam Ababsa (2014). Jordan's Land Cover. P.485. Chapter: A Land of Contrasts. p. 40-41. Éditeur: Presses de l'Ifpo. ISBN: 9782351593783, ISBN Multi-formats: 978-2-35159-438-4.

[49] Robertson, W. G. 2012. Stone formation in the Middle Eastern Gulf States: A review, Arab Journal of Urology, 10: 265–272. http://dx.doi.org/10.1016/j.aju.2012.04.003.

[50] Robertson, W. G., Heyburn, P. J., Peacock, M., Hanes, F. A., and Swaminathan, R., 1979. The effect of high animal protein intake on the risk of calcium stone formation in the urinary tract, Clin. Sci. (Colch), 57: 285–8.

[51] Safarinejad, M. R. 2007. Adult urolithiasis in a population-based study in Iran: prevalence, incidence, and associated risk factors, Urol. Res., 35(2): 73–82. doi: 10.1007/s00240-007-0084-6.

[52] Scales, C. D. Jr., Smith, A. C., Hanley, J. M., and Saigal, C. S., 2012. Prevalence of Kidney Stones in the United States, Elsevier B.V. on behalf of European Association of Urology. Urologic Diseases in America Project, European Urology, 62: 160–165. doi: 10.1016/j.eururo.2012.03.052.

[53] Serio, A., and Fraioli, A., 1999. Epidemiology of nephrolithiasis, Nephron 81(suppl 1): 26–30.

[54] Sierakowski, R., Finlayson, B., and Landes, R., 1979. Stone incidences as related to water hardness indifferent geological regions of the United States, Urol. Res., 7: 157–160.

[55] Tasian, G. E., Pulido, J. E., Gasparrini, A., Saigal, C. S., Horton, B. P., Landis, J. R., Madison, R., and Keren, R., 2014. For the Urologic Diseases in America Project. Daily mean temperature and clinical kidney stone presentation in five U.S. metropolitan areas: a time-series analysis, Environ. Health Perspect., 122: 1081–1087. doi.org/10.1289/ehp.1307703.

[56] Tiu, A., Tang, V., Gubicak, S., Knight, P., and Haxhimolla, H., 2010. Seasonal variation of acute urolithiasis at an Australian tertiary hospital, Australas Med. J., doi:10.4066/AMJ.2010.502.

[57] Vahlensieck, E. W., Bach, D., and Hesse, A., 1982. Incidence, prevalence and mortality of urolithiasis in the German Federal Republic, Urol. Res., 10: 161–164.

[58] Weather online. 2016. See this link: http://www.weatheronline.co.uk/weather/maps/city?FMM=1&FYY=2001&LMM=12&LYY=2001&WMO=40270&CONT=asie&REGION=0023&LAND=JD&ART=PRE&R=0&NOREGION=0&LEVEL=162&LANG=en&MOD=tab

JJEES
Jordan Journal of Earth and Environmental Sciences

Volume 9, (Number 1), April, 2018
ISSN 1995-6681
Pages 39 - 46

Characterization of Architectural Mortars from Buildings at Umm Qais (Gadara), Northwest Jordan: Provenance Input

[1]Saeb A. Al-Shereideh, [2]Ibrahim A. BanyYaseen, [1]Mahmoud H. Al-Tamimi, [1]Nazem M. El-radaideh and [3]Khaled Al-Bashaireh.

[1]Yarmouk University, Faculty of Sciences, Earth and Environmental Division, Irbid, Jordan.
[2]Institute of Earth and Environmental Science, University of Al al-Bayt, Mafraq, Jordan.
[3]Yarmouk University, Faculty of Archaeology and Anthropology, Department of Archaeology, Irbid, Jordan.

Received 13 December, 2017; Accepted 28 March , 2018

Abstract

This paper aims at characterizing architectural mortars taken from structures at Umm Qais (Gadara) in northwest Jordan. The study intends to shed light on the mortar production technology, and to determine the provenance of the raw materials used in the mortar production. The Mortar samples were collected from the Western Theater and the Roman Market built during the Roman Period. The samples were analyzed by Optical Lenses, X-Ray Diffractometer, Optical and Scanning Electron Microscopes. The collected data was compared with some published literature on the geology of the Gadara area. The results show that the mortars are lime-based mixed with different local aggregates mainly fossiliferous micritic limestone, quartz, tuff, ceramic and basalt. The hydraulicity of the mortars was obtained through the addition of natural and artificial pozzalinic materials. Most likely, the high reactivity of the lime binder originated from the soft burning of the raw limestone. The results shed light on the Roman mortar production technology and the technology of ancient mortar production at other archaeological sites in Jordan.

Keywords: Lime mortar, Hydraulicity, Provenance, Fossiliferous limestone, Mineralogy, Petrography, West Theater, Roman Market, Gadara, Jordan

1. Introduction

The Greco-Roman and the Decapolis city of Gadara (Umm Qais) is considered one of the important archaeological sites in Jordan (Daher, 1999). It is located on a plateau that overlooks the Jordan Valley, Tiberius Lake, and the Yarmouk River in the northeastern part of Jordan, about 115 km from the Amman (Fig. 1). In antiquity, it connected several trade routes between Palestine and Syria, and the seashores and lowlands with the central and eastern uplands (Weber, 1990). Gadara was inhabited by Greeks, Romans, Byzantines, and Muslims. Its poets, fortunes, theaters, hippodrome, gates, nymphaeum, shops, churches, Ottoman village, and many other archaeological structures and remains attest for the wealth and prosperity of the city during this period. Unfortunately, the city was leveled and most of these buildings were destroyed by the devastating earthquake of 747 AD (Tsafrir and Foertser, 1992). The city was mainly constructed out of basalt, limestone, and caliche rocks bound and lined with mortar and plaster cement materials (Al-Bashaireh, 2003).

Unlike other sites and despite the great significance of Gadara, its cement materials have not been studied, however, other materials were analyzed. Al-Bashaireh (2003) and Al-Bashaireh (2011) characterized and provenanced the marble used in the construction of several structures at Gadara. El-Gohary and Al-Naddaf (2009) characterized the bricks used in building the walls of the Gadara's Roman Baths. El-Khouri (2014) investigated the early Byzantine glass production excavated from the area at Gadara in 2011. Al-Bashaireh (2013) and Al-Bashaireh and Hodgins (2012) investigated the production technology of mortar and plaster samples from different structures at Petra and Udruh to radiocarbon

Figure 1. Location map

* Corresponding author. e-mail: shereideh@yahoo.com

date them. Al-Bashaireh (2014) investigated and produced a radiocarbon date of the plaster samples from House XVII-XVIII at Umm el-Jimal. Dunn and Rapp (2004) investigated the mortar and plaster of different structures at Umm el-Jimal. Al-Bashaireh (2016) characterized the lightweight mortar of the fallen dome of the West Church at Umm el-Jimal. Yaseen et al. (2013) investigated mortar samples from different structures at Gerasa.

This research is an archaeometric study of mortar samples collected from two of the Gadara structures (the West Theater and Roman Market) to describe their production technology and identify the material sources used during their production.

2. Geological Setting

Umm Qais is located in the southwestern part of Harrat Al-Jabban which belongs to Harrat Al-Shaam. It is mainly composed of basalt (El-Akhal, 2004) and flows of basic volcanic tuff (Kwatli et al., 2015). Gadara is built on the northwestern end of the Jordanian Highlands,which include the carbonate rock sequences of the Belqa Group, namely Muwaqqar Chalky Marl Formation (MCM) and Umm Rijam Chert-Limestone Formation (URC) (Bassam, 2000), Fig.2.

Muwaqqar Formation (MCM) contains massive, soft, white chalky marl rich in planktonic foraminifera. Umm Rijam Chert-Limestone Formation (URC) contains a variety of chalky, marly and kerogenous limestones in its lower part, while those of its upper part have chert beds and/or concretions (Moh'd, 2000).

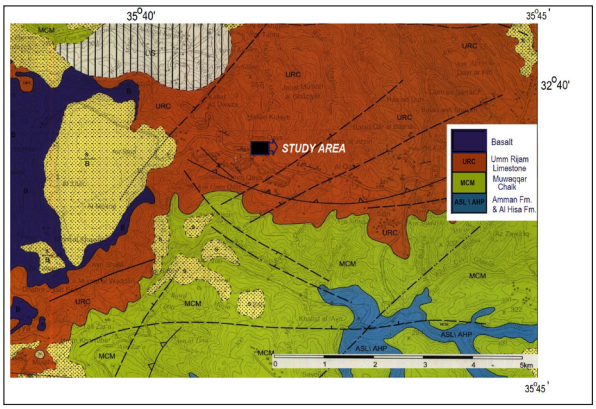

Figure 2. Geological map of the study area; after Bassam (2000).

2. Geological Setting

Umm Qais is located in the southwestern part of Harrat Al-Jabban which belongs to Harrat Al-Shaam. It is mainly composed of basalt (El-Akhal, 2004) and flows of basic volcanic tuff (Kwatli et al., 2015). Gadara is built on the northwestern end of the Jordanian Highlands,which include the carbonate rock sequences of the Belqa Group, namely Muwaqqar Chalky Marl Formation (MCM) and Umm Rijam Chert-Limestone Formation (URC) (Bassam, 2000), Fig.2.

Muwaqqar Formation (MCM) contains massive, soft, white chalky marl rich in planktonic foraminifera. Umm Rijam Chert-Limestone Formation (URC) contains a variety of chalky, marly and kerogenous limestones in its lower part, while those of its upper part have chert beds and/or concretions (Moh'd, 2000).

3. Sampled Structures

The mortar samples were collected from two structures of Gadara, namely, the West Theater, and the Roman Market (Fig. 3). Both structures face the west and are located on the east bank of Cardo Street facing the North-South. The two structures date back to the Roman period (they were most likely constructed during the 2nd century AD), but they were reused during later periods (Zayadine, 1973, Weber, 1990, Al-Dahash, 1993). They are mainly constructed of basalt blocks bonded with mortar.

The basalt seats of the West Theater are distributed into lower, middle, and upper sections. The upper part is supported by a vault in the form of an entrance facing east (Figure 3a). The Roman Market consists of twenty rows of shops adjacent to the north of the West Theater below the western extension of the basilica terrace (Guinée et al., 1996).

4. Materials and Methods

and from light to dark gray. They are moderately hard, compacted, and brittle. Small chips were taken by a sharp chisel and a hammer from the cement mortars filling the boundaries between stone courses. The samples were in their original position and did not show signs of reuse or refilling; therefore, their expected construction dates back to the Roman Period, (2nd Century AD). Small parts of the chips were ground into powder for the XRD analysis, and the rest were used for thin section preparation and analysis by the Scanning Electron Microscopy. The thin sections were prepared by a vacuum impregnation process using an epoxy resin to harden the mortar. The samples were then carefully

polished until the resulting thin section was about 0.03 µm in thickness following standard procedures (see Al-bashaireh, 2013:10).

The XRD analyses were performed to determine the mineralogical composition (mineral crystalline phases) of the samples. The polarized light microscope was used to identify the types of the aggregates added to the binding material (binder), their distribution within the binder, and the ratio between the binder and aggregates. The polarized light microscope can also show the interaction of pozzalanic materials with the lime binder (Elsen, 2006).

The thin sections were prepared and examined using the Leitz 7062 Polarizing Microscope at the laboratories of the Faculty of Archaeology and Anthropology at Yarmouk University in Jordan. A Shimadzu Lab X, 6000 X- Ray Diffractometer was used for the XRD analysis. Powder diffraction patterns were obtained under the following conditions: CuKα radiation (λ = 1.5418 Å) with 30 kV, 30 mA energy and Graphite Monochromatic.

Scanning Electron Microscopy (SEM) analysis was used for further investigations of the components of the mortars, their morphology and textural interrelationships which cannot be observed by the optical microscope. The EDX spectra provide an elemental analysis of the mortar components. Initially, the samples were coated with a thin film of gold and then analyzed by an FEI Quanta 200 scanning electron microscope equipped with EDS (Energy Dispersive X-ray Microanalyzer) at the SEM laboratory in the Department of Earth and Environmental Sciences of the Faculty of Science at Yarmouk University. The analyses were performed under the following conditions: they were run at an accelerating voltage between 0.3 and 30 kV with the chamber's pressure being at about 50 Pa in a variable-pressure mode.

The data collected to determine the mineralogical composition of the binders and aggregates of the mortars and their content of fossils were compared to the available geology of the study area, including charts, maps and related literature; see for example Bender (1974), Abded (2000), (Bassam (2000), El-Akhal (2004), and Moh'd (2000), to identify the provenance of the original raw materials used in the production of the mortars.

5. Results and Discussion

5.1. X-Ray diffraction analysis

The XRD analyses of the samples show the presence of calcite as a major mineral, quartz as a minor mineral, and the absence of gypsum (Fig. 4a,b) in the composition of the mortars. Analyses show the presence of quartz in different quantities in all of the samples examined, and the presence of pyroxene (augite) and anorthite in sample 10 (Fig. 4c). The absence of gypsum and the high content of carbonates in the samples that came from the binder and/or the aggregates indicate that the studied samples are lime-based mortars.

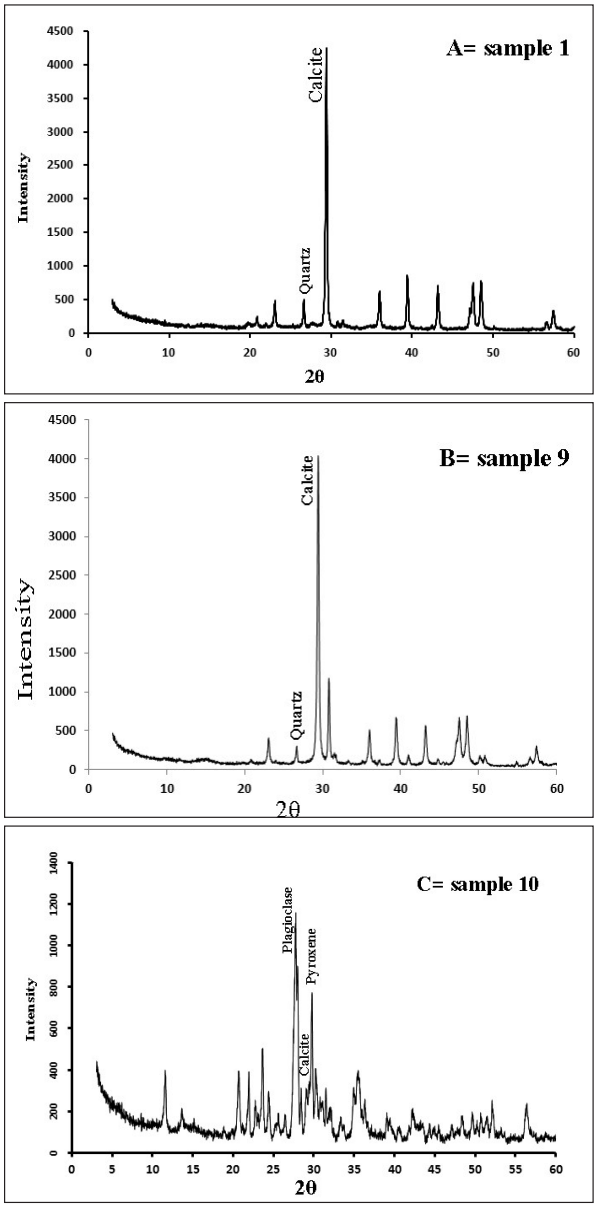

Figure 4. XRD patterns showing the mineralogical composition of samples 1 (A), 9 (B) and 10 (C).

5.2. Petrographic analyses

Ancient mortar is a composite material made of a binder and aggregates (fillers). Lime and gypsum were common binders and a variety of aggregates were also used. The colors of the binder samples vary from grey in samples 7, 8, 9, 10, and 11 to light brown in samples 2,4, and 6 and brown in samples 1,3, and 5. Petrographic analyses showed a strong cohesion between the binder and aggregates except for in sample 7 which showed a weak cohesion and some cracks (Fig. 5a). They showed that the studied mortars contain different types of aggregates, including micritic chalky and fossiliferous limestones, porphyritic basalt, reused mortars, ceramics, clays, quartz grains, and an organic matter of wood and charcoal.

 - Volume 9, (Number 1), (ISSN 1995-6681)

The limestone fragments are micritic, chalky, fine, sometimes very coarse, and rich in planktonic foraminifera (Fig. 5b). The quartz grains are small in size and round to angular in shape (Fig. 5c). While the basalt fragments are porphyritic ranging from medium to large in size (Fig. 5d), the ceramics are small in size, sub-rounded and rich in fine quartz grains (Fig. 5e). The old, reused, mortar fragments are large and contain fossiliferous micritic limestone fragments, basalt particles, and fine quartz grains (Fig. 5f). The small clay particles were likely an accidental addition during the preparation and mixing of raw materials. The ratio of binder and aggregates ranges between 1.2 and 2.1, where their percentages ranging from 50-60: 30-35% to 65-70:25-30%. The sample contents of binders and aggregates are presented in percentages in Table 1. Eventhough limestone is a common aggregate, its abundance differs in the tested samples. Other present aggregates differed in type and abundance. They can be classified into three groups. The first group includes samples (1, 2, 5, and 7), the second group includes samples (4, 6, and 9), and the third group includes samples (6, 8, and 10).

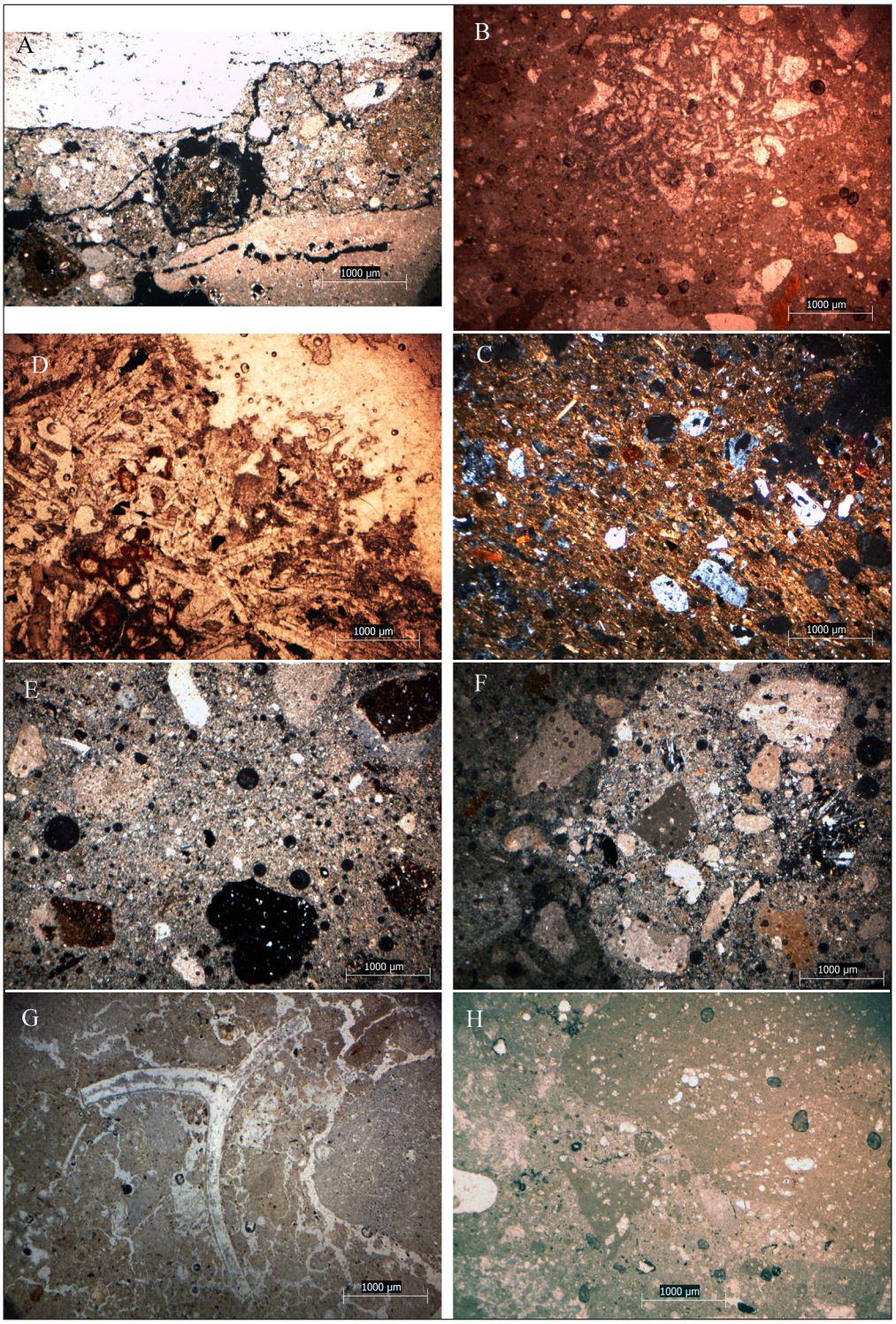

Figure 4. Microphotograph of Gadara mortars showing micritic lime binder and different kinds of aggregates. A. the weak cohesion, cracks and tuff (middle) of sample 7, B. fossiliferous limestone aggregate, C. quartz grains, D. porphyritic basalt fragment, E. ceramic grains, F. reused mortar, G. recrystallized calcite and shells, H. underburned angular fossiliferous micritic limestone.

The three groups differ mainly in the type and the amount of the available aggregate. The first group is comprised mainly of limestone rich in fossils, large shell fragments, and some tuffs. Small fragments are angular while large ones are sub-rounded. The second group is mainly comprised of limestone fragments rich in fossils, and has reused mortar rich in limestone, basalt, and quartz. These aggregates are angular and vary in size from fine to very coarse. The third group has limestone rich in fossils and high quantities of ceramic, porphyritic basalt, and quartz particles of angular to sub- angular shapes.

Table 1. The colors of the binders and percentages of the samples components (S =sample, b/a binder/aggregate, Lst.= limestone, Q= quartz, Cer.= ceramic, Or. M. = organic materials).

S.	b/a ratio	Binder		Aggregates%							
		Color	%	Lst.	Q.	R.M.	Bas.	Tuff	Cer.	Or. M.	Clay
1	1.2	Brown	50-60	30	3	-	-	2	5	3	2
2	1.2	Light brown	50-60	28	3	-	2		5	3	-
3	1.9	Brown	65-70	12	14	-	3	-	3	2	-
4	1.6	Light brown	60-65	35	1	-	-	-	-	2	-
5	1.4	Brown	50-60	30	1	-	-		7	4	-
6	1.5	Light brown	60-65	35	1	-	-	-	-	2	2
7	1.4	Grey	50-60	30	1	-	-		7	4	-
8	2.1	Grey	65-70	10	13	-	4	-	2	3	-
9	1.6	Grey	60-65	35	1	-	-	-	-	2	-
10	1.9	Grey	65-70	10	15	-	3	-	2	2	2

Petrographic analyses confirmed the XRD results that calcite, quartz, and pyroxene are major minerals present in the samples resulting from the addition of limestone, silica, and basalt aggregates.

It is worth mentioning that both the natural (tuff) and the artificial (ceramics) pozzolanic materials gave the mortars their hydraulicity, durability, adhesion to the stones and resistance to the environmental conditions. The hydraulicity of the samples is confirmed by the reaction rim between the pozzalanic materials and the lime (Fig. 5a and 5e) (Pavia and Caro, 2008, Izzo et al., 2016). The presence of some charcoals and other few fine wooden fragments could be contaminants from kiln fuels and are therefore accidental. Their reaction with the lime-binder might have given the mortars the hydraulic properties, reinforcement, and reduced fracturing (Leslie et al., 2002, Pavia and Caro, 2008). The results indicate that the stone builders at Gadara used hydraulic materials not only in buildings exposed to humidity, but also to improve the performance of mortars that were exposed to aerial conditions (Baronio et al., 1997, Fichera et al., 2015).

The sample contents containing the rounded nodules of quicklime (CaO) (Fig. 5g), might be an indication of poor mixing or dry slaking (with the minimal amount of water) (Bakolas et al., 1995). Some samples showed secondary calcite partially filling the pores and the cracks which is a result of the shrinkage effects (Fig. 5g). Abundant areas of recrystallization of binders in the small pores and larger cracks were observed in several of these samples.

Angular limestone fragments within the lime-binder (Fig. 5h) indicate low firing temperatures of below 850°C, which is the temperature needed to break up limestone. In accordance with Pavia and Caro (2008), Goffer (1980), and Boynton (1980), analytical results showed that the low firing temperature of the raw materials in the Gadara samples resulted in a lime binder with a large specific surface, low shrinkage, and high chemical reactivity.

5.3. Scanning Electron Microscopic Analysis (SEM)

The SEM analyses of the samples' microstructures are shown in Fig. 5. The analyses showed that all mortars have compact microstructures of aggregates embedded in the fine lime binder of calcite particles (Fig. 5a), organic inclusions, wood (Fig. 5B), and quartz grains (Fig. 5C). The SEM images reveal micro pores and cracks, particularly at the binder-aggregate interface (Fig. 5D). The pores presented in sample 9 are filled with new calcite crystals formed possibly by the recrystallization processes of the binder (Fig. 5F). The bond between the lime binders and the aggregate grains is mostly strong, especially those with the hydraulic properties, and shows good cohesion through the SEM observations. It is probable that the acicular (needle-like shape) crystals seen in figures 5E and 5F are formed of calcium silicate hydrates (C-S-H) and are obtained through the reaction between the pozzolanic materials rich in reactive silica and the lime binder.

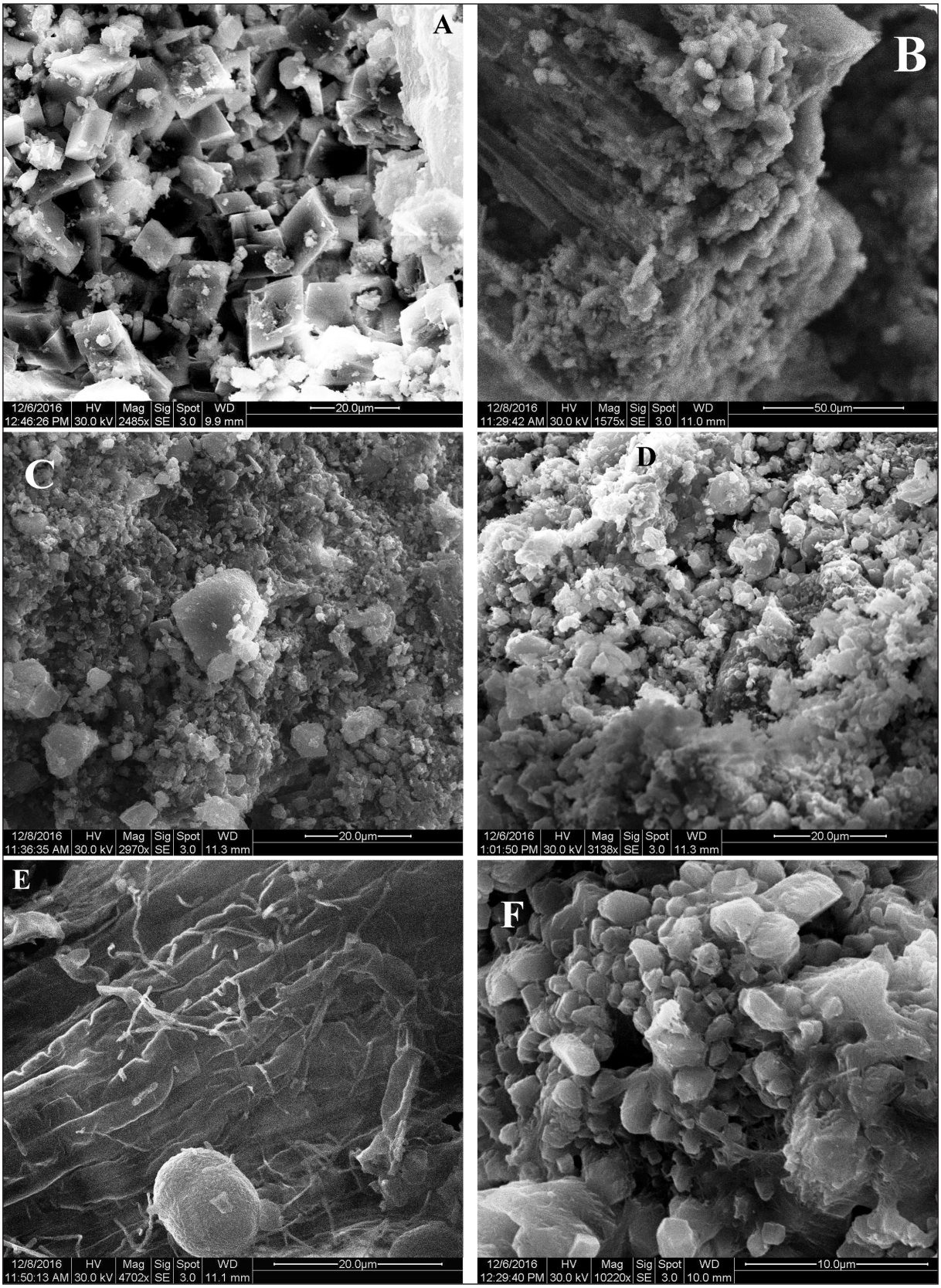

Figure 5. General microstructures of Gadara mortars. Aggregates represented are A) calcite particles, B) wood, C) quartz are embedded in lime binders, D) pores and cracks, needle-like shapes of hydraulic crystals (E and F).

6. Raw Materials Sources

Correlating the fossils and mineralogical composition of the underburned limestone fragments present in the lime-binder and the added aggregates to those of possible raw materials can determine their source within the surrounding area; see similar works of Elsen, (2006) and Ontiveros-Ortega et al. (2016). The planktonic foraminifera observed in the underburned limestone and the limestone aggregates were most likely sourced from the limestone layers of the Muwaqqar formation rich in foraminifera outcropping in the vicinity of Gadara. The most likely source of the quartz present are the sands from the valleys surrounding Gadara. The Mediterranean sands can still be their possible source because of their proximity to Gadara. Similarly, basalt and tuff that crop out in the area and its surroundings are the most likely source for the porphyritic basalt and tuff particles added to the mortars. The angularity of some limestone and quartz fragments might indicate a deliberate crushing of the source rocks. The basalt presence could be either a deliberate addition by the stone builders or was just an accidental addition resulting from the crushing processes of the rocks using basalt millstones. Some basalt fragments are inadvertently present in some of the studied mortars through the addition of reused mortar. These results indicate that local raw material sources were utilized in the production of the cementing materials used for the construction of the Gadara structures.

Conclusion

This multidisciplinary study of some archaeological mortars from Gadara provides information about their production techniques and the sources of raw materials used to produce them.

The micritic binder is lime mixed with aggregates of fossiliferous limestone fragments, quartz grains, basalt, clay, tuffs, ceramics, and organic materials. Because of the variation in the sample contents of their components, they are divided into three categories. The Hydraulicity of the lime binder was obtained by the addition of the pozzalinic materials to the mixture such as basalt, tuffs, and ceramics. Hydraulicity was observed through the reaction rims between the pozzolanic fragments and the lime binder. The samples showed good cohesion between the binder and aggregates.

The presence of lime lumps indicated that the lime was slaked with the minimum amount of water or poor mixing. Low firing temperatures (soft burning) were proven and verified by the presence of limestone fragments in the binder, the high chemical reactivity of the binder, and lack of cracks normally formed because of the shrinkage. The Raw materials used in the production of mortars were most likely local from the outcropping limestones, tuffs, basalts rock surrounding the archaeological site. The analytical results concerning the Gadara mortars are similar to the results of the examination of Gerasa mortars found by Yaseen et al. (2013) who observed that the cementing mortars were formed by a soft burning of the limestone which produced the high reactivity of the lime and the low shrinkage.

Acknowledgments

The authors would like to express their sincere thanks to the Department of Antiquities of Jordan for granting permission to collect and study the needed samples. The authors would like to extend their thanks to the Dean of the Scientific Research and Graduate Studies at Yarmouk University for the opportunity and support provided through the use of XRD, SEM, and XRF to carry out the analyses.

References

[1] Abed, A.M. 2000. The Geology of Jordan and Its Environment and Water. The Jordanian Geologists Association, Amman (In Arabic).

[2] Al-Bashaireh, K. 2003. Determination of Provenance of Marble and Caliche Used in Ancient Gadara (Umm-Qais), N. Jordan, Unpublished M. Sc. thesis, Yarmouk University.

[3] Al-Bashaireh, K. 2011. Provenance of Marbles from the Octagonal Building at Gadara Umm-Qais, northern Jordan, Journal of Cultural Heritage, 12:317–322.

[4] Al-Bashaireh, K. 2013. Plaster and Mortar Radiocarbon Dating of Nabatean and Islamic Structures, South Jordan, Archaeometry, 55(2): 329-354.

[5] Al-Bashaireh, K. 2016. Use of Lightweight Lime-Mortar in the Construction of the West
Church of Umm el-Jimal, Jordan: Radiocarbon Dating and Characterization, Radiocarbon, 58(3): 583–598.

[6] Al-Bashaireh, K. 2014. Reconstructing the Chronology of the House XVII–XVIII Complex at Umm el-Jimal, East Jordan: Radiocarbon Dates of Organic Inclusions of Architectural Mortars, Radiocarbon, 56(1): 245–56.

[7] Al-Bashaireh, K, Hodgins G.W.L., 2012. Lime Mortar and Plaster: A Radiocarbon Dating Tool for Dating Nabataean Structures in Petra, Jordan, Radiocarbon, 54(3–4): 905–14.

[8] Bassam, K., 2000. Geological Map of Ash-Shuna Ash Shamaliyya. Natural Resources Authority (NRA), Geology Directorate, Amman, Jordan.

[9] Baronio, G., Binda, L., and Lombardini, N., 1997. The Role of Brick Pebbles and Dust in Conglomerates Based on Hydrated Lime and Crushed Bricks, Construction and Building Materials, 11(1): 33-40.

[10] Bakolas, A., Biscontin, G., Moropoulou, A., and Zendri, E., 1995. Characterization of the Lumps in the Mortars of Historic Masonry, Thermochimica Acta, 269: 809-816.

[11] Bender, F. 1974. Geology of Jordan. Gebruder Borntrager, Berlin.

[12] Boynton, R. S. 1980. Chemistry and Technology of Lime and Limestone. John wiley, New York.

[13] Dahash, M. 1993. The Building Techniques of the Roman Theaters in Amman and Umm Qais, Comparative Study. Unpublished M. Sc. thesis, Yarmouk University.

[14] Daher, R. F., 1999. Gentrification and the politics of power, capital and culture in an emerging Jordanian heritage industry. Traditional Dwellings and Settlements Review, 33-45.

[15] Dunn, E., and Rapp G.R., 2004. Characterization of Mortars and Pozzolanic Materials from Umm al-Jimal, Studies in Conservation, 49(3): 145–60.

[16] El-Akhal, H. 2004. Contribution to the Petrography, Geochemistry, and Tectonic Setting of the Basalt Flows of the Umm-Qais Plateau, North Jordan, Geological Bulletin of Turkey, 47: 1-12.

[17] El-Gohary, M. A., and Al-Naddaf, M. M., 2009. Characterization of Bricks Used in the External Casing of Roman Bath Walls «Gadara-Jordan», Mediterranean Archaeology and Archaeometry, 9(2): 29-46.

[18] El-Khouri, L. 2014. Glass Production in the Early Byzantine Period (4th–7th Century) at Gadara (Umm Qais), Jordan, Area W, 2011 Season of Excavation, Levant, 46(1): 89-97.

[19] Elsen, J. 2006. Microscopy of Historic Mortars—A Review, Cement and Concrete Research, 36(8): 1416-1424.

[20] Al Kwatli, M.A., Gillot, P.Y., Lefèvre, J.C. and Hildenbrand, A., 2015. Morpho-Structural Analysis of Harrat Al Sham Volcanic Field Arabian Plate (Syria, Jordan, and Saudi Arabia): Methodology and Application, Arabian Journal of Geosciences, 8(9): 6867-6880.

[21] Fichera, G. V., Belfiore, C. M., La Russa, M. F., Ruffolo, S. A., Barca, D., Frontoni, R., Galli G., and Pezzino, A., 2015. Limestone Provenance in Roman Lime-Volcanic Ash Mortars from the Villa dei Quintili, Rome, Geoarchaeology, 30(2): 79-99.

[22] Goffer, Z. 1980. Archaeological Chemistry: A Sourcebook on the Applications of Chemistry to Archaeology. Wiley-Interscience, New York.

[23] Guinée, R.L., Mulder, N. F. and Vriezen, K. J., 1996. The Façade of The Vaulted Rooms along the So-called Cardo in Umm Qeis Ancient Gadara, Area III: Archaeological Design and Reconstruction, ADAJ, 40: 207-215.

[24] Izzo, F., Arizzi, A., Cappelletti, P., Cultrone, G., De Bonis, A., Germinario, C., Graziano, S. F., Grifa, C., Vicenza, G., Mercurio, M., Morra, V., and Langell, A., 2016. The Art of Building in the Roman Period (89 BC–79 AD): Mortars, Plasters and Mosaic Floors from Ancient Stabiae (Naples, Italy), Construction and Building materials, 117: 129-143.

[25] Leslie, A. B., and Hughes, J. J., 2002. Binder Microstructure in Lime Mortars: Implications for the Interpretation of Analysis Results, Quarterly Journal of Engineering Geology and Hydrogeology, 35(3): 257-263.

[26] Moh'd B. 2000. The geology of Irbid and Ash Shuna Ash Shamaliyyah (Waqqas) Map Sheet no. 3154-II and 3154-III, Bulletin 46. Geology directorate, NRA, Amman.

[27] Ontiveros-Ortega, E., Rodríguez-Gutiérrez, O., and D. Navarro, A., 2016. Mineralogical and Physical–Chemical Characterisation of Roman Mortars Used for Monumental Substructures on the Hill of San Antonio, in the Roman City of Italica (Prov. Baetica, Santiponce, Seville, Spain), Journal of Archaeological Science: Reports, 7: 205-223.

[28] Tsafrir, Y., and Forester, G., 1992. The Dating of the «Earthquake of the Sabbatical Year» of 749 C.E. in Palestine, Bulletin of the School of Oriental and African Studies, 55: 231-35.

[29] Pavia, S., and Caro, S., 2008. An investigation of Roman Mortar Technology through the Petrographic Analysis of Archaeological Material, Construction Building Materials, 22:807–1811.

[30] Weber, Th., 1990. Umm Qais, Gadara of Decapolis. Al-Kutba publisher, Amman.

[31] Yaseen, I.A.B., Al-Amoush, H., Al-Farajat, M., and Mayyas, A., 2013. Petrography and Mineralogy of Roman Mortars from Buildings of the Ancient City of Jerash, Jordan, Construction and Building Materials, 38: 465-471.

[32] Zayadine, F., 1983. Un Fascinum Pr'es de l'Odeon d'Amman-Philadelphia, ZDPV, 99: 184-188.

JJEES
Jordan Journal of Earth and Environmental Sciences

Volume 9, (Number 1), April, 2018
ISSN 1995-6681
Pages 47 - 56

A Regional Scale Photovoltaic Site Selection Based On Geospatial Techniques

Khaled Hazaymeh[1]*, Mohammad Zeitoun[1], Abdulla Al-Rawabdeh[2], and Noah Al-Sababhah[1]

1Department of Geography, Faculty of Arts, Yarmouk University, Irbid, 21163, Jordan.
2Department of Earth and Environmental Science, Faculty of Sciences, Yarmouk University, Irbid, 21163, Jordan.

Received 16 December, 2017; Accepted 21 March , 2018

Abstract

The current study is aimed at defining the suitable areas for establishing photovoltaic (PV) farms in Jordan utilizing geospatial techniques, remote sensing and GIS data. The methodology includes a GIS-based multi-criteria evaluation which converts and integrates geospatial data in the form of map criteria and decision-makers' preferences to define the most suitable sites for the photovoltaic site selection. The study consists of four major components: (1) identifying the potential regions for the PV farms, (2) determining the score values and relative weights of nine spatial criteria, (3) synthesizing the nine criteria according to the fuzzy-AHP method, and (4) evaluating the suitability of the potential sites for PV farms. The results show that the major contributing factors in defining the suitable PV sites are the solar radiation, aspect, and distance from a major electricity network (with relative weights of 30%, 22% and 15%, respectively). The percentage of potential regions in Jordan for PV sites was found to be 58.4%; however, the percentage of suitable regions represented 68.4% of the potential areas which were divided into four groups: "suitable" (8.3%), "slightly more suitable" (14.6%), "moderately suitable" (18.1%), and "highly suitable" (27.4%). The statistical results at the administrative-unit level (governorate) show that 11.2% of the "highly suitable" areas are located in the Ma'an governorate in the southern part of the country. Thus, utilizing the "highly suitable" areas for PV farms can generate much more electricity than the current demand in Jordan.

Keywords: Remote sensing, GIS, topography, renewable energy, solar radiation, environment

1. Introduction

Responding to the global calls to reduce fossil fuel emissions, the world is witnessing remarkable steps being taken towards improving the production of renewable energy, storage, usage, and planning strategies. The necessity for these efforts is enforced by two major revelations: (1) climate change occurring as a result of fossil fuel burning, and (2) increased energy-safety feelings and policies [1]. In general, renewable energy is defined as the energy generated from natural and sustainable resources, which include solar radiation, wind, waves and tides, rivers and reservoirs, and geothermal heat [2]. Among these resources, solar energy is receiving increased attention worldwide due to the enormous amount of the solar radiation the Earth receives, and the remarkable advances in photovoltaic (PV) panels and concentrated solar power (CSP) technologies [3]. However, the contribution of solar energy as a source of power generation is still minimal compared to other conventional resources. The World Energy Council (WEC) estimated the total amount of power generated by PV panels as being 227 gigawatts, which was only 1% of world power production by the end of 2016 [4]. According to the WEC, major solar installations exist in regions with relatively fewer solar resources (e.g., Europe and China), whereas the potentially high solar resource regions (e.g., Africa and Middle East) remain undeveloped. China leads in new solar exploration followed by Japan, Germany, the United States, and Italy [4].

Furthermore, the incorporation of geospatial technologies, including remote sensing and geographical information systems (GIS), in solar energy capacities has significantly increased. These technologies are providing continuous, large spatial coverage, cost-effective data, and useful analysis tools for the assessment of solar energy potentials, and the selection of suitable sites for solar energy farms. Of these two issues, the selection of suitable sites is more challenging for the following reasons: (1) the amount of required spatial and non-spatial datasets, (2) the need for suitable integration models for data having different formats, (3) the potential costs, (4) environmental impacts, (5) public and community acceptance, and (6) the need to consider the future demand, which may be unpredictable in some cases [3,5–7]. However, under the framework of decision support systems (DSS), GIS-based multi criteria evaluation (GIS-MCE) has emerged in the spatial selection, planning, and management of suitable locations [8]. The GIS-MCE process converts and integrates geospatial data (i.e., in the form of map criteria) and decision-makers' preferences to define the most suitable sites [9–11]. To date, several GIS-MCE methods have been developed and used in renewable energy studies, such as the weighted sum method (WSM), the analytical hierarchy process (AHP), the technique for order preference by similarity to ideal solutions

* Corresponding author. e-mail: khazaymeh@yu.edu.jo

(TOPSIS), fuzzy overlay analysis (FOA), and fuzzy AHP (FAHP). Wang et al.[10], Pohekar and Ramachandran [9], and Ishizaka [12] conducted critical reviews and comparisons of MCE methods concluding that the methods which combine the AHP and fuzzy logic methods produced the most comprehensive evaluation tool for subjective and consistent results in sustainable energy decision-making. In solar energy projects, this approach requires mathematical simulations and optimizations of several criteria (e.g., climate variables, topographic variables, and human variables) [13]. In the present study presented, the potential regions for PV sites in Jordan were identified, and the suitable regions for PV farms were allocated utilizing a FAHP approach.

2. Description of the Study Area and the Status of Solar Energy Sector

In this study, the whole land area of Jordan (~ 88788km^2) was selected as the study area. Jordan is a developing country located in a semi-arid hot zone in the Middle East (between 29^o and 32^{o}north and 35^o and 39^{o}east) (see Figure 1). Jordan's population amounts to 9.5 million and experienced a relatively high growth rate of 4.2% at the end of 2015 [14]. Its Mediterranean climate provides hot dry summers and wet cold winters, and the average annual temperature varies with the topography, and is typically predicted as 16-18C^o in mountainous areas, 24C^o in the Jordan valley, and 18C^o in Badia. There are growing concerns about Jordan's energy demands, including rising energy prices, the security of energy supplies, the effects of industrial and population growth, environmental sustainability, and the national security. These reasons prompted both the governmental and private sectors to consider the renewable energy technologies as the main workable alternatives, above all, the PV industry.

Being a semi-arid (hot) country, Jordan is a potential source of abundant solar energy. With an average of 300 sunny days annually, and an average daily sunshine of approximately 8.7 hours, its average direct normal irradiation (DNI) is approximately 6.3 KWh/m^2/day (i.e., ~ 2,400 KWh/m^2/year)[15,16]. As for the electricity sector, the volume of electricity generated by different sources reached 18,911 GWh in 2015, which reflected a 1% growth compared to the previous year. Electricity consumption has increased in all sectors, and reached 5% in 2015 compared to 2014 [15]. Therefore, many action plans have been advanced to meet this demand, including inviting global companies to explore potential oil and gas sources, the direct burning of oil shale to generate electricity, and investing in the renewable energy.

Jordan's achievements in renewable energy in 2015 included three finished PV projects (one project in the Mafraq governorate with a capacity of 10 MW, and two projects in the Azraq area with a capacity of 2 MW and 3 MW, and 12 projects with a capacity of 200 MW in the Ma'an governorate). Another four projects are planned for the coming five years with an expected total capacity of 200 MW (50 MW each) in the northern, central, and eastern areas of Jordan and one project with a capacity of 103 MW in the Qweirah/Aqaba area [15].

In addition, under the instructions of the Energy and Minerals Regulatory Commission, the Jordan government has begun to allow domestic entities (e.g., households, universities, commercial and industrial enterprises, hospitals, farms, etc.) to secure their electricity needs using renewable energy and sell the excess (if any) to the electricity grid by installing small-scale renewable energy systems. By the end of 2015, 35 MW additional capacities were provided in a grid-connected PV system from such small-scale projects [15]. The Jordanian strategic plan of energy has set the ambitious goal of generating 8% of its total electricity capacity using the solar energy technology by the year 2023 [15].

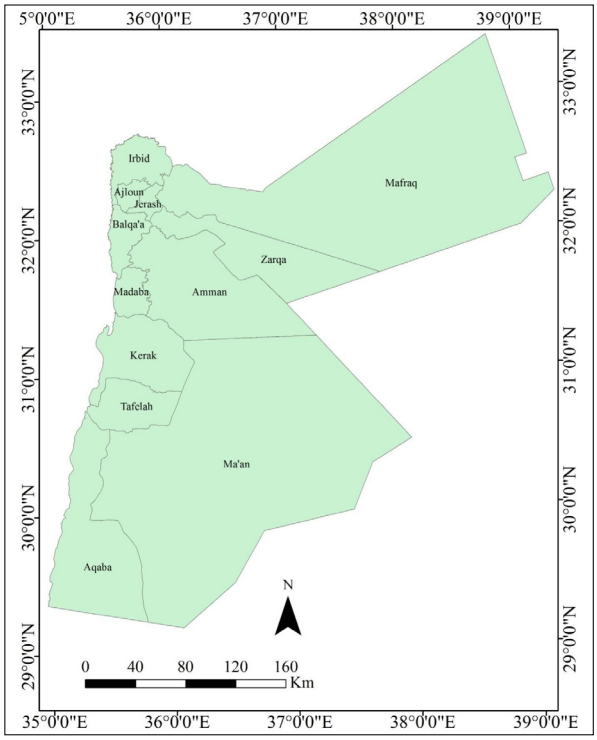

Figure 1. Study area representing the whole geographic extant of Jordan.

3. Materials and Methods

3.1. Defining the Criteria for Potential Suitable Sites for PV Farms

There are no clear-cut rules for PV site selection. However, the process of site selection must take in consideration several constraints that may impact the cost of the electricity generated from that site [17]. To identify and evaluate the potential suitable sites for PV farms in Jordan, nine criteria were determined and grouped into three categories according to their relevance: solar radiation, topographic criteria, and human-related criteria. The criteria were defined by considering the economic, technical, social, environmental, and other constraints [17] based on the past literature and experts' opinions (the Delphi method [18]). The criteria are summarized in Table 1.

Table 1. Description of criteria used in this study for identifying suitable PV sites.

Criterion	Data source	Rule and reasoning
Solar radiation	Remote sensing-derived (i.e., Metosat data, 2.5 km resolution)	- Major criterion represents the source of energy for PV panels. In general, the higher the solar irradiance the better the location for establishing PV farms.
Elevation	Remote sensing-derived (i.e., ASTER-GDEM data, 30m resolution)	- Elevation affects atmospheric depth. Generally, higher elevation regions are having thinner atmosphere. Therefore, less interaction between incident radiation and atmospheric components happen. Thus, these regions receive greater solar radiation. The higher the elevation the better the location for PV farms.
Slope	==	Flat or slightly gradient slope makes installation simpler and reduces the cost of technical modifications of ground adjustment [17].
Aspect	==	Generally, south-facing slope in the northern hemisphere is more appropriate. Such aspect ensures more irradiance and reduces the cost of technical modifications to adjust the ground [17].
Streams	==	Closer site to stream network might be more vulnerable to electrical equipment damage due to potential for flooding. Also, it might increase the risk of erosion of the soil structure and PV foundations [17].
Land use/cover	Remote sensing-derived (i.e., Landsat-8 data, 30m resolution)	In general, open and vacant areas are highly preferable for sites selection due to economic reasons. Forests, archeological, and protected areas are considered as restricted areas for potential PV sites.
Residential areas	Delineated from dense road network map, and Landsat-8 images	The major utilization of electricity demand in Jordan is for residential purposes. Therefore, residential areas were considered apart from other land use types. On the other side, the potential growth should be taken in consideration.
Electricity transmission lines	Ministry of Power	PV-generated electricity is distributed through local electricity transmission network. Thus, this network should be considered in PV site selection. Generally, PV sites should be close to the electricity transmission lines to increase the economic and efficiency potential.
Main road network	Royal Jordanian Geographic Center	PV sites should be served by good road networks for instruments supply and accessibility. The closer the sites are to a road network, the higher the cost reduction and availability of technical support for PV farms.

3.2. Data Preparation

3.2.1. Preparing a Solar Radiation Map

Solar radiation in this study was calculated as the global horizontal irradiance (GHI) (Figure 2a), which was obtained from the Solar Atlas for the Mediterranean (http://www.solar-med-atlas.org/solarmed-atlas/about.htm) in raster format. The data were provided by Solar Energy Mining (SOLEMI) and the Heliosat method [19], which is mainly based on Meteosat images (i.e., spatial resolution of 2.5 km and half-hourly temporal resolution). The Heliosat method was conducted in two steps:(1) the cloud index was derived from the Meteosat images, and (2) the derived cloud index was correlated to the clear-sky index, which relates the actual ground irradiance to the irradiance of the cloud-free case. These data have been validated in several studies [20–22]. The GHI map was re-projected to the Jordan Transfers Mercator (JTM) coordinate system, and then was subset to the Jordanian boundary. The GHI pixel values are in KWh/m^2/year ranging between 1,648 and 2,950. It is important to note that solar radiation is the most important criterion in PV projects being the source of energy [23]. In general, the higher the solar radiation, the better the location is for establishing PV farms [17].

3.2.2. Preparing the Maps of Topographic Criteria

The topographic maps contained the elevation, slope, and aspect (Figures 2b–2c) and streams network (Figure 2f). All the topographic maps were derived from ASTER-GDEM data[24]. Two DEM files were obtained from NASA and mosaicked and masked within the Jordanian boundaries. After that, the mosaicked file was re-projected to the JTM coordinate system. Several pre-processing steps were taken prior to generating the topographic maps, including a quality check and filling in the missing values in the DEM, to remove the small imperfections of the data. The elevation, slope, and aspect maps were, then, derived using the appropriate spatial analysis tools. The stream network map was derived in accordance with the protocols of the ArcHydro tools [25]. Steps to delineate the stream order network were followed in the required sequential order, and they included calculating the functions of flow direction, flow accumulation, stream definition, and stream order identification. Finally, the streams that were level (order) 5 and greater were extracted and used for further analysis.

3.2.3. Preparing the Maps of Human-related Criteria

The human-related criteria included land use types, main electricity transmission lines, and major roads (see Figures 2e and 2f). The map of major transmission lines was obtained as an image file (**.jpg) from the National Electric Power Company, which then was georeferenced to the JTM coordinate system and was digitized accordingly. The map of major roads was obtained from the Royal Jordanian Geographic Center, and was visually checked by overlaying it on the Google Earth base imagery. Residential areas were delineated based on the road density analysis of a detailed road network map combined with a classification procedure for Landsat-8 images. The land use map was identified through a supervised process utilizing a vegetation index-based classification technique for eleven Landsat-8 images covering the geographic extent of Jordan. Accordingly,

seven land-use/ cover type classes were identified, namely, residential areas, open area, quarries, agriculture, chert plain, forest, and water bodies. Each image was exclusively classified, then the eleven maps were combined into one land-use map. The average overall accuracy and Kappa coefficient values of the classified maps of the eleven images were 89.3 % and 82.7 %, respectively. Table 2 shows statistical measures of average user's and producer's accuracies for the eleven classified maps. All the datasets were clipped within the Jordan boundaries and projected to the JTM coordinates.

Table 2. Average values of statistical measures of 11 landsat-8 classified images generated through confusion matrices

Average producer's % accuracy	Average user's % accuracy	Land use / cover type
85.3	89.3	Residential areas
82.4	90.2	Open area
94.3	93.4	Quarries
80.7	82.3	Agriculture
96.8	97.4	Chert plain
86.3	85.1	Forest
97.8	98.3	Water bodies

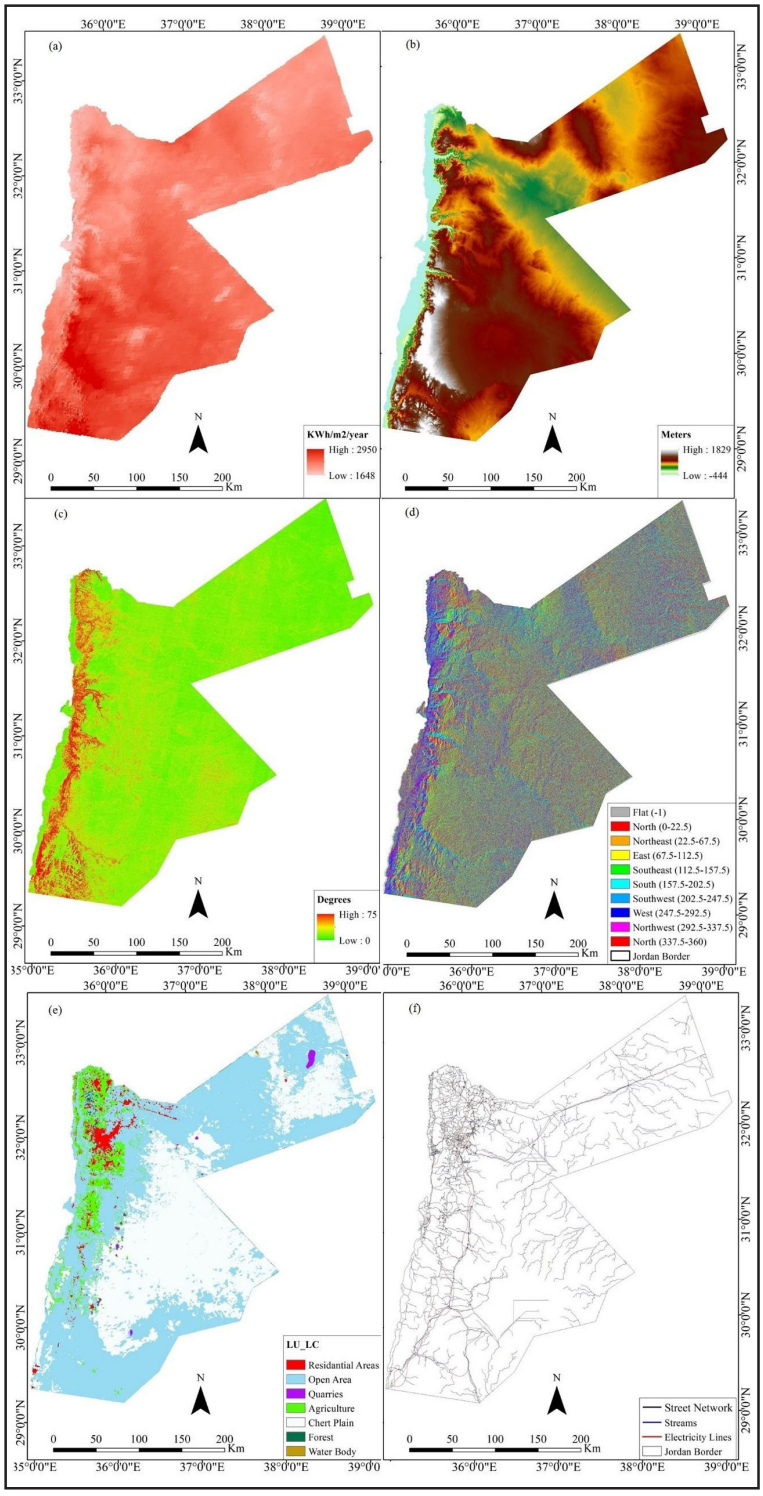

Figure 2. Maps of selected criteria used in this study for defining potential sites of photovoltaic farms: (a) solar radiation, (b) elevation, (c) slope, (d) aspect, (e) land use/cover, and (f) streets, streams, and electricity network.

3.3. Methods

Figure (3) shows a schematic diagram of the methodology, which consisted of four major components: (1) identifying potential regions for PV farms, (2) determining the score values and relative weights of each criterion, (3) synthesizing the criteria according to the GIS-MCE function, and (4) evaluating suitable sites for PV farms.

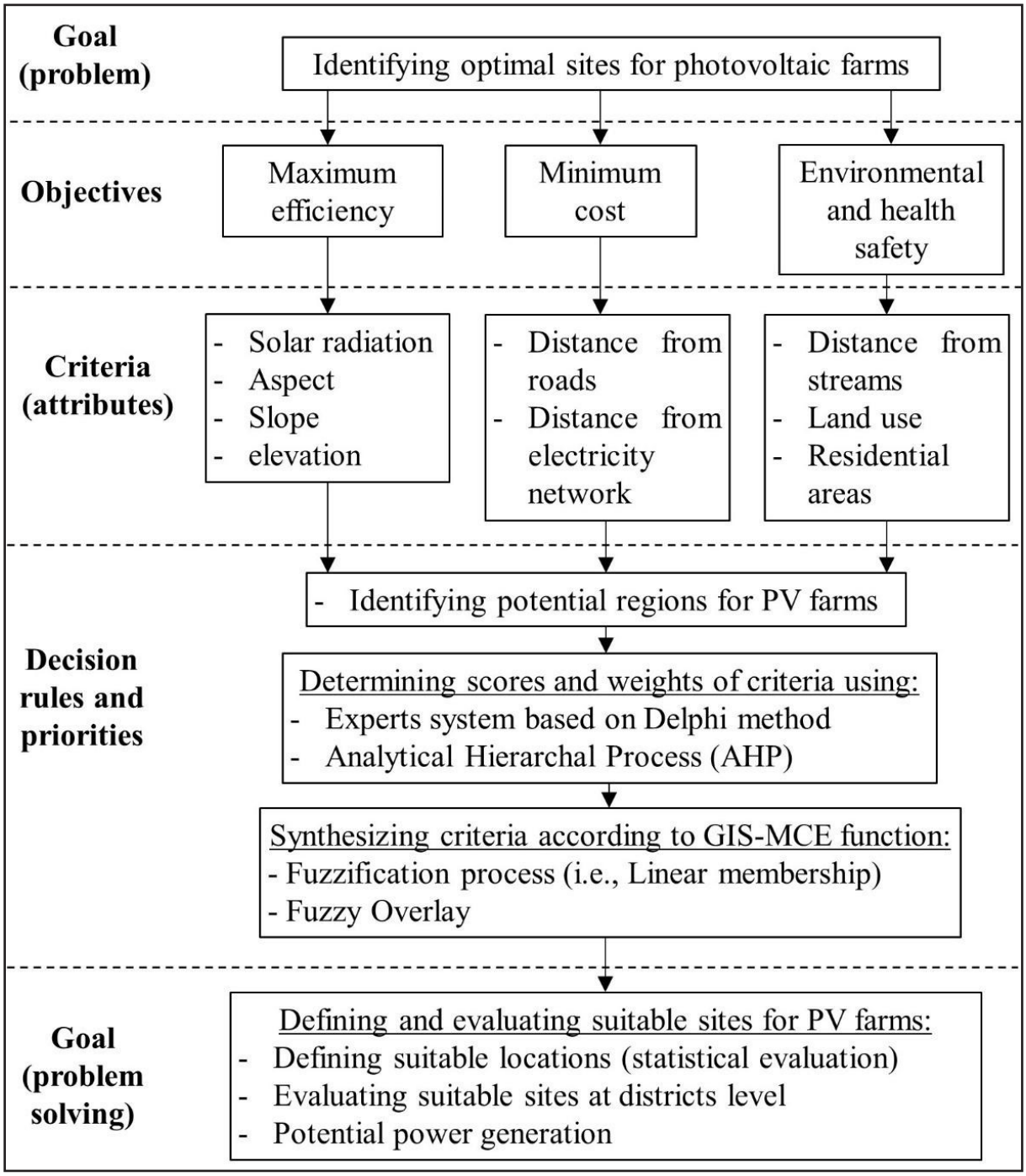

Figure 3. Schematic diagram of the proposed model for photovoltaic farms site selection; the bold terms represent the general steps of multi-criteria evaluation process.

3.3.1. Identifying Potential Regions for PV Farms

To identify potential regions for PV farms and to reduce the processing time of the MCE site selection functions, several spatial masks were applied to define the potential regions for PV farms excluding the unsuitable regions as the first step. The excluded regions were determined based on several constraints, including environmental, technical, safety/security, social and economic constraints [13]. The spatial masks included the following regions:

- Regions with less than 1,300 KWh/m^2/year of solar radiation (technical and economic constraints).
- Protected regions such as forests, national parks, wildlife conservations, lakes, and reservoirs (environmental constraints) [17].
- Regions within a buffer of 0.5km from protected regions (environmental constraints).
- Regions within a buffer of 2km from residential areas (safety, social, and environmental constraints).

- Regions at a distance greater than 50 km from roads and power transmission lines (technical and economic constraints).
- Regions with a distance less than 0.5 km from streams, and less than 0.1 km from roads (technical and safety constraints).
- Regions with a slope greater than 11% (technical and safety constraints).

3.3.2. Determining the Score Values and Relative Weights for each Criterion

The next step entailed that the potential regions determined in the first step were tested for their suitability for establishing PV farms based on the score values and the relative weights of each criterion. Based on an expert system procedure (the Delphi method), the score values for each criterion were set to define the spatial proportional importance of a tested location compared to other locations within the single criterion.

The relative weight for each criterion was defined in relation to the other criteria and was calculated using the AHP protocols. For these protocols, the AHP hierarchy was developed by defining the overall goal (the best PV sites) as well as the sub-goals (suitable site per criterion) based on the attributes assigned for each alternative (e.g., a raster cell or cluster representing a score value). Then, a pairwise comparison matrix A between the defined criteria was designed based on the Saaty scale of preferences [26] (see Table (2) for details), and calculated the relative weights following Equation (1), the consistency index [CI: Equation (2)], and the consistency ratio [CR: Equation (3)] to measure the inconsistency associated with the pairwise comparison matrix A. As a rule of thumb, CR values less than or equal to 0.1 indicate an acceptable level of consistency in matrix A and vice versa [27].

$$W_{(i)} = \frac{\sum v_{(ij)}}{\frac{s_{(j)}}{n}} \quad \text{.....(1)}$$

$$CI = \frac{\lambda_{max} - P}{P - 1} \quad \text{.....(2)}$$

$$CR = \frac{CI}{RI} \quad \text{.....(3)}$$

where is the relative weight for criterion i, is the value of criterion i in column j in matrix A is the sum of column j, and n is the number of criteria. is the largest eigenvalue that could be obtained once its associated eigenvector was determined. P is the number of columns of matrix A. RI is the random inconsistency index as defined in Table (3) [26].

Table 3. Saaty's preferences in the pairwise comparison process (matrix).

Numerical rating	**Verbal description of preference between criterion *i* and criterion *j***
1	*Ai* is equally important to *Aj*
3	*Ai* is slightly more important than *Aj*
5	*Ai* is strongly more important than *Aj*
7	*Ai* is very strongly more important than *Aj*
9	*Ai* is extremely more important than *Aj*
2, 4, 6, 8	Intermediate values
Aj has the reciprocal value when compared with criteria *Ai*	Reciprocals of above non-zero number

Random inconsistency indices (RI)*.

n criteria	1	2	3	4	5	6	7	8	9	10
RI	0	0	0.58	0.9	1.12	1.24	1.32	1.41	1.45	1.49

3.3.3. Synthesizing Criteria according to the GIS-MCE Method

The combined FOA-AHP method is selected for this study to address the two main sources of inaccuracies in the attribute data that can severely affect decision-making selection, namely, the definition of the classes in a classification, and the imprecision in assigning phenomena to classes. Also, the FOA-AHP method can provide an overlay analysis closer to natural human thinking [28]. In FOA-AHP, all the input variables must be in raster format to allow for the map algebra processes.

The FOA-AHP method was conducted through two major steps: (1) the fuzzification process in which each individual raster cell in each map criterion was reclassified or assigned a value between 0 and 1 representing the possibility of that cell value being a member of a certain suitability set (i.e., 0 was not in a set, other values were at various levels of possibility), (2) a fuzzy overlay analysis in which the locations that best met all the criteria (i.e., having high likelihood of membership in all sets) were multiplied by the relative weight value of the corresponded criterion. Then, the results were totaled to assign the final relative level of suitability for each location on the final suitability index map, which is expressed below in Equation (4) [29].

$$S = \sum w_{(i)} * x_{(ij)} \quad \text{.....(4)}$$

Where S is the suitability index for each pixel in the final map, w_i is the weight of ith criterion map, and x_{ij} is the criteria score of class j in criterion i. This equation returns the highest potential membership or suitability value for each cell in all the multiple criteria simultaneously.

Finally, the suitability index map was regrouped into four different classes of suitability: "suitable" , "slightly more suitable", "moderately suitable" , and "highly suitable".

3.3.4. Evaluating Suitable Sites for PV Farms

Results for the twelve governorates were investigated and analyzed according to the Jordanian administrative system. The land suitability index of each governorate was then determined according to the four classes of suitability. In addition, the location of an already existing PV farm in Jordan (i.e., Shams Ma'an) was evaluated. Finally, the potential power generation from the selected "highly suitable" sites was calculated for different PV systems in Table 4 using Equation (5)[30,31].

$$GP = SR * CA * AF * \eta \quad \text{.....(5)}$$

Where GP is the potential power generation capacity (GWh/year); SR is the annual solar radiation (GWh/km^2/

year); CA is the total area of suitable locations (km^2); AF is the area factor (portion) of CA that can be covered by solar panels (%); and η is the efficiency with which the PV solar system converts sunlight into electricity (%) as shown in Table 4 [32].

Table 5. Efficiencies of different PV systems evaluated under standard test conditions (STC)* that manufacturers use (i.e., 1000 W/m^2) from annual data.

PV solar panel technologies	Efficiency η, (%)
Micromorph silicon (μ-Si)	7.7
Monocrystalline silicon (M-Si)	14.5
Amorphous silicon (a-Si)	6.9
Polycrystalline silicon (Poli-Si)	13.5

** STC is defined as the solar irradiation of one kilowatt (kW) per square meter, a module temperature of 25 degrees Celsius and a solar irradiation angle of 45 degrees.*

4. Results and Discussion

4.1. Potential Regions for PV Sites

After applying the appropriate spatial masks for the protected/restricted areas, the potential regions for establishing PV farms in Jordan were identified as shown in Figure 4. The total potential areas were located mainly in the southern and eastern regions (approximately 51818.6km^2), representing 58.4% of the whole country.

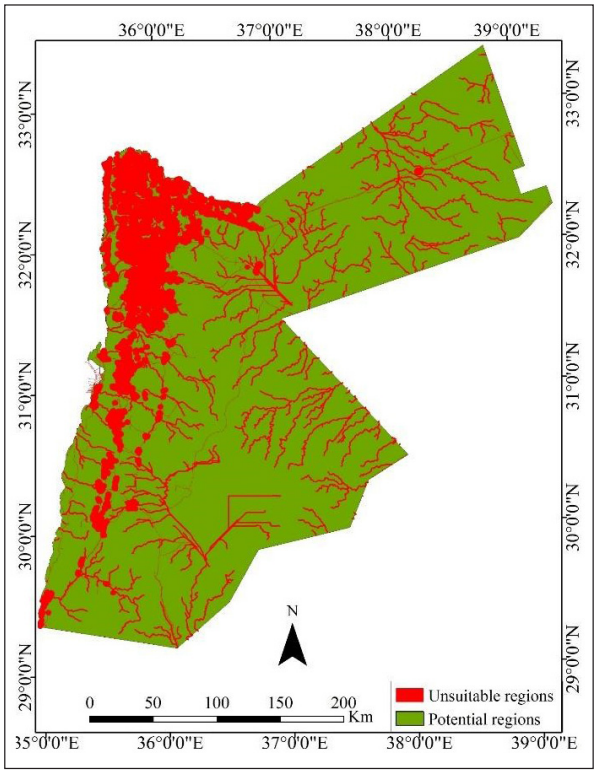

Figure 4. Potential regions for photovoltaic farms in Jordan, the unsuitable regions show the restricted areas according to specific spatial masks discussed in Section 3.2.1.

4.2. AHP Analysis and FOA Results

Table 5 shows the pairwise matrix generated in this study and the calculated relative weight for each criterion. Based on the above-mentioned calculations, the solar radiation, aspect, and distance from electricity network lines, variables were found to be the most important criteria with relative weights of 30%, 22%, and 15%, respectively. The slope, distance to main roads, and land-use type variables came having moderate importance with relative weights of 10 %, 9% and 6 %, respectively. The distance to streams, elevation and the distance from residential areas were found to have minimal influence on the PV site selection and the relative weights as low as 4 % and 2 %, respectively. Tarhi et al., [33], Sánchez-Lozano et al., [34], Charabi and Gastli [35], Uyan [36], and Noorollahi et al., [13] also considered solar radiation as the most important criterion. The consistency analysis of the pairwise matrix and the relative weights revealed a consistency ratio of 0.088, indicating an acceptable and consistent pairwise matrix as its value was less than 0.10. Thus, the resultant relative weights have been validated for use in further analysis.

Table 5. Pairwise comparison matrix of multiple criteria for PV site selection and its calculated relative weights based AHP analysis. Values in the crossed cells represent the scale of importance for comparison pair in row i and column j as defined in Table (2) or its replicable.

Criteria*	SR	E	S	A	LU	DR	DE	DS	DRA	W (%)
SR	1.00	7.00	5.00	3.00	5.00	5.00	3.00	5.00	7.00	30
E	0.14	1.00	0.20	0.14	0.20	0.20	0.20	0.33	1.00	2
S	0.20	5.00	1.00	0.20	3.00	3.00	0.33	3.00	5.00	10
A	0.33	7.14	5.00	1.00	5.00	3.00	3.00	5.00	7.00	22
LU	0.20	5.00	0.33	0.20	1.00	0.33	0.20	3.00	3.00	6
DR	0.20	5.00	0.33	0.33	3.03	1.00	0.33	3.00	5.00	9
DE	0.33	5.00	3.03	0.33	5.00	3.00	1.00	5.00	5.00	15
DS	0.20	3.03	0.33	0.20	0.33	0.33	0.20	1.00	3.00	4
DRA	0.14	1.00	0.20	0.14	0.33	0.20	0.20	0.33	1.00	2

** SR = solar radiation, E = elevation above sea level, S = slope degree, A = aspect, LU = land use, DR = distance from roads, DE = distance from electricity network lines, DS = distance from stream network, DRA = distance from residential areas, W = relative weight.*

The results for the total suitable areas shown in Figure 5 were found to be approximately 35468 km^2 (~ 68.4% of the potential area for PV). These areas were reclassified into four levels of suitability: "suitable" (suitability index less than 0.4), "slightly more suitable" (0.4 > suitability index < 0.5), "moderately suitable" (0.5 > suitability index < 0.6), and "highly suitable" (suitability index < 0.6). As can be seen in Figure 5, most of the "highly suitable" sites were located in the open land use areas having flat south-oriented topographies and higher solar radiation exposure and were closer to power sources and road networks.

The land use and distance from streams or residential areas were found less important in the PV farms-site selection. The statistical measurements showed that the "suitable," "slightly more suitable," "moderately suitable," and "highly suitable" areas represented approximately 8.3%, 14.6%, 18.1%, and 27.4% of the potential areas, respectively. The statistical results for the administrative units (i.e., governorates) showed that 11.2% of the "highly suitable" areas were located in the Ma'an governorate in the southern part of the country. In

contrast, the less suitable areas were identified in the districts of the Jordan Valley in the western part of the country because although they have high potential for solar radiation, these areas have low land-terrain topographies.

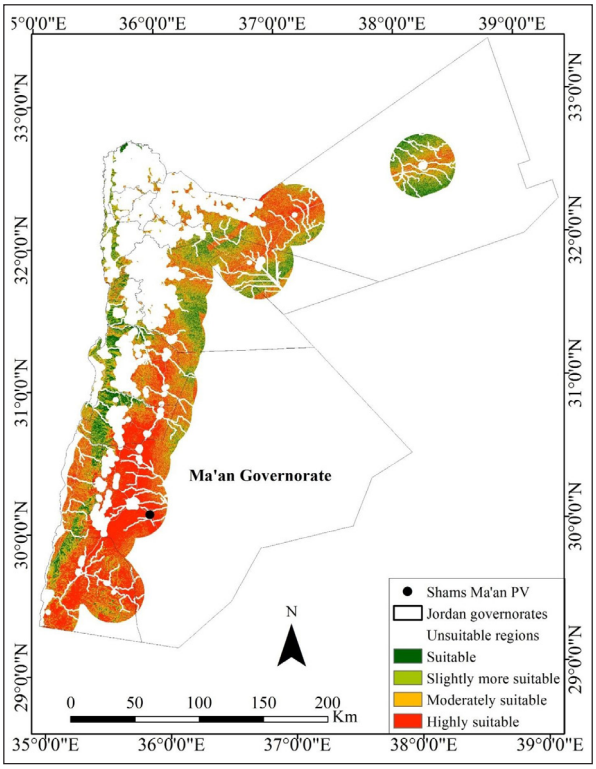

Figure 5. Suitable areas for photovoltaic sites in Jordan as calculated by Fuzzy-AHP method.

4.3. Evaluation of Suitable Sites for PV Farms

Our evaluation of the existing PV project [i.e., Shams Ma'an (2km^2) in the governorate of Ma'an showed that it was in a "highly suitable" area (see Figure5). The advantages of this site include the excellent environmental economic and safety factors for allocating the PV farms. Our assessment results confirmed that the region of Ma'an is indeed highly suitable for PV projects. The solar radiation high potential, the distance from electricity networks, the south-facing orientation, and the large open areas are unsurprisingly key factors that increase the suitability indexing of this area. In comparison to other areas in the Mediterranean region, Ma'an offers competitive opportunities. For example, the percentage of "highly suitable" areas was 3% in Cartegena, Spain [37], 5% in Granada, Spain [38], 14% in Karapinar, Turkey [7], 23% in Ouarzazate, Morocco [33], 4% in Oman [35], 14.7% in Iran (e.g., 38.4% in Kerman province)[13], and 20% in Lake Nasser Region, Egypt [39].

The evaluation of potential power generation for the highly suitable areas (see Equation 4) for the four PV technologies is presented in Table 6. Note that an AF of 70% was used based on the maximum land occupancy and distance between PV panels, which ensured a minimal shading effect [40]. Dolara et al., [41] and Altarawneh et al., [16] addressed the shading effect on the potential power generation of a PV system, and demonstrated that 50% shading of a PV single cell may result in reducing the PV potential of power generation by more than 30%. The efficiency η percentage of each PV system was considered in this study for typical high temperatures and low solar-radiation region applications. Table 6 shows that all the tested PV systems could produce huge amounts of electricity. For instance, if monocrystalline silicon (M-Si) system was selected for installing PV farms in "highly suitable" areas, it has a power generation potential of 104,886,738 GWh/year for various electricity demand sources in Jordan. Note that in 2015, the total annual electricity production in Jordan was 18,911 GWh. Thus, utilizing "highly suitable" areas for PV farms would generate many multiples of the current demand for electricity in Jordan. It is worthwhile to mention that such large projects require highly trained professionals and can be costly. Therefore, collaboration with other interested parties in the world is necessary. It is important to note that in this study, only the potential use of PV technology was considered, while other technologies, such as CSP were not investigated because, compared to PV systems, they require large amounts of water for the purposes of cooling and mirror washing. Therefore, for arid and semi-arid countries with scarce water resources, as is the case for Jordan [42], PV technologies would be the best choice, since PV technologies are more environment-friendly, economical, flexible, and faster to be implemented and connected to electric grids than CSP technologies [30].

Table 6. The potential power generation for the highly suitable areas for the four PV technologies.

PV solar panel technologies	Potential power generation (GWh/y)
Micromorph silicon (μ-Si)	55,698,474
Monocrystalline silicon (M-Si)	104,886,738
Amorphous silicon (a-Si)	49,911,620
Polycrystalline silicon (Poli-Si)	97,653,170

Concluding remarks

This study applied the geospatial-based fuzzy multi-criteria approach in the evaluation of the suitability of land areas for installing PV farms in Jordan. The evaluation module of this approach incorporated expert opinions on the criteria and their weights, and applied a fuzzification process to identify the suitable sites based on several environmental, human, and topographic variables. The results show that approximately 16.1% of the country contains highly suitable locations for PV farm implementation with the governorate of Ma'an leading the list of the most suitable sites among all the other governorates of Jordan. In addition, we evaluated the potential electricity generation for four different PV technologies for highly suitable areas, and found that PV could produce surplus electricity that exceeds the current power demand of Jordan. It should be noted that for the successful implementation of the PV technology, long-term strategies must be developed and followed.

Acknowledgments

We thank the following agencies and individuals for their assistance with this research, namely, the United States Geological Survey (USGS), and the National Aeronautics and Space Administration (NASA) for providing Landsat-8 images free of cost. We express our thanks also to the Ministry of Economy, Trade, and Industry (METI) of Japan jointly with NASA for providing the Advanced Spaceborne Thermal Emission and Reflection Radiometer (ASTER) Global Digital Elevation Model data free of cost, and to the Royal Jordanian

Geographic Center and Ministry of Power for providing the required data and also to the experts who contributed to the evaluation of the criteria.

References

[1] Ramachandra, T.V. and Shruthi, B.V. 2007. Spatial Mapping of Renewable Energy Potential, Renew. Sustain. Energy Rev. 11, pp. 1460–1480, doi:10.1016/j.rser.2005.12.002.

[2] Pryor, S.C. and Barthelmie, R.J. 2013. Renewable Energy Resources - Ocean Energy. Wind-Wave-Tidal-Sea Currents. doi:10.1016/B978-0-12-384703-4.00311-7.

[3] Kucuksari, S., Khaleghi, A.M., Hamidi, M., Zhang, Y., Szidarovszky, F., Bayraksan, G., and Son, Y.J. 2014. An Integrated GIS, Optimization and Simulation Framework for Optimal PV Size and Location in Campus Area Environments, Appl. Energy. 113, pp. 1601–1613. doi:10.1016/j.apenergy.2013.09.002.

[4] REN21, Renewables 2017 Global Status Report.

[5] Jahangiri, M., Ghaderi, R., Haghani, A., and Nematollahi,O. 2016. Finding the Best Locations for Establishment of Solar-Wind Power Stations in Middle-East Using GIS: A Review, Renew. Sustain. Energy Rev. 66, pp. 38–52. doi:10.1016/j.rser.2016.07.069.

[6] Yunna, W. and Geng, S. 2014. Multi-criteria Decision Making on Selection of Solar-Wind Hybrid Power Station Location: A Case of China, Energy Convers. Manag. 81, pp. 527–533. doi:10.1016/j.enconman.2014.02.056.

[7] Uyan, M. 2013. GIS-based Solar Farms Site Selection Using Analytic Hierarchy Process (AHP) in Karapinar Region, Konya/Turkey, Renew. Sustain. Energy Rev. 28, pp. 11–17. doi:10.1016/j.rser.2013.07.042.

[8] Kou, G., Shi, Y., and Wang, S. 2011. Multiple Criteria DecisionMaking and Decision Support Systems - Guest Editor's Introduction, Decis. Support Syst. 51, pp. 247–249. http://sci-hub.cc/http://www.sciencedirect.com/science/article/pii/S0167923610002083 (accessed June 12, 2017).

[9] Pohekar, S.D. and Ramachandran, M. 2004. Application of Multicriteria Decision Making to Sustainable Energy Planning - A Review, Renew. Sustain. Energy Rev. 8, pp. 365–381. doi:10.1016/j.rser.2003.12.007.

[10] Wang, J.J., Jing,Y.Y., Zhang, C.F., and Zhao, J.H. 2009. Review on Multicriteria Decision Analysis Aid in Sustainable Energy Decision Making, Renew. Sustain. Energy Rev. 13, pp. 2263–2278. doi:10.1016/j.rser.2009.06.021.

[11] Kowalski, K., Stagl, S., Madlener, R., and Omann, I. 2009. Sustainable Energy Futures: Methodological Challenges in Combining Scenarios and Participatory Multi-Criteria Analysis, Eur. J. Oper. Res. 197, pp. 1063–1074. doi:10.1016/j.ejor.2007.12.049.

[12] Ishizaka, A. 2014. Comparison of Fuzzy Logic, AHP, FAHP and Hybrid Fuzzy AHP for New Supplier Selection and Its Performance Analysis, Int. J. Integr. Sypply Manag. 9, pp. 1–22. doi:10.1007/s13398-014-0173-7.2.

[13] Noorollahi, E., Fadai, D., Akbarpour Shirazi, M., and Ghodsipour, S. 2016. Land Suitability Analysis for Solar Farms Exploitation Using GIS and Fuzzy Analytic Hierarchy Process (FAHP) - A Case Study of Iran, Energies, 9, 643. doi:10.3390/en9080643.

[14] DPS (Department of Population Statistics), Population and Social Statistics. 2015. http://web.dos.gov.jo/wp-content/uploads/2016/04/No_of_pop_depand_on_GOV.pdf (accessed June 13, 2017).

[15] MEMR (Ministry of Energy and Mineral Resources), Ministry of Energy, and Mineral Resources Annual Report. 2015. http://www.memr.gov.jo/echobusv3.0/SystemAssets/6df2053d-ee21-4fa0-ada8-613049ab7015.pdf (accessed June 13, 2017).

[16] Altarawneh, I.S., Rawadieh, S.I., Tarawneh,M.S., Alrowwad, S.M. and Rimawi, F. 2016. Optimal Tilt Angle Trajectory for Maximizing Solar Energy Potential in Ma'an Area in Jordan, J. Renew. Sustain. Energy, 8, 33701. doi:10.1063/1.4948389.

[17] International Finance Cooperation. 2015. Utility-Scale Solar Photovoltaic Power Plants in Partnership With A Project Developer's Guide. https://www.ifc.org/wps/wcm/connect/f05d3e00498e0841bb6fbbe54d141794/IFC+Solar+Report_Web+_08+05.pdf?MOD=AJPERES (accessed June 17, 2017).

[18] Hsu, C. and Ohio, T. 2007. The Delphi Technique : Making Sense Of Consensus, Pract. Assessment, Res. Eval. 12. doi:10.1080/02688867.1988.9726654.

[19] Cano, D., Monget, J.-M., Albuisson,M., Guillard, H., Regas,N., and Wald, L. 1986. A Method for the Determination of the Global Solar Radiation from Meteorological Satellite Data, Sol. Energy. 37, pp. 31–39. http://www.sciencedirect.com/science/article/pii/0038092X86901040 (accessed June 14, 2017).

[20] Meyer, R., Lohmann, S., Schillings, C. Hoyer, Climate Statistics for Planning and Siting of Solar Energy Systems, Sol. Resour. from Local Lev. to Glob. Scale Support Resour. Manag. Renew. Electr. Gener. (2007). http://elib.dlr.de/10316 (accessed June 14, 2017).

[21] Beyer, D., Costanzo, H.G., and Heinemann, C. 1996. Modifications of the Heliostat Procedure for Irradiance Estimates from Satellites Images, Sol. Energy. 56, pp. 207–212. http://www.sciencedirect.com/science/article/pii/0038092X95000926 (accessed June 14, 2017).

[22] Ineichen, P. 2013 Long-term Satellite Hourly, Daily, and Monthly Global, Beam and Diffuse Irradiance Validation: Interannual Variability Analysis. https://www.researchgate.net/profile/Pierre_Ineichen/publication/259400149_Long_term_satellite_hourly_daily_and_monthly_global_beam_and_diffuse_irradiance_validation_Interannual_variability_analysis/links/00b7d52b7d1adc5ce7000000.pdf (accessed June 14, 2017).

[23] Meral,M.E. and Diner, F. 2011. A Review of the Factors Affecting Operation and Efficiency of Photovoltaic-based Electricity Generation Systems, Renew. Sustain. Energy Rev. 15, pp. 2176–2184. doi:10.1016/j.rser.2011.01.010.

[24] Tachikawa, T., Hato, M., Kaku, M., andIwasaki, A. 2011. Characteristics of ASTER GDEM Version 2, In: Int. Geosci. Remote Sens. Symp., 2011: pp. 3657–3660. doi:10.1109/IGARSS.2011.6050017.

[25] Maidment, D.R. 2002. Arc Hydro: GIS for water resources, ESRI, Inc. https://books.google.com/books?hl=en&lr=&id=07vH7Sf0v6MC&oi=fnd&pg=PP7&dq=Arc+Hydro+Tools+-+Tutorial+&ots=aiSBABcfiz&sig=4EAj8QXFvACoaaBNh_fqzz5AN28 (accessed June 14, 2017).

[26] Saaty, T.L. 1994. How to Make a Decision: The Analytic Hierarchy Process, Eur. J. Oper. Res. 1 (1994) 19–43. http://www.sciencedirect.com/science/article/pii/037722179090057I (accessed June 15, 2017).

[27] Boroushaki, S. Malczewski, J., Boroushaki, S.. and Malczewski, J. 2008.Implementing an Extension of the Analytical Hierarchy Process Using Ordered Weighted Averaging Operators With Fuzzy Quantifiers in ArcGIS, Comput. Geosci. 34, pp. 399–410. doi:10.1016/j.cageo.2007.04.003.

[28] Malczewski, J. 2004. GIS-based Land-use Suitability Analysis: A Critical Overview, Prog. Plann. 62, pp. 3–65. doi:10.1016/j.progress.2003.09.002.

[29] Malczewski, J. 2006. Ordered Weighted Averaging with Fuzzy Quantifiers: GIS-based Multicriteria Evaluation for Land-Use Suitability Analysis, Int. J. Appl. Earth Obs. Geoinf. 8, 270–277. doi:10.1016/j.jag.2006.01.003.

[30] Charabi, Y. and Gastli, A. 2011. PV Site Suitability Analysis Using GIS-based Spatial Fuzzy Multicriteria Evaluation, Renew. Energy. doi:10.1016/j.renene.2010.10.037.

[31] Gastli, A. and Charabi, Y. 2010. Solar Electricity Prospects in Oman Using GIS-based Solar Radiation Maps, Renew. Sustain. Energy Rev. 14, pp. 790–797. doi:10.1016/j.rser.2009.08.018.

[32] Guenounou, A., Malek, A., and Aillerie, M. 2016. Comparative Performance of PV Panels of Different Technologies over One Year of Exposure: Application to a Coastal Mediterranean Region of Algeria, Energy Convers. Manag. 114, pp. 356–363. doi:10.1016/j.enconman.2016.02.044.

[33] Tahri, M. Hakdaoui, M. Maanan, M. 2015. The Evaluation of Solar Farm Locations Applying Geographic Information System and Multi-Criteria Decision-Making Methods: Case Study in Southern Morocco, Renew. Sustain. Energy Rev. 51, pp.1354–1362. doi:10.1016/j.rser.2015.07.054.

[34] Sánchez-Lozano, J. Geographical Information Systems (GIS) and Multi-Criteria Decision Making (MCDM) Nethods for the Evaluation of Solar Farms Locations: Case Study in Southeastern Spain, Renew. Sustain. Energy News. 24, pp. 544–556. doi:http://dx.doi.org/10.1016/j.rser.2013.03.019.

[35] Charabi, Y. and Gastli, A. 2011. PV Site Suitability Analysis Using GIS-Based Spatial Fuzzy Multi-Criteria Evaluation, Renew. Energy. 36, pp. 2554–2561. doi:10.1016/j.renene.2010.10.037.

[36] Uyan, M. 2013. GIS-based Solar Farms Site Selection Using Analytic Hierarchy Process(AHP) in Karapinar Region, Konya/Turkey, Renew. Sustain. Energy Rev. 28 pp. 11–17. doi:10.1016/j.rser.2013.07.042.

[37] Sánchez-Lozano, J. M., Teruel-Solano, J., Soto-Elvira, P. L., Socorro García-Cascales, M. 2013. Geographical Information Systems (GIS) and Multi-Criteria Decision Making (MCDM) Methods for the Evaluation of Solar Farms Locations: Case Study in Southeastern Spain, Renew. Sustain. Energy Rev. 24, pp. 544–556. doi:10.1016/j.rser.2013.03.019.

[38] Arán Carrión, J., Espín Estrella, A., Aznar Dols, F., Zamorano Toro, M., Rodríguez, M., and Ramos Ridao, A. 2008. Environmental Decision-support Systems for Evaluating the Carrying Capacity of Land Areas: Optimal Site Selection for Grid-connected Photovoltaic Power Plants, Renew. Sustain. Energy Rev. 12, pp. 2358–2380. doi:10.1016/j.rser.2007.06.011.

[39] Effat, H. 2016. Mapping Solar Energy Potential Zones, using SRTM and Spatial Analysis, Application in Lake Nasser Region, Egypt, Int. J. Sustain. L. Use. 3 (2016). https://www.sciencetarget.com/Journal/index.php/IJSLUP/article/view/551 (accessed June 29, 2017).

[40] Effect of Shading on the Performance of Solar PV Panel, (n.d.). http://article.sapub.org/10.5923.c.ep.201501.01.html (accessed July 12, 2017).

[41] Dolara, A., Lazaroiu, G.C., Leva, S., and Manzolini, G. 2013. Experimental Investigation pf Partial Shading Scenarios on PV (Photovoltaic) Modules, Energy. 55 (2013) 466–475. doi:10.1016/j.energy.2013.04.009.

[42] [42] Hazaymeh, K. and Hassan,Q.K. 2017. A Remote Sensing-based Agricultural Drought Indicator and its Implementation over a Semi-arid Region, Jordan, J. Arid Land. 9 (2017) 319–330. doi:10.1007/s40333-017-0014-6.

JJEES
Jordan Journal of Earth and Environmental Sciences

Volume 9, (Number 1), April, 2018
ISSN 1995-6681
Pages 57 - 61

Royalty of Using Jordanian Oil Shale as an Alternative Fuel in the Cement Industry

Awwad H. Titi[1], Hani M. Alnawafleh[1], Mohammad K. Dweirj[1,2], and Rami O. Alrawashdeh[1]

[1]*Department of Mining and Mineral Engineering, Faculty of Engineering, Al-Hussein Bin Talal University, Ma'an, Jordan*
[2]*Natural Resources and Chemical Engineering, Tafila Technical University, Tafila, Jordan*

Received 19 December, 2017; Accepted 16 January, 2018

Abstract

The Jordanian oil shale (JOSh) is considered as a strategic mineral similar to oil. The government of Jordan seeks to earn a new royalty rate from the oil shale extraction industry to cope with the constantly changing fuel oil prices in the world. This paper discusses the royalty rate when using oil shale in the cement industry. The royalty rate is estimated by creating formulas of substitute portions of different types of fuel used in the cement industry. The suggested mathematical equation of the royalty rate determination for each tonne extracted has been calculated, taking into account the stripping ratio and the variability in the oil content percentage in different oil shale (OS) deposits. The purpose of royalty rate determination is to control the mining operations and the quantities of the extracted oil shale. Results indicate that as the portion of oil shale or Petcoke in the mixture increases, the saving rate increases as well. Moreover, the cost of using portions of oil shale or Petcoke in the fuel mixture tends to be less than the cost of utilizing pure fuel oil. The current study recommends using oil shale mixed with fuel as an energy alternative in the manufacturing of cement in Jordan.

Keywords: Oil shale, Jordan, Royalty, Fuel oil, Oil shale ash, Cement industry.

1. Introduction

Jordan has to cope with its growing demand for energy. The implementation of suitable measures to face the increasing demand is urgently needed. The high consumption of imported oil has become a heavy burden on the gross national product (GNP), and an obstacle for the economic development in Jordan.. One important solution could be the use of domestic Jordanian oil shale (JOSh) resources.

Coal is a primary fuel used in the cement industry. A wide range of other fuels such as natural gas, oil, liquid waste materials, solid waste materials, and Petcoke have all been successfully used as sources of energy for firing cement-making kilns, either on their own or in various combinations. Other alternative materials that can be used as thermal energy in the cement maufacture include waste oil, saw dust, tyres, plastics, mixed industrial waste, and alternative fuels biomass (ECRA, 2014).

Up to 30-40 % of the operating costs of cement manufacturing are related to energy consumption; thus, a cement manufacturing plant that takes measures to save the costs of energy has a competitive advantage over cement plants that use traditional fuels (Mokrzycki and Bochenczyk, 2003). The high energy costs prompted major cement producers to look for and use alternative energy sources including oil shale (OS) and Petcoke to reduce the operating costs of the cement production. One tonne of commercial-grade OS contains up to 200 liters (Dyni, 2010), and can be used as an alternative energy source in the cement industry. Up to 6 % of the global OS production is used in cement manufacturing and other industries (Brendow, 2002). An example of the use of OS in the cement industry is that of Estonia (Veiderma, 2003).

In Jordan, the cement industry depends mainly on fuel oil (FO) as a major resource of energy. Over the recent years, oil prices increased dramatically which directly affected the cost of cement manufacturing and production in Jordan. The Jordan Cement Company has already started to look for other alternative energy sources in accordance with the governmental policies in this regard. So far, the only important indigenous source of energy found is the JOSh. The use of JOSh in the cement industry has attracted the Jordanian Lafarge Company since 2006. They ran a pilot experiment to test the use of JOSh along with FO in the manufacturing of cement. The results of their experiment were promising, and they reported 25% possible substitution of FO by JOSh (Jordan Lafarge Cement, 2017).

Jordan has potential OS deposits containing more than 40 billion tons of OS (Alali, 2006). The major JOSh deposits of commercial scale are located near the surface in central Jordan (Figure 1). They are easily accessible from the desert Highway and a substantial part of the infrastructure is already available (Alali, 2006; Besieso, 2007). The JOSh is not true shale (Abed, et. al, 2009; Alnawafleh, and Fraige, 2015). It is kerogen-rich, bituminous, argillaceous limestone that was deposited in shallow marine during the Maestrichtian-Danian periods (Abed, 2000; Pufahl, et. al., 2003; Dyni, 2006). Characteristics and physical properties of the potential JOSh deposits are presented in Table 1.

* Corresponding author. e-mail: hanialnawafleh@ahu.edu.jo

 - Volume 9, (Number 1), (ISSN 1995-6681)

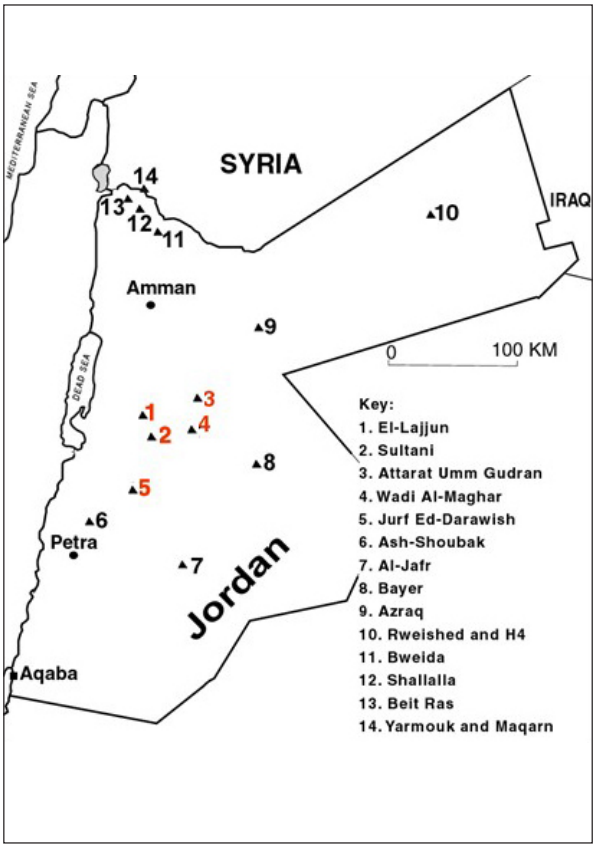

Figure 1. Major Oil Shale deposits in Jordan (Alnawafleh, et al., 2015).

The JOSh deposits in central Jordan have been extensively studied. They represent the potential OS resources for future utilization due to the following factors: They are good in quality and shallow in depth, and the ratio of overburden to OS is very low which makes them favorable for surface mining conditions. Moreover they are located in a thinly- populated area with ease of accessibility, reasonable infrastructure, as well as the availability of adequate amounts of water for the industrial utilization (Alali, 2006; Besieso, 2007; Jaber et al., 2008; Alnawafleh et al., 2015). In addition to the previous factors, and the abundance of JOSh resources in these areas, the supportive business environment offered by the government of Jordan is highly considered. The JOSh reveals local and lateral variability that should be considered in any potential uses of this resource (Alnawafleh et. al., 2015).

This paper highlights the advantage of using JOSh as fuel in the cement industry. More economic utilization of JOSh can be achieved by using both OS energy and oil shale ash (OSA). The most effective way is the use of OSA as a feedstock for the cement production. Studies showed that the addition of about 30% OSA into Portland cement clinker can enhance the compressive strength of the ordinary Portland cement (Al-Hasan, 2006). The royalty rate of JOSh utilization in the cement industry will be calculated. This will be done through the development of royalty equations that will be derived on the basis of the available data on the FO prices, in addition to OS stripping ratio and the percentage of oil content in different JOSh deposits.

Table 1. Specifications of the most important JOSh deposits (Hamarneh, 1998; Alali, 2006).

Description	El-Lajjun	Sultani	Juf Ed-Darawish	Attarat Umm Gudran	Wadi Maghar	Eth Thamad
Geological Reserve (M tonne)	1.3	0.99	8.6	11.3	32	11.4
Area (km^2)	20	24	150	226	29	150
Overburden (O.B) (m)	31	69	47	47	40	400-142
Oil shale (m)	29	32	68	36	40	200-72
Organic materials%	28	25	18	29	20	25
Oil%	10.5	9.7	5.7	11	6.8	10.5
Humidity%	2.1	5.5	4.5	3.25	2.9	2.5
Ash%	54.7	55.5	58.4	53.2	57.5	54.7
Sulfur%	3.1	2.4	2.4	2.6	2.6	3.2
Density (g\cm3)	1.8	1.9	2.1	1.8	2.03	1.8
(kj\kg)	6906	6380	4603	7235	4773	6903
(kcal\kg)	1650	1526	1100	1730	1090	1800

2. Methodology

The data required for the purpose of this study were collected from specific resources including published and unpublished reports, and personal communications. Calculations were made to determine the cost of JOSh extracting, the cost of transporting JOSh from the mine to the factory, and the cost of using and comparing different types of fuel in the cement industry, as well as the royalty rate. Calculation details will be presented in section 3. The expected cost of extracting and transporting one tonne of JOSh from the mine to the factory is 25.34 JOD excluding the saving rate of 1.5 JOD resulting from the use of OSA in the cement industry (Table 2).

one way through which the cement factories in Jordan can save the FO cost can be by using alternative fuel resources such as natural gas, Petcoke, and JOSh. Data were collected to calculate the low heat value (LHV) of each of these fuel types or their mixtures suggested for use in manufacturing cement. The equivalent low heat value (LHV_{eq}) of the mixed fuel is calculated in relation to the FO low heat value (Table 3).

Table 2. The expected cost of JOSh extraction, transportation, and OSA used in the cement industry.

Subject	*Cost (JD/tonne)
Cost of mining operations	4
Cost of crushing	2
Cost of transfer oil shale to the cement factory	4
Cost of Grinding oil shale in cement factory	10
Salaries costs, Maintenance, Diesel for drying and Electricity	3.74
Cost of burning	0.8
Cost of Grinding Cement	0.8
Total Cost	25.34
The advantage of using the oil shale ash	1.5
Cost of one tonne of oil shale	

** Cost data based on some personal communications (11/11/2017) with different Jordanian mining companies.*

Table 3. A comparison between the costs of OS with different kinds of fuel, taking into account the energy content of each kind.

Items	Unit	Fuel Oil *	Natural Gas *	Petcoke **	JOSh***
LHV(Low Heat Value)	Kcal/Kg	9600	11782	7500	1500
LHV$_{eq}$(equivalent to mixed fuel)	Times	1	0.81	1.28	6.4
Average Fuel oil price, 2016	JOD/ Ton	254	514.2	116	23.84
Comparative prices of fuel type	JOD/ Ton	254	391.60	148.48	152.58
Saving	JOD	0	---	105.052	101.42
Saving per 1ton raw oil shale	JOD/ Ton	---	---	---	16

Fuel oil and natural gas prices according to MEMR (2016) and Statista (2017).
*** Price and calorific value of Petcoke by Personal Communication (11/11/2017) with the Crushing Unit Manager of Al-Rashadieh Cement Factory.*
**** Based on data reported by Alali (2006).*

The average crude oil price annually from 2004 to 2017 is shown in Figure 2. Data of 2017 is used for the purpose of calculation the saving rate using different ratios of JOSh and Petcoke with FO as a mixture, in addition to the royalty rate.

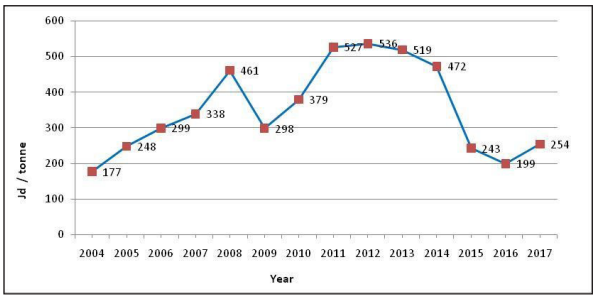

Figure 2. Average crude oil price annually from 2004 to 2017 released by the Organization of the Petroleum Exporting Countries (OPEC) [in JOD per metric ton, note:1 U.S Dollar equal 0.7 JOD] (Statista, 2017).

3. Discussion and Results

3.1. Saving Rate Calculation

Natural gas is not utilized in Jordanian industries due to the resource unavailability in Jordan and the special setup needed for the carrying and using this resource. Due to the repeated disruption of the pipeline that carries the imported Egyptian natural gas as a result of unstable regional conditions, and the need for special equipment to use gas as fuel in the cement industry all make the utilization of natural gas in the cement industry in Jordan quite unfeasible. However, the use of Petcoke can be promising taking into consideration that cement companies must import it from abroad as it is not produced locally. Because there are large reserves of good quality JOSh in Jordan and because of the ease of the extraction of JOSh through surface mining methods, and the possibility to use OSA in the cement industry, all make the use of JOSh as an energy resource in the cement industry a very good option. Studies show that OSA is a very good additive to cement (Smadi and Haddad, 2003).

Tables 4 and 5 show the average FO prices used in the cement industry, in addition to the calculation of the saving rate after using different ratios of JOSh and Petcoke with FO as a fuel mixture in order to save the cost of fuel used in the cement industry. Data indicate that the cost of JOSh and Petcoke used in the mixture is less than that of the FO. Moreover as the JOSh and Petcoke ratios in the mixture increase, the saving rate also rises.

Table 4. Calculation of the saving rate using different ratios of FO and OS mixtures.

FO Price JOD/T *	Gov. OS price JOD/T	OS%	OS price JOD	OS weight Kg	FO%	FO price JOD	FO weight Kg.	OS and FO mix. price JOD/T	Saving Rate JOD/T
254	131.82	5	7	320	95	241	950	248	6
254	131.82	10	13	640	90	229	900	242	12
254	131.82	15	20	960	85	216	850	236	18
254	131.82	20	26	1280	80	203	800	230	24
254	131.82	25	33	1600	75	191	750	223	31
254	131.82	30	40	1920	70	178	700	217	37

** Based on FO latest prices reported in MEMR (2016) and Statista (2017).*

Table 5. Calculation of the saving rate using different ratios of FO and Petcoke mixtures.

FO Price JOD/T *	Petcoke Price JOD/T	Petcoke%	Petcoke Price JOD/%	Petcoke weight Kg.	FO %	FO price JOD	FO weight Kg.	Petcoke and FO mix. price JOD/T	Saving Rate JOD/T
s254	148.48	5	7.4	64	95	241	950	249	5
254	148.48	10	14.8	128	90	229	900	243	11
254	148.48	15	22.3	192	85	216	850	238	16
254	148.48	20	29.7	256	80	203	800	233	21
254	148.48	25	37.1	320	75	191	750	228	26
254	148.48	30	44.5	384	70	178	700	222	32

** Based on FO latest prices reported in MEMR (2016) and Statista (2017).*

Figure 3 shows a comparison between the use of FO mixed with different ratios (5-30%) of JOSh and Petcoke with pure FO used in the cement industry. Results show that the savings are charged when using both JOSh and Petcoke in cement industry. The saving rates after using different ratios of FO and JOSh mixtures are slightly higher than that obtained when using different ratios of FO and Petcoke mixtures.

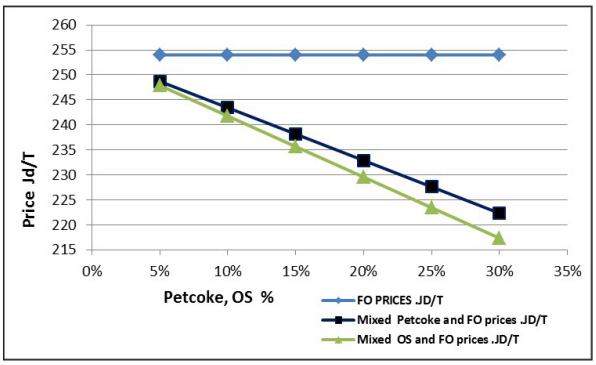

Figure 3. Comparative prices of FO and FO with JOSh and Petcoke mixtures.

3.2 Royalty Rate Determination

The government of Jordan has regarded JOSh as a strategic resource and has decided to put in place an appropriate mechanism for the royalty determination required of the mining companies to extract one tonne of JOSh. For this purpose, a concept for calculating the required royalty rate will be developed, taking into account the JOSh deposit conditions in various areas in Jordan including the overburden thickness above the JOSh (stripping ratio), and the oil content percentage in each area. In order to control the mining operations and the quantities of the extracted JOSh so that the companies will not be able to exclude quantities of extracted low-grade OS, it is necessary to link the royalty rate with the global FO price.

To formulate the royalty equation in relation to the different global FO prices, the FO prices are plotted against suggested progressive ratios (Figure 4). It is considered that the lowest FO price from which the royalty rate can be calculated equals 200 JOD/t which is weighted as 1%. As the suggested progressive ratio increases; the price of FO increases as well. Therefore, the developed royalty ratio equation is:

Y= 0.0148 X – 2.02 ……..…….. (1)

Where; Y: Royalty%, X: FO price.

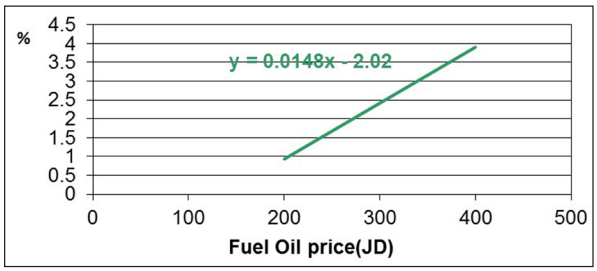

Figure 4. Royalty equation developed through the connection between different FO prices and suggested progressive ratios.

The difference in the stripping ratio and the oil content percentage in different JOSh deposits (areas) should to be taken into account in the process of royalty calculation. Firstly, for the purpose of variability in oil content, the highest percentage of oil content in the JOSh is 11% reported in Attarat Umm Ghudran deposit (Alali, 2006). This highest percentage of oil content is weighted as 100%. Therefore, the oil content in other deposits is calculated in relation to this ratio (Table 6). Secondly, for the purpose of variability in stripping ratio (SR), the standard SR value (1:1) for OS is found in Wadi Maghar deposit which is calculated from the overburden and JOSh thickness (data shown in Table 1). The standard SR value (1:1) is weighted as 100%, therefore, SR in other deposits is calculated in relation to this ratio (Table 6).

Table 6. The stripping ratio (SR) and oil content percentage calculation.

No.	Area/ JOSh Deposit	Oil content %	Oil content percentage compared with the highest percentage	Stripping Ratio (SR)*
1	Attarat Umm Ghudran	11	100	1.3
2	El-Lajjun	10.5	95.5	1.1
3	Eth Thamad	10.5	95.5	2
4	Sultani	9.7	88.1	2.2
5	Khan AzZabib	6.9	62.7	1.6
6	Wadi Maghar	6.8	61.8	1
7	Juf Ed-Darawish	5.7	51.8	0.7

**Calculated on the basis of the data reported in Table 1, where SR = O.B thickness/OS thickness.*

Based on previous assumptions, the government royalty ratio equation will be:

Y = (0.0148X-2.02)*(Oil content %) / SR .....(2)

Where; Y: Royalty %, X: FO price, SR: Stripping ratio.

As shown in Table 7, and based on equation (2), the royalty ratio is calculated for all deposits in relation to the different FO prices. Based on that, the royalty rate (JOD/t) can be obtained by equation (3). The results are shown in Figure 5.

Y (JD/t OS) = Y% * X .....(3)

Where; Y: Royalty %, X: FO price.

Table 7. Government royalty of different JOSh deposits according to equation (2).

	Area/ JOSh Deposit	Oil content percentage	SR	Y%, Oil price 200 J/t	Y%, Oil price 250 J/t	Y%, Oil price 300 J/t	Y%, Oil price 350 J/t	Y%, Oil price 400 J/t	Y%, Oil price 450 J/t	Y%, Oil price 450 J/t
1	Attarat Umm Ghudran	1	1.3	1.41	2.89	2.89	3.63	4.37	5.11	5.85
2	El-Lajjun	0.955	1.1	1.21	1.95	2.69	3.43	4.17	4.91	5.65
3	Eth Thamad	0.955	2	2.00	2.74	3.48	4.22	4.96	5.70	6.44
4	Sultani	0.881	2.2	2.15	2.89	3.63	4.37	5.11	5.85	6.59
5	Khan AzZabib	0.627	1.6	2.17	2.91	3.65	4.39	5.13	5.87	6.61
6	Wadi Maghar	0.618	1	1.71	2.45	3.19	3.93	4.67	5.41	6.15
7	Juf Ed-Darawish	0.518	0.7	1.47	2.21	2.95	3.69	4.43	5.17	5.91

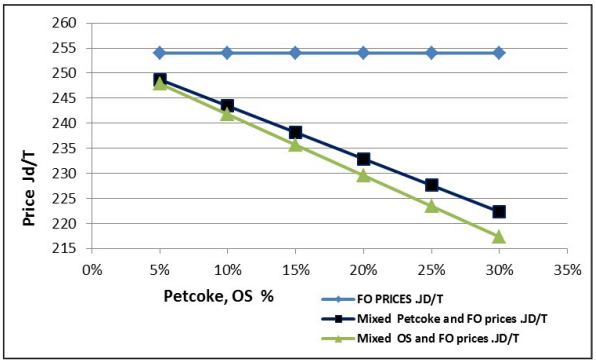

Figure 5. Royalty (JD/t) for major JOSh deposits.

Conclusion

In order for the Jordanian cement factories to save the fuel oil cost in cement manufacturing, they have to depend on alternative fuel resources such as natural gas, Petcoke, and oil shale. In Jordan, the energy sector depends primarily on imported crude oil. However oil shale is the only available indigenous fossil fuel resource. Jordan is a country with a large volume of Oil Shale reserves. One good strategy for the companies that manufacture cement in Jordan is the use of oil shale to partially substitute fuel oil in the cement production. In short Oils shale will be the alternative source of energy in the Jordanian cement factories. Also, oil shale ash is considered as an important additive raw material in cement. The results of this study show that the expected cost of one tonne of oil shale extracted from the mine and transported to the cement factory is 25.34 JOD (deduct 1.5 JOD saved after using oil shale ash in the cement industry). The cost of oil shale or Petcoke used in the fuel mixture is less than the cost of using pure fuel oil. As the oil shale or Petcoke ratios in the mixture increase, the saving rate will increase as well. The government royalty rate is calculated in order to control the mining operations and the quantities of the extracted oil shale. Therefore, the low-grade oil shale will not be excluded. By taking into consideration the variation in oil content percentage and the stripping ratio, the royalty equation gurantees justice for both the Jordanian government and the mining companies as well,. The formulated royalty equation can be applied in all oil shale mining projects in Jordan.

References

[1] Abed, A. M. (2000) The geology of Jordan and its environment and water (in Arabic). Publication of the Jordanian Geologists Association. Amman, Jordan.

[2] Abed, A.M.; Arouri, K.; Amiereh, B.S.; and Al-Hawari, Z. (2009) Characterization and Genesis of Some Jordanian Oil Shales. Dirasat, Pure Sciences. Vol. 36, No. 1. Pp 7-17.

[3] Alali, J. (2006) Jordan Oil Shale, Availability, Distribution, and Investment Opportunity. Unpublished report. The NRA, Jordan. Rtos-A117.

[4] Al-Hasan. M. (2006) Behavior of Concrete Made Using Oil Shale Ash and Cement Mixtures. Oil Shale. Vol. 23, No. 2. Pp. 135–143.

[5] Alnawafleh, H.M. and Fraige, F.Y. (2015) Analysis of Selected Oil Shale Samples from El-Lajjun, Central Jordan. Geomaterials, 5, 77-84. http://dx.doi.org/10.4236/gm.2015.53008.

[6] Alnawafleh, H.M., Fraige, F.Y., Al-khatib, L.A. and Dweirj, M.K. (2015) Jordanian Oil Shales: Variability, Processing Technologies, and Utilization Options. Journal of Energy and Natural Resources. Vol. 4. Pp 52-55. http://dx.doi.org/10.11648/j.jenr.20150404.11

[7] Besieso, M. (2007) Jordan's Commercial Oil Shale Strategy. 27th Oil Shale Symposium, Colorado, USA. 15-19 October 2007, 12 p.

[8] Brendow, K. (2002) Global Oil Shale Issues and Perspectives. Synthesis of the Symposium on Oil Shale held in Tallinn (Estonia) on 18 and 19 November 2002. World Energy Council, Geneva, Oil Shale, 2003, Vol. 20, No. 1, pp. 81-92.

[9] Dyni, J.R. (2006) Geology and Resources of Some World Oil-Shale Deposits. Scientific Investigations Report 2005- 5294, USGS, U.S. Geological Survey, Reston, VA, 42 p.

[10] Dyni, J.R. (2010) Oil Shale. In Clarke, A.W.; Trinnaman, J.A. (Eds.), 2010 Survey of Energy Resources. World Energy Council. London, UK. p. 93-123.

[11] ECRA (European Cement Research Academy) (2014) Modern Techniques used in the Industry for quality control of cement. Newsletter No. 1. Page 3. Available on line: https://ecraonline.org/fileadmin/ecra/newsletter/ECRA_Newsletter_1-2014.pdf

[12] Hamarneh, Y. (1998) Oil shale resources development in Jordan. Unpublished report. The NRA. Amman, Jordan.

[13] Jaber, J.O., Thomas A. Sladek, T.A., Mernitz,S., and Tarawneh, T. M. (2008) Future Policies and Strategies for Oil Shale Development in Jordan. Jordan Journal of Mechanical and Industrial Engineering. Vol. 2. No. 1. Pp 31-44.

[14] Jordan Lafarge Cement (2017) Jordanian Oil Shale in Cement Industry: Experience of Jordan Cement Company in utilizing Oil shale in Cement Process. Available on line: http://www.sdnp.jo. Accessed date: 11/11/2017 at 3:23 pm.

[15] MEMR (Ministry of Energy and Mineral Resources) (2016) Unpublished Annual Report. Amman, Jordan. 67pages. Available on line: http://www.memr.gov.jo/Pages/viewpage.aspx?pageID=190.

[16] Mokrzycki, E. and Bochenczyk, A. (2003) Alternative Fuels for the Cement Industry. Applied Energy.Vol. 74. No. 1-2. Pp. 95-100.

[17] Pufahl P. K., Grimm K. A., Abed A. M., and Sadaqah R. M. (2003) Upper Cretaceous (Campanian) Phosphorites in Jordan: Implications for the Formation of a South Tethyan Phosphorite Giant. Sedimentary Geology. Vol 161. Pp175-205.

[18] Smadi, M. and Haddad, R. (2003) The use of oil shale ash in Portland cement concrete. Cement and Concrete Composites. Vol. 25. Pp 43-50. DOI: 10.1016/S0958-9465(01)00054-3.

[19] Statista – The portal for statistics (2017) Chemicals & Resources: Fossil Fuels-Annual OPEC oil prices 1960-2017: Average annual OPEC crude oil price from 1960 to 2017. Available on Line: https://www.statista.com/statistics/262858/change-in-opec-crude-oil-prices. Accessed date 28/11/2017.

[20] Veiderma, M. (2003) Estonian Oil Shale – Resources and Usage. Estonian Academy of Sciences Tallinn. Oil Shale. Vol. 20, No. 3 Special. Pp. 295-303.

JJEES
Jordan Journal of Earth and Environmental Sciences

Volume 9, (Number 1), April, 2018
ISSN 1995-6681
Pages 63 - 66

Index Properties of Alkali-Activated Cement Mortar Affected by the Addition of Phosphatic Clay

Faten Mustafa Al-Slaty

Department of Earth and Environmental Sciences, Faculty of Natural Resources and Environment, The Hashemite University, Zarqa- Jordan.

Received 13 December, 2017; Accepted 18 April, 2018

Abstract

Phosphatic clay (PhC) is a by-product waste released from beneficiation processes during phosphatic mining. This study presents an analysis of the effects of PhC on the characteristics of the alkali-activated aluminosilicate mixture to formulate a cement mortar. The mix proportion of cement mortar was prepared from aluminosilicate materials (kaolin and silica sand). PhC was added to the mix proportion with an appropriate ratio. The quality-indicating parameters were tested. The results indicated that, the bulk density of hardened mortar increased from 2 g/cm^3 to 2.21 g/cm^3. The compressive strength accounted for the 12.5% improvement. The cement mortar absorbed less amount of water and showed less shrinkage behavior. This study found that using PhC as admixture in activated aluminosilicate cement mortar shows a tendency to improve the index properties of the activated mortar.

Keywords: Phosphatic clay, by-product materials, mining wastes, activated aluminosilicates, cement mortar

1. Introduction

Phosphate is one of the most essential commodities mined in large quantities yearly around the world. It is considered as the main source of the element phosphorus used essentially in the agricultural sector as a form of fertilizer (Abu-Hamatteh, 2007). The phosphate layer, known as the matrix, is made up of nearly equal parts of sand, clay, and phosphatic minerals (Beavers et al., 2015). Jordan has huge resources and reserves of phosphate with high quality P_2O_5 content in the middle of country; namely in Al Hassa area, Al-Abiad area, and Eshidiya area (Sadaqah, 2000). The mines require processing of flotation and beneficiation to reduce the content of accessory minerals, including quartz, clay, calcite, and dolomite (Abouzeid & Seifalnassr, 1996). The process of beneficiation depends upon the grain size. The Phosphate pebble is separated by a series of screens and washers, then the concentrates are utilized directly. The finer material is separated from the final phosphate concentrate as waste tailings, thus so-called phosphatic slime (Pittman and Sweeney, 1983). A typical mine can generate millions of tons of phosphate clay tailings annually. On the whole, for each ton of phosphate produced, approximately one ton of clay must be disposed (El-Shall, 2009). In Jordan, almost 10,000 tons of clay waste are produced daily during the phosphate beneficiation and flotation processes at the Eshidiya mine (Al-Hwaiti et al., 2015). This product is dispersed in water as a dilute colloidal suspension. The use of a conventional clay settling areas is the dominant method of storing phosphatic clay during the phosphate mining operations (Beavers et al., 2015). The PhC creates one of the most difficult disposal problems in the mining industry, due to the pollution of streams by turbid or toxic effluents (Abouzeid and Seifalnassr, 1996). The PhC of the Jordanian phosphate mines was characterized by several work studies (Khoury et al., 1988); (Al-Hwaiti, 2000); (Al-Hwaiti et al., 2005); and (Slaty, 2005). The solubility of PhC indicated that PhC can be used as a source material for the immobilization process of heavy metals.

Very little research has been done in the past on the utilization of PhC around the world. Goode and Sadler (1975) tested the PhC as a substitute for bentonite in geothermal drilling fluids. The results indicated that, PhC base drilling fluids have more favorable rheological behavior than bentonite base fluids but poorer filtration properties. Wissa et al. (1983); Hardianto & Ericson (1993), and Boyd et al. (2007) investigated the stabilization potential of PhC with different materials as a lime and gypsum. Srinivas et al. (2106) studied the possibility of recovering phosphate minerals from the rejects of the Eshidiya beneficiation plant. He found that PhC can be used for direct application in soils as phosphate-rich organic manure in highly saline soil. Khoury et al. (1988) estimated the possibility of utilizing PhC from El-Hasa and Russifaha phosphate mines in Jordan. He concluded that PhC is more suitable as a lightweight for thermal insulation due to the small density, low water absorption, and good thermal conductivity. In Jordan, a low-cost building material with an acceptable compressive strength (32 MPa) was developed through the alkali activation of Jordanian Hiswa kaolinite, and was assessed in several research papers by Khoury and Al-Shaaer (2009); Al-Shaaer et al. (2009); and Slaty et al. (2013). Physical, thermal, mineralogical and microstructural results indicate that the activation process has decreased the porosity due to the formation of sodium zeolite phases and feldspathoids that fill the pore spaces and bind the matrix.

In this study the potential utilization of PhC in constructions as a cement admixture is examined by studying

* Corresponding author. e-mail: fatenm@hu.edu.jo

the effects of adding PhC on the index properties of hardened aluminosilicate mortar through alkali activation.

2. Methodology

2.1. Characterization of PhC

The PhC sample of this study was collected from Al-Hasa Phosphate Mine plant (about 130 km south of Amman, Jordan). The sample was collected directly from hydrocyclones after the beneficiation process. Filtration was done to separate the fine particles of PhC from water. The sample was oven-dried at 105 ºC for twenty-four hours. Its color was determined by visual observation. The specific gravity was measured by the standard testing methods ASTM D854-00, using the pycnometer. The particle size distribution was determined using sieve analysis and hydrometer methods (for particle sizes pass sieve No. 200), according to ASTM D 422. The Atterberg limits were determined according to ASTM D4318-17. The chemical and mineralogical composition of PhC was determined using X-ray diffractometers (XRD) by Philips 2KW model and SHIMADZU Sequential X-ray Fluorescence Spectrometer (XRF) at the University of Jordan.

2.2. Preparation of cement mortar

An activated cement mortar from Jordanian kaolinite was developed and characterized previously by the researchers (Khoury and Al-Shaaer, 2009); (Al-Shaaer et al., 2009); and (Slaty et al., 2013). The activated cement mortar was prepared by the alkali activation of untreated kaolinite (HK) from a deposit in Hiswa area (South Jordan). HK consists mainly of 74% of silica (SiO_2) and alumina (Al_2O_3) of the total content. The selected grain size was less than 425µm after the crushing and sieving of the oven-dried sample (at 105 °C). Silica sand (SS) was used as an inert filler (with purity being about 99% and the grain size between 90 and 250 µm) to improve the workability of the mixture and its mechanical strength. NaOH pellets of 99% purity (Merck) and distilled water were used to prepare 16 M of alkaline activator for dissolution aluminosilicate phases. The mixing process of the constituents was done according to the following equation.

$$\underset{\text{(Kaolinite)}}{Si_2Al_2O_5(OH)_4} + 2NaOH \xrightarrow{H2O} \underset{\text{(Feldspatoid or Hydroxysodalite)}}{Na_2Si_2Al_2O_5(H_2O)_6} \quad .....(1)$$

In order to investigate how PhC affects the activated mortar characteristics, two mixtures of raw materials were prepared. The first mix was composed of 2HK: 1SS proportion, and acted as the reference mixture. The second mix was composed of 2HK:1SS:1PhC proportion, to investigate the potential influence of PhC on the final quality of the product. The water ratio was added according to the plasticity limit of each mixture. The prepared mixture was mixed for 10.0 minutes to obtain a homogenized paste. The produced cement paste was molded and processed at the 60.0 °C for twenty-four hours. The final activated mortars were dried at room temperature in lab conditions for seven days and characterized. The unconfined compressive strength was tested by the CBR Tester device according to ASTM C39/C39M-18.

2.3. Characterization of cement mortar

The effect of adding PhC to the activated cement mortar was evaluated by calculating the mortars density (the ratio between the weight and volume of the cement mortar after curing). The amount of water absorption after immersing the mortars in de-ionized water for seven days (ASTM C187-16), according to equation 2:

$$A = ((W_w - W_d)/W_d) \times 100 \quad .....(2)$$

Where A is the absorption of water expressed in percentage, W_w is the weight of the immersed specimen (g), and W_d is the weight of the dry specimen after curing (g).

The shrinkage percentage was tested by measuring the change in the height of cement mortars after storage in dry conditions for twenty-one days (ASTM C827/C827M-16). According to the S equation:

$$S = [(H_0 - H_1)/H_0]*100 \quad .....(3)$$

Where S is the difference in specimens high after curing (H_0) and after twenty-one days of storage at room temperature (H_1).

3. Results and discussion

3.1. Characterization of PhC

The PhC sample was characterized physically by testing the color appearance, specific gravity of solids (Gs), Atterberg limits (LL, PL, and PI) and hydrometer analysis to obtain the physical properties of PhC as presented in table 1. The collected sample of the PhC appeared as fine particles with a light creamy yellow color. The Gs was 2.43 g/cm^3. The particle size analysis indicated that about 68% of PhC particles are in the range of silt fraction size (< 0.075 mm). The plasticity indices of LL, PL, and PI, are 33%, 21%, and 12%, respectively. According to USCS classification, the plasticity index of the present PhC is medium plastic sediments. The clay activity depending on the ratio between the plasticity index and clay size particle percentage indicated that PhC is a less active material. According to Skempton (1953), when the activity is less than 0.75 the material has low-volume change when wetted and low shrinkage when dried.

Chemically, PhC consists mainly of about 34.40% silica (SiO_2), 32.35% lime (CaO), and 19.46% phosphorous (P_2O_5), as shown in table 2. PhC contain also a high concentration of some trace elements like, Cr, Ni, Sr, V, Zn, and U. Most of the trace elements are substituted in apatite and clay minerals or are adsorbed by organic matter in the phosphatic ore; being washed out after the beneficiation process causes a concentrate of these elements in the PhC (Dudka et al., 1994); (Al-Hwaiti, 2000).

Table 1. Physical properties of PhC

Color	Yellow or creamy
Gs	2.43 g/cm^3
Particle size distribution Texture USCS	7% Fine sand, 68% silt, 24% clay Silt clay loam CL
Plasticity Limits Degree of plasticity Activity = PI / (% clay particles)	33% LL, 21% PL, 12% PI Medium plasticity 0.5%

Table 2. Major element composition of PhC

Major oxides	Al_2O_3	CaO	Fe_2O_3	K_2O	MgO	Na_2O	P_2O_5	SiO_2	SO_3	LOI
%	1.45	33.35	1.02	0.09	0.71	0.86	19.46	34.40	0.51	6.22
Traces	Cd	Cr	Cu	Ni	Sr	V	Zn	Zr	U	
PPm	3.23	231.80	15.41	97.21	575.31	127.94	132.58	18.27	45.72	

The X-Ray Diffractogram of the PhC is shown in Fig.1. The result indicated that the PhC is composed mainly of quartz, calcite, and carbonate apatite minerals as well as a minor amount of kaolinite and montmorlonite. PhC is represented as an argillaceous matrix that intercalated with all phosphate beds associated with pellets, teeth, and bones in the phosphatic ore (Khoury et al., 1988). The main conclusion from previous studies is that PhC should not be directly discharged into the environment (Slaty, 2005); (Al-Hwaiti et al., 2014). The utilization of PhC in industrial applicatios is considered as an effective waste management plan.

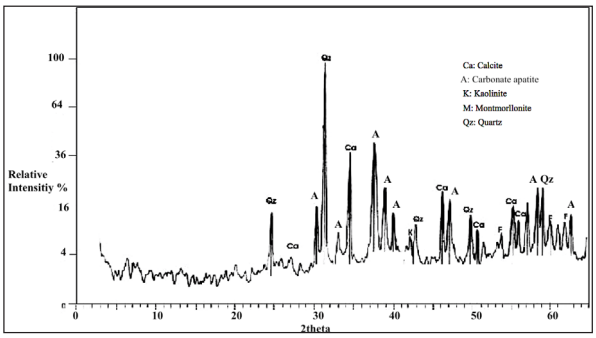

Figure 1. X-ray diffractogram of PhC

3.2. Characterization of the cement mortar

The effects of the addition of PhC to the aluminosilicate mixture were investigated by studying the changes in the index properties of cement mortars as presented in table 3. The workability of the cement mixture is largely dependent on the amount of added water. The ratio of water was measured according to the plasticity limits for solid components over which the mixture is in the plastic behavior. The plastic limit of HK as a raw material was around 30%.

The plasticity limit of 2HK: 1SS and 2HK: 1SS: 1PhC mixtures were 22% and 28%, respectively. The Addition of SS to HK already decreased the plasticity limit due to the increased porosity and air content. On the other hand, the adding of PhC to the aluminosilicate mixture resulted in increasing the limit of plasticity for the cement mixture. The increase of water content provides greater lubrication and helps increase the workability of the cement paste (Johnson, 1926); (Yen et al., 2012). The addition of PhC to the cement mixture resulted in increasing the mortar density (2.21 g/cm^3) because of the increased plasticity limit. This has immensely affected the strength of the cement mortar giving the mortar more stiffness (Yen et al., 2012). After adding the PhC content, the activated cement mortar absorbed less water in immersing conditions for seven days of about (8.4%) compared to (10%) in the reference mortar. The shrinkage test indicated that the addition of PhC caused less shrinkage in the cement mortar of about (0.08%) compared to (1,5 %) in the reference mortar . The compressive strength test showed increase in the mortar strength after adding the PhC (36.48 MPa), compared to (32.53 MPa) of the reference mortar. This study found that the addition of PhC to aluminosilicate mixture could simultaneously accelerate the activation process and achieves better performance.

Table 3. The index properties of the activated cement mortars

	2HK:1SS (Reference)	2HK:1SS: 1PhC
Pl%	22.0	28.0
Bulk Density (g/cm^3)	2.0	2.21
Water absorption%	10.0	8.4
Shrinkage %	0.15	0.08
Compressive Strength (MPa)	32.53	36.48

Conclusion

PhC is a medium plastic moldable material. In accordance with the results of this study, adding PhC with an appropriate ratio to the aluminosilicates mixture improve the characteristics of the cement mortar. The results showed an increase in the mortar density and the compressive strength of the cement mortar and a decrease in the percentage of water absorption and shrinkage. On the basis of these results, PhC could be a situable by-product waste to be used in constructions as a cement admixture. After all, it can be truly useful for managing the huge amounts of PhC produced daily from the phosphate mines. However, further experiments on the quality and permanence of the cement mortar are recommended.

Acknowledgement

The author would like to thank the Jordan Phosphate Mines Company (JPMC) for their help in the sampling process. Many thanks go to the analysts at the Hashemite University for their technical support.

تأثير اضافة مادة الطين الفوسفاتي في خواص قوالب الاسمنت المفاعل قلويا

فاتن مصطفى السليتى

قسم علوم الأرض والبيئة – الجامعة الهاشمية – الأردن

خلاصة

يهدف هذا البحث الى دراسة تأثير اضافة مادة الطين الفوسفاتي – التي تطرح من عملية تركيز الفوسفات الاردني– في خواص القوالب الاسمنية المصنعة من مواد قليلة التكلفة. يهدف البحث في امكانية اعادة استخدام هذه المادة في البناء عوضا عن طرحها في برك طينية حيث تتراكم بكميات ضخمة مع زيادة عملية التعدين ويتزايد تركيز العناصر الثقيلة فيها مما يجعلها تشكل خطرا على النظام البيئي في منطقة التعدين. خلال الدراسة تم تحضير خليط اسمنتي من مواد المنيوسيلكاتيه ومفاعلته قلويا لتشكيل قوالب اسمنتية قوية ومتماسكة. ومن ثم تشكيل قوالب اسمنتية من نفس الخليط الاول مضافا له نسبة٢٥٪ من مادة الطين الفوسفاتي. وقد دلت الفحوصات المخبرية للخواص الاساسية للقوالب الاسمنية المحضرة، ان كثافة القوالب الاسمنتية قد زادت بعد اضافة الطين الفوسفاتي لها مما ادى الى زيادة في قوة القوالب الاسمنتية. وقد اشارت النتائج الى حدوث انخفاض في قابلية العينات لامتصاص الماء والانكماش في حجم العينات. وقد اوصت الدراسة بان امكانية استخدام هذه المادة مع خليط من المواد الالومنيوسيلكاتية يعتبر مجدي لتحسين خصائص الخليط الاسمنتي.

References

[1] Abouzeid, A. Z., & Seifelnassr, A. S. 1996. Polymeric Flocculation of Phosphate Slimes. Fizykochemiczne problems mineralurgii (30): 71-83.

[2] Abu-Hamatteh, Z. 2007. Geology, Geochemistry and Ore Characteristics of the Jordanian Phosphates. Central European Geology, (50/3): 283–295.

[3] Al-Hwaiti, M. 2000. Geostatistical and Geochemical Investigation on Eshidiya Phosphorites, Western Ore body, South Jordan: variation in ore composition and its content of toxic heavy metals available for plant absorption. Ph.D Thesis, University of Jordan.

[4] Al-Hwaiti, M. Ali, Q. M. Saffarini, G. & Al-Zhughoul, K. 2014. Assessment of Elemental Distribution And Heavy Metals Contamination In Phosphate Deposits: Potential Health Risk Assessment Of Finer-Grained Size Fraction. Journal Environmental Geochemistry and Health. (36): 651–663.

[5] Al-Hwaiti, M. S., Brumsack, H. J., & Schnetger, B. 2015. Fraction Distribution and Risk Assessment of Heavy Metals in Waste Clay Sediment Discharged Through the Phosphate Beneficiation Process in Jordan. Environ Monit Assess. 187-401

[6] Al-Shaaer, M., Slaty, F., Khoury, H, Rahier, H., & Wastiels, J. 2009. Development of Low-Cost Functional Geopolymeric Materials. Ceramic Transactions, Advances in Materials Science for Environmental and Nuclear Technology, (222): 159–167.

[7] Beavers, C., Hanlon, E., Wilson, M., Cates, J., & Hochmuth, G. 2015. Sand-Clay Mix in Phosphate Mine Reclamation: Characteristics and Land Use. IFAS Extension. University of Florida. SL423.

[8] Boyd, A. J., Birgisson, B., Beatty, C. & Zaman, A. 2007. Utilization of Phosphatic Clay Waste in Concrete, Final Report prepared for Florida Institute of Phosphate Research. Pub. No. 02-164-223

[9] Dudka, S., Piotrowska, M., & Chlopecka, A. 1994. Effect of Elevated Concentrations of Cd and Zn in Soil on Spring Wheat Yield and the Metal Contents of the Plants. Water, Air, and Soil Pollution. (76): 333–341.

[10] El-Shall, H. 2009. Field Demonstration and Evaluation of Rapid Clay Dewatering and Consolidation Process Using other Wastes (FIPR/DIPR Process) to Minimize Clay Setting Ponds. Final Report prepared for Florida Institute of Phosphate Research. Pub. No. 02-168-232.

[11] Goode, A. & Salder, L. (1975) Substitution of Phosphate Slime for Bentonite in Geothermal Well Drilling Fluids. Report of investigation 8032. U.S. Bureau of mines.

[12] Hardianto, F. S., & Ericson, W. A. 1993. Stabilization of Phosphatic Clay Using Lime Columns. Final Report Prepared for Florida Institute of Phosphate Research. . Pub. No. 02-088-102.

[13] Johnson, H. V. 1926. Cement-Lime Mortars. Technologic Papers of the Bureau of Standards, Vol. 20.

[14] Khoury, H., Al-Hawari, Z., & El-Suradi, S. 1988. Clay Minerals Associated With Jordanian Phosphates and their Possible Industrial Utilization. Elsevier Science (3): 111-121.

[15] Khoury, H. & Alshaaer, M. 2009. Production of Building Products through Geopolymerization, Proceeding of the Global Conference on Renewable and Energy Efficiency for Desert Regions (GCREEDER 2009, Amman-Jordan. pp. 1-5.

[16] Pittman, W. E., Jr., & Sweeney, J. W. 1983. State-Of-The-Art of Phosphatic Clay Dewatering Technology and Disposal Techniques: A Review of Phosphatic Clay Dewatering Research. Florida Institute of Phosphate Research. Pub. No. 02-017-021.

[17] Sadaqah, R. 2000. Phosphogenesis, Geochemistry, Stable Isotopes and Depositional Sequence of the Upper Cretaceous Phosphorite Formation in Jordan, Ph.D. Thesis, University of Jordan.

[18] Skempton, A.W. 1953. The Colloidal Activity of Clays. Proc. 3rd Int. Conf. Soil Mech. Found. Eng. vol.1, pp. 57-61.

[19] Slaty, F. 2005. Environmental Aspects of Phosphate Beneficiation Processes in Al-Abeid Mine, Central Jordan: Migration and Dispersion of Heavy Metals in the Sediment, Soil and Water Systems, M.Sc. Thesis, The Hashemite University.

[20] Slaty, F., Khoury, H., Wastiels, J., & Rahier, H. 2013. Characterization of Alkali Activated Kaolinitic Clay. Appl. Clay Sci., 75(76): 120–125.

[21] Srinivas, K., Dassin, Y., Prabhulingaiah, G., & Sekhar, D. 2010. Utilization of Eshidiya Phosphate Beneficiation Plant Rejects. Final Report for Jordan Phosphate Mines Company Limited, Eshidiya Mines, Jordan.

[22] Wissa, A., Fuleihan, N., & Ingra, T. 1983. Evaluation of Phosphatic Clay Disposal and Reclamation Methods, Florida Institute of Phosphate Research.Vol. 4: Consolidation Behavior of Phosphatie Clays.

[23] Yen, C. L., Tseng, D. H., & Wu, Y. Z. 2012. Properties of Cement Mortar Produced from Mixed Waste Materials with Pozzolanic Characteristics. Environ Eng Sci., 29(7): 638–645.

JJEES
Jordan Journal of Earth and Environmental Sciences

Volume 9, (Number 1), April, 2018
ISSN 1995-6681
Pages 67 - 74

Analyses of Climate Variability in Jordan using Topographic Auxiliary Variables by the Cokriging Technique

Mohammed I. Al-Qinna

Department of Land Management and Environment, Faculty of Natural Resources and Environment, The Hashemite University, Zarqa, Jordan

Received 13 December, 2017; Accepted 18 April, 2018

Abstract

Climatic variability in Jordan is unequivocal resulting from various atmospheric circulations that have complex site-specific characteristics. Trends of change in daily and monthly precipitation, mean air temperature, maximum air temperature, minimum air temperature, relative air humidity, and potential evapotranspiration across the country were investigated by the Mann-Kendall rank and linear regression trend tests using long-term historical meteorological data collected on daily and monthly bases from about 143 stational points. Trend tests indicated significant changes at both national and station levels, where the mean annual precipitation tended to decrease significantly by time at a rate of 1.2 mm per year. Mean air temperature, maximum air temperature, minimum air temperature, relative humidity, and mean annual potential evapotranspiration all tended to increase significantly by 0.02°C/year, 0.01°C/year, 0.03°C/year, 0.08%/year, and 17mm/year, respectively.

The Integrated Geographic Information System (GIS), and a geostatistic approach were used for spatial interpolation of selected climatic variables. Cokriging fine resolution maps were generated from integrating climatic variables with elevations obtained from digital elevation maps. The cross validations indicated the efficient use of auxiliary information to aid the interpolation with a very high coefficient of determination and low root mean square errors. The cokriging with elevation as an auxiliary variable is a very flexible and robust interpolation method that exhibited great improvement for estimating several climatic variables in the country.

Keywords: Cokriging, digital elevation model, climatic variability, Jordan

1. Introduction

Warming of the climate system is unequivocal. Since the 1950s, many of the observed changes are unprecedented over decades to millennia (IPCC, 2007). The increase in concentrations of greenhouse gases (GHGs) was detected to be mainly responsible for the atmosphere and ocean warming, changes in the global water cycle, reductions in snow and ice, global mean sea level rise, and changes in some climate extremes. It is *extremely likely* that human influence has been the dominant cause of the observed warming since the mid-twentieth century (IPCC, 2013).

The globally-averaged land and ocean surface temperature has risen from 0.85 [0.65 to 1.06] °C over the period from 1880 to 2012. Continued emissions of GHGs will cause further warming and changes in all components of the climate system. Climatologists project that the tempreture may rise another 0.3 and 4.8 **°C** over the next century depending on the world's ability to reduce emissions (IPCC, 2014).

Many of the world countries, including the Hashemite Kingdom of Jordan, already struggle under various pressures such as water scarcity, food insecurity, ecological, economical and social development (MoEnv, 2012). These pressures will be significantly exacerbated by the climate change creating several hazards for many regions such as reduced rainfall, increased temperatures, increased frequency and intensity of floods, increased chances of the occurrences of weather extreme events (e.g. flash floods and warm waves), intensified erosion, reductions in snow cover, sea-level rise, and damage to water quality and ecosystems (MoEnv, 2013; UN, 2009). In order to improve climate change resilience, proper understanding of the current and future climate changes are acquired.

Several investigations of the variability of the meteorological parameters in Jordan were conducted over the last decade (Abandeh, 1999; Al-Ansari et al., 1999; Al-Houri, 2014; Al-Qinna et al., 2011; Bani-Domi, 2005, Dahamsheh and Aksoy, 2007; Freiwan and Kadioglu, 2006; Freiwana, and Kadioğlu, 2008; Ghanem, 2010; Ghanem, 2011; Ghanem, 2013; Matouqa, et al., 2013; Ragab and Prudhomme, 2002; Smadi and Zghoul, 2006; Tarawneh and Kadioğlu, 2002)

Most of the literature indicated the existence of huge spatial and temporal variability especially in precipitation with unclear and/or insignificant trends of increase or decrease at station levels (MoEnv, 1999; MoEnv, 2006; MoEnv, 2009; MoEnv, 2012; MoEnv, 2013; MoEnv, 2014a; MoEnv, 2014b). However, researchers were able to conclude that the reliability of data in terms of availability, accuracy, and precision play an important role in the final results. The spatial and temporal meteorological trends vary by data source, measurement techniques, and accuracy assessment, especially when dealing with missing values. Limited data and the lack of models and tools specifically designed for local conditions result in high uncertainty regarding the impact of climate change on Jordan (MoEnv, 2013).

* Corresponding author. e-mail: qinna@hu.edu.jo

Up to now, there is a lack of understanding of the consequences of climate change at the local level due to imprecise status analyses of the historic and current climatic variability As a consequence, decision-makers are unable to link the regional and national conditions with the global conditions, which hampers their ability to take the most appropriate planning decisions regarding vulnerability and adaptation. One of the best methods used to reduce the prediction errors is the cokriging technique with well-defined auxiliary variables such as elevation (Goovaerts, 2000; Diodato, 2005). The multivariate geostatistical incorporating of the digital elevation model into the spatial prediction of climatic variables such as precipitation yields more accurate predictions (Wang et al., 2011; Adhikary et al., 20017). The objective of this paper is to investigate the climatic variability through the trend analyses of many long reliable historical climatic data across the country, and to generate detailed climatic spatial interpolation maps through integrating the geographic information system and the geostatistic approach of cokriging with elevation as an auxiliary variable.

2. Methodology

2.1. Study Area

Jordan is located about 80 km to the East of the Mediterranean Sea between 29º 11´ to 23º 22´ North, and 34º 19´ to 39º 18´ East. Its predominant Mediterranean climate is characterized hot dry summers and wet cool winters.

Jordan is divided into three main climatic regions (FAO, 2012); the Ghor Region (lowlands), the Highlands, and the Badia or Desert region (Figure 1). The Lowlands region is part of the Great Rift Valley with elevation ranging from 197 m below MSL in the north to 417 at the Dead Sea. The lowlands consist of three parts; the Jordan River, the Dead Sea, and Wadi Araba. The Highlands and the Marginal Steeps Region extend north-south to the east of the Ghor, i.e. from the Yarmouk River in the north to Ras El-Naqab in the south. The mountain peaks' elevation varies from 1150 m above MSL in Ras Muneef to 1365 m above MSL in Al–Shoubak, and exceeds 1500 m above MSL at El-Qurain. The Desert Region extends north to south from the eastward foot of the Highlands with elevation ranging from 600 to 750 above MSL.

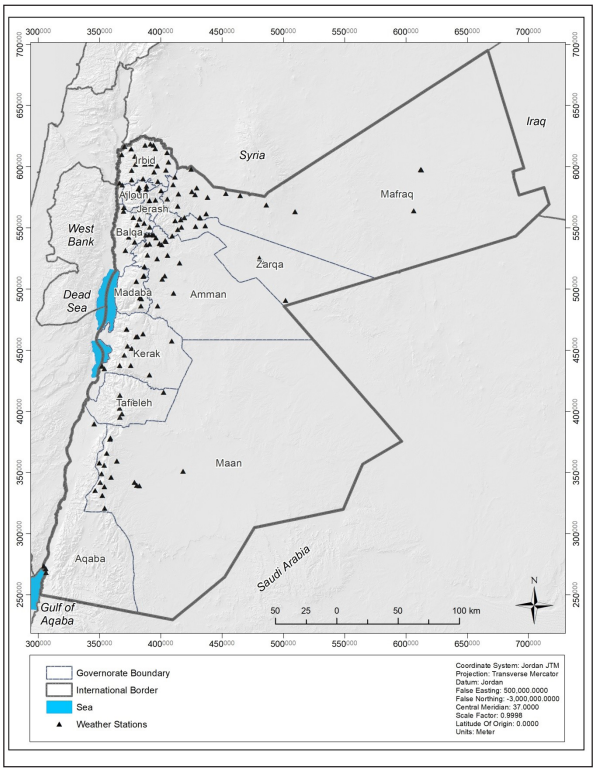

Figure 1. Meteorological stations locations within the Jordan study area.

2.2. Data Sources and Description

Although there are many stational points available within the country, reliable and continuous local daily meteorological data sets were selectively obtained from both the Jordanian Meteorological Department (JMD) and the Ministry of Water and Irrigation (MWI) for the period between (1961-2012). For precipitation, a total of 143 station points (twenty-four station points from JMD and 119 station points from MWI) were implemented in this study. On the other hand, only forty meteorological stational points (twenty-four station points from JMD and sixteen station points from MWI) were selected for the following climatic variables: mean temperature, maximum temperature, minimum temperature, relative humidity, and Class A-Evaporation Pan (Figure 1).

Weather data quality-assessment, including outlier detection and filling missing values, was achieved using the Quality Control (QC) tool to assess the validity of weather data of long-term stations. Both threshold and step-change tests were conducted using JMP statistical software (Guttman et al., 1988; Fiebrich et al., 2010; Shulski et al., 2014). On the other hand, missing values were treated in four different manners depending on the range of the gap; mean substitution, simple regression, multiple regressions, and spatial distribution based on the nearest station (Kotsiantis et al., 2006; Grzymala-Busse Hu, 2001).

2.3. Trend Analyses

The climatic trend of a monotonic increase or decrease in the average meteorological values between the beginning and the end of an available time series was detected using two methods: (1) the linear regression trends, and (2) the nonparametric "Mann-Kendall rank trend test" (Kendall, 1975; Mann, 1945; Nelsen, 2001). The trend analyses were cnducted on both monthly and yearly bases to assess monotonic changes dominancy over the historical period using the JMP statistical software (version 11) (JMP, 2014).

2.4. Spatial Variability

Before commencing the modeling analysis, it was useful to identify the strength of the relationships between the climatic variables and the auxiliary variables such as altitude. This was achieved by creating a Pearson's product moment correlation matrix using Equation (1).

$$r = \frac{\sum_{1}^{n}(Z_i - \bar{Z})(A_i - \bar{A})}{\sqrt{\sum_{1}^{n}(Z_i - \bar{Z})^2}\sqrt{\sum_{1}^{n}(A_i - \bar{A})^2}} \quad \text{.....(1)}$$

where n is the number of observations, Z_i is the selected climatic variable, A_i is the auxiliary variable, is the mean of the first selected climatic variable, and is the mean of the auxiliary variable. The strength of the correlation was classified into three levels: weak correlation when $0 \leq |r| < 0.3$, moderate correlation when $0.3 \leq |r| < 0.6$, and strong correlation when $0.6 \leq |r| \leq 1.0$.

In order to have a fine resolution map for the climatic variables across the country (i.e. down to 30m pixel range), spatial interpolation was achieved using the ordinary Co-kriging technique between the climatic variable and the altitude, taking into account the existing huge variability of the altitudes within the country.

Cokriging is a method for interpolation that minimizes the variance of the estimation error by exploiting the cross-correlation between several variables, thus the cross-correlated information contained in the auxiliary variable will help reduce the variance of the estimation errors (Wackernagel, 1995; Journel, 1986; Journel, 1989; Isaaks and Srivastava, 1989). The digital elevation map (DEM) including altitude, orientation, slope, roughness, and encasement was obtained from the Royal Jordanian Geographic Center on a 30 m interval.

A multiple regression technique was adopted to interpolate the climatic variable of magnitude at an unknown pixel (i.e. between the climatic variable and DEM data). The cross-correlation was achieved using geostatistical tools within Arc Map (ArcGIS 10.3, ESRI, 2017). The ordiniary cokriging assumes the following two equations (2) and (3):

$$Z(x) = \mu_1 + \varepsilon_1(x) \quad \text{..... (2)}$$

$$A(x) = \mu_2 + \varepsilon_2(x) \quad \text{..... (3)}$$

where Z(x) is the climatic variable of interest at location x, A(x) is the covariate/auxiliary at location x, μ_1 and μ_2 are unknown constants, $\varepsilon_1(x)$ and $\varepsilon_2(x)$ are random errors representing autocorrelation of Z variable and cross-correlation between Z and A, respectively.

The unknown value Z_0 at any pixel is then a linear combination of N values of two regionalized variables. The general equation for a two-variable cokriging was estimated locally within each set of the neighborhood control points using Equation (4) (Goovaerts, 2000).

$$Z_0 = \sum_{i=1}^{n} W_i Z_i + \sum_{j=1}^{n} \beta_j A_j + \beta_0 A_0 \quad \text{..... (4)}$$

where Z_0 = the estimate at the unknown location, W_i = the undetermined weight assigned to Zi varying between 0 and 100 %, Zi = the regionalized variable at a given location, with the same units as for the regionalized variable, Ai = the auxiliary regionalized variable co-located with Zi, with the same units as for the secondary regionalized variable, β_j = the undetermined weight assigned to Ai varying between 0 and 100 %, A_0 = the auxillary variable located at the target location, with the same units as for the secondary variable, and β_0 = the undetermined weights assigned to A_0 varying between 0 and 100 %.

$$\gamma_{za} = \frac{1}{2N(h)} \sum_{i=1}^{N(h)} [Z_i(x) - Z_i(x+h)] \times [A_i(x) - A_i(x+h)] \quad \text{..... (5)}$$

The cokriging accuracy were investigated using cross-validation between actual measured values and predicted climatic variables at the same pixel using the root mean square error (RMSE) and the coefficient of determination (r) performance indicators as indicated by Equations (5) and (6) respectively.

$$RMSE = \frac{1}{n} \sum_{i=1}^{n} [Z_i(x) - Z_i(x)] \quad \text{..... (6)}$$

$$r = \frac{\{\sum_{i=1}^{n} [Z_i(x) - Z_i(x)] \times [Z_i(x) - \bar{Z}_i(x)]^2\}}{\sum_{i=1}^{n} [Z_i(x) - Z_i(x)]^2 \times \sum_{i=1}^{n} [Z_i(x) - \bar{Z}_i(x)]^2} \quad \text{..... (7)}$$

where (x) is the predicted climatic variable at location x using the cokriging technique.

3. Results and Discussion

3.1. Trend Analyses

According to the preliminary statistical description of all the tested climatic variables, there exist clear trends either decreasing or increasing with time as indicated by both Mann-Kendall and linear trends (Table 1). The resulted trends are a clear evidence of climate change in Jordan over the last fifty years.

According to the historic climatic linear analyses, the annual precipitation tends to decrease significantly (P<0.0021) by time with an average rate of 1.2 mm/year (ranging from 0.5 to 2.2 mm/year regarding the stational point). On the contrary, the mean, maximum and minimum air temperatures tend to increase significantly by 0.02, 0.01, and 0.03 °C/year, respectively. On the other hand, the relative humidity and mean annual potential evapotranspiration tend to increase significantly by an average of 0.08 %/year and 17mm/year.

Table 1. Mann-Kendall trend statistics of climatological time series for selected climate variables for all of Jordan.

	Mann-Kendall τ	Prob>|τ|	R	RMSE	Linear Model	P value
Precipitation	-0.0590	0.0044*	-0.0964	184.1829	= 2632.01 - 1.214*YEAR	0.0021*
Mean Temp	0.0930	<.0001**	0.0933	3.282705	= -24.31 + 0.022*YEAR	0.0039*
Max Temp	0.0424	0.0463*	0.0463	3.583504	= 2.02 + 0.012*YEAR	0.1425
Min Temp	0.1104	<.0001**	0.1098	3.430952	= -41.07 + 0.027*YEAR	0.0005**
Relative Humidity	0.0663	0.0056*	0.1125	7.678434	= -102.14 + 0.080*YEAR	0.0015*
Evapotranspiration	0.1501	<.0001**	0.2357	189.5767	= 16370.75 + 17.052*YEAR	<.0001**

** sign indicates significant trends at the 5 percent confidence level, and ** sign indicates significant trends at the 1 percent confidence level.*

The trend statistics of precipitation on a monthly basis indicated that the reduction is highly significant during the whole rainy season (which extends from October to May of the next year) except for January where it increases by time (Table 2). The maximum rate of decrease was during March followed by January, while the maximum increase was found to be associated with February with a rate of 0.245mm/year. Coinciding with (Salahat and Qinna, 2015), the trends show a clear shift in the rainy season with significant narrowing of precipitation magnitudes; however, the rate of decrease in rainfall seems to be affecting not only the quantities but also the number of rainy days.

Table 2. Historic Trend Analyses of Average Monthly Precipitation across the country.

	Month	Linear Model	Mann-Kendall τ	Prob>|τ|	R^2	RMSE	Prob > F
Precipitation	JAN	= 567.57 - 0.259 * Year	-0.0179	0.3848	0.0047	55.273	0.0241*
	FEB	= -440.65 + 0.245 * Year	0.0581	0.0047*	0.0043	54.712	0.0313*
	MAR	= 861.15 - 0.416 * Year	-0.124	<.0001**	0.0217	40.839	<.0001**
	APR	= 435.65 - 0.213 * Year	-0.1272	<.0001**	0.0176	23.300	<.0001**
	MAY	= 79.96 - 0.039 * Year	-0.005	0.8214	0.0070	6.754	0.0062*
	JUN	= -4.89 + 0.003 * Year	0.0005	0.9834	0.0007	1.463	0.4013
	JUL	= -0.26 + 0.0001 * Year	0.0156	0.532	0.0001	0.168	0.6995
	AUG	= -0.66 + 0.0003 * Year	0.0067	0.7889	0.0008	0.181	0.3676
	SEP	= -13.38 + 0.007 * Year	0.1123	<.0001**	0.0063	1.265	0.0089*
	OCT	= 60.53 - 0.027 * Year	-0.0301	0.1603	0.0011	11.799	0.2769
	NOV	= 149.46 - 0.064 * Year	-0.0704	0.0007**	0.0008	33.249	0.3551
	DEC	= 1066.97 - 0.516 * Year	-0.0678	0.001**	0.0208	51.935	<.0001**
Mean air temperature	JAN	= -9.09 + 0.009 * Year	0.0776	0.017*	0.0014	3.421	0.2447
	FEB	= 4.88 + 0.003 * Year	0.0339	0.2973	0.0001	3.474	0.7335
	MAR	= -11.06 + 0.012 * Year	0.0579	0.0749	0.0024	3.558	0.1325
	APR	= -23.85 + 0.021 * Year	0.1032	0.0015**	0.0075	3.428	0.0078**
	MAY	= -20.71 + 0.021 * Year	0.0947	0.0036**	0.0077	3.454	0.0070**
	JUN	= -10.74 + 0.018 * Year	0.0855	0.0085**	0.0052	3.506	0.0258*
	JUL	= -43.08 + 0.035 * Year	0.1459	<.0001**	0.0188	3.601	<.0001**
	AUG	= -37.16 + 0.032 * Year	0.1376	<.0001**	0.0155	3.648	0.0001**
	SEPT	= -19.401 + 0.022 * Year	0.1023	0.0016**	0.0084	3.435	0.0046**
	OCT	= -27.88 + 0.025 * Year	0.1324	<.0001**	0.0105	3.417	0.0016**
	NOV	= 5.47 + 0.005 * Year	0.0508	0.118	0.0004	3.575	0.5406
	DEC	= -25.41 + 0.018 * Year	0.1197	0.0002**	0.0060	3.350	0.0173*
Maximum air temperature	JAN	= 1.85 + 0.006 * Year	0.0299	0.1648	0.0005	3.800	0.4644
	FEB	= 33.87 - 0.009 * Year	-0.0114	0.5974	0.0010	3.945	0.3095
	MAR	= 3.59 + 0.008 * Year	0.0231	0.2833	0.0008	4.019	0.3751
	APR	= -10.25 + 0.018 * Year	0.047	0.0288*	0.0043	3.815	0.0400**
	MAY	= 11.35 + 0.009 * Year	0.0266	0.2172	0.0012	3.785	0.2836
	JUN	= 24.54 + 0.004 * Year	0.0208	0.3327	0.0002	3.864	0.6316
	JUL	= -6.24 + 0.020 * Year	0.0537	0.0125*	0.0052	4.007	0.0238*
	AUG	= -1.96 + 0.018 * Year	0.0514	0.0166*	0.0043	3.932	0.0387*
	SEPT	= 22.03 + 0.005 * Year	0.0179	0.4049	0.0004	3.550	0.5119
	OCT	= 16.57 + 0.006 * Year	0.0255	0.2348	0.0006	3.509	0.4511
	NOV	= 26.71 - 0.003 * Year	0.0028	0.8962	0.0001	3.784	0.7674
	DEC	= -30.55 + 0.024 * Year	0.0739	0.0006**	0.0085	3.600	0.0035**
Minimum air temperature	JAN	= -16.18 + 0.010 * Year	0.0464	0.0314*	0.0017	3.482	0.1960
	FEB	= -15.47 + 0.010 * Year	0.0491	0.0228*	0.0018	3.386	0.1791
	MAR	= -19.04 + 0.013 * Year	0.0445	0.0391*	0.0030	3.424	0.0869
	APR	= -32.06 + 0.022 * Year	0.0803	0.0002**	0.0081	3.373	0.0046*
	MAY	= -44.39 + 0.030 * Year	0.0825	0.0001**	0.0143	3.476	0.0002**
	JUN	= -39.71 + 0.029 * Year	0.0867	<.0001**	0.0129	3.540	0.0003**
	JUL	= -73.75 + 0.047 * Year	0.1296	<.0001**	0.0331	3.585	<.0001**
	AUG	= -69.37 + 0.045 * Year	0.1257	<.0001**	0.0272	3.788	<.0001**
	SEPT	= -51.59 + 0.035 * Year	0.1072	<.0001**	0.0162	3.842	<.0001**
	OCT	= -62.03 + 0.038 * Year	0.1118	<.0001**	0.0196	3.847	<.0001**
	NOV	= -7.23 + 0.008 * Year	0.0401	0.0616	0.0009	3.882	0.3355
	DEC	= -16.84 + 0.011 * Year	0.0476	0.0264*	0.0019	3.630	0.1668

** sign indicates significant trends at the 5 percent confidence level, and ** sign indicates significant trends at the 1 percent confidence level.*

Although the lack of data on the rainfall intensity hinders the investigation of the potentials of extreme events in the country, it was found through the exploration of the number of rainy days within each month at the station level that there exists a high potential of increase in rainfall intensity with time. The significant decrease in the number of rainy days with time supports the increase postulation of intensity with the assumption of keeping the precipitation quantity around the same annual average. On the other hand, it was clear that the precipitation quantity varies spatially and temporally across the country, thus the rainfall intensity and, therefore, extreme events are likely to appear with spatial and temporal dependents as well. This justifies the increase in flooding events at some locations in Jordan during the last decade.

On the other hand, the statistical trends of mean, maximum and minimum temperatures on daily and monthly bases indicated significant increasing for most of the months and within the majority of the stational points. The climate change trends are clearer and more affective at the minimum air temperature as shown by the probability of significance compared to mean and maximum temperatures. The increase trends in maximum air temperatures were detected to be insignificant; however, they are spatial-dependent rather than being temporal-dependent. This coincide with Freiwan and Kadioğlu (2008a and 2008b) where warming climate trends were recognized in two spells in the time series of the early 1970s and beyond the year 1992, when maximum temperature was less statistically-significant compared to the minimum temperature. The minimum air temperature increase was detected to be more sever in the dry season (May to September) compared to the wet season (October to April) as indicated by the rate of change and the trend tests' significance.

3.2. Spatial Cokriging Mapping

The strength of the relationships between the climatic variables and auxiliary variables were ranging between moderate to strong. Pearson correlation matrix indicated that the auxiliary variable correlation with precipitation, maximum air temperature, mean air temperature, minimum air temperature, relative air humidity, and potential evapotranspiration were 0.56, 0.67, 0.71, 0.78, 0.81, and 0.75, respectively.

The cross-variogram model indicates the anisotropical behavior of all climatic variables with a logarithmic behavior of change for most of the climatic variables, except for relative air humidity where the best fit model is Gaussian. The cross-validation between the auxiliary variable and the climatic variables were very satisfactory. The coefficients of determination of the final cokriging map were 0.92, 0.80, 0.84, 0.91, 0.86, and 0.74 for precipitation, mean air temperature, maximum air temperature, minimum air temperature, relative air humidity, and potential evapotranspiration, respectively. The root low magnitudes of residuals are indicative of the improvement of the accuracy of prediction compared to the general kriging technique; therefore, the cokriging technique for the generation of precipitation maps especially in regions with high spatial variation of rainfall as well as elevation was employed.

Table 3. Cross-validation statistics of cokriging spatial interpolation.

Climatic Variable	R^2	RMSE
Precipitation	92	31.2
Mean Air Temperature	0.80	2.3
Maximum Air Temperature	0.84	1.9
Minimum Air Temperature	0.91	1.5
Relative Air Humidity	0.86	5.4
Potential Evapotranspiration	0.74	55.4

Based on the generated cokriging precipitation map, the long mean annual precipitation appears to be spatially and temporally dependent (Figure 2)t. The minimum rainfall was recorded at the southern Badia region with an average value of less than 30 mm similar to Al–Jafr and Aqaba. The cokriging precipitation map was able to show the detailed variation in precipitation especially along the Ghor region, starting from 280 mm at the highest point in the north, declining towards the south until reaching 71 mm in Ghor Safi. The high average annual precipitation in the mountains was found to vary from 298 mm in Tafeeleh and 270 mm in Al–Shoubak to 540 mm at Bulqa mount and 615 mm in Ras Muneef.

On the other hand, the generated cokriging temperature maps indicated that the average mean temperature across the country varies from 13 C in the southern Badia region to 28 C at Aqaba with a mean of 18.6 C all over the country (Figure 3). The variability in the mean air temperature is attributed to the existing variability in the minimum temperature ranging from 5.6 in the eastern region to 19.8 C in the western region (Figure 4), while the maximum temperature is almost distributed uniformly with an average of 25.3 C varying from 18.7 to 31.3 C (Figure 5).

The country seems to have an oriented spatial distribution of both potential evapotranspiration and relative humidity. The average annual potential evapotranspiration was estimated at about 2502 mm varying from 1460 mm in the northern highlands of Ras Muneef to 3886 mm in the eastern region, especially in Aqaba (Figure 6). Similarly, the relative humidity was about 57% varying from 76.2% in the northern highlands of Ras Muneef to 48.8 % in the northern Badia region and to 47.6 % in Aqaba (Figure 7f).

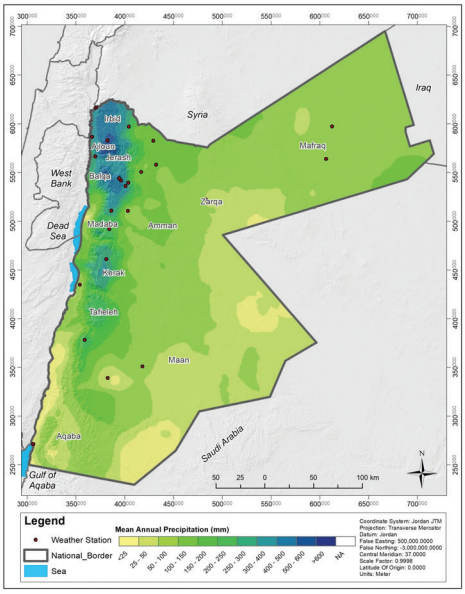

Figure 2. Generated gokriging precipitation map

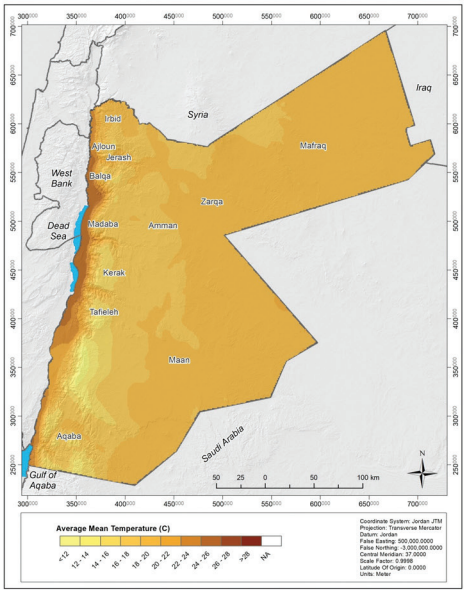

Figure 3. Generated cokriging average mean air temperature map

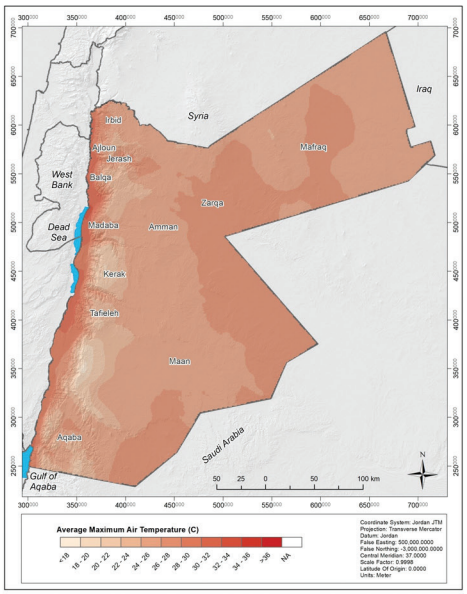

Figure 4. Generated cokriging maximum air temperature map

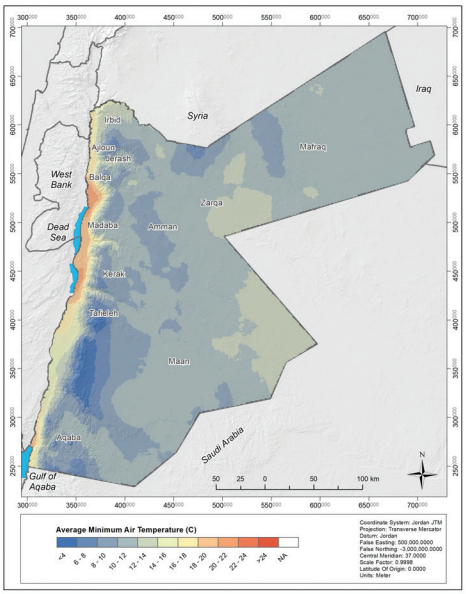

Figure 5. Generated cokriging maximum air temperature map

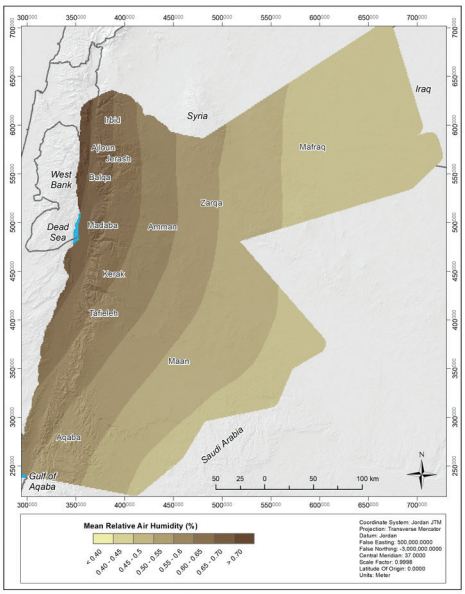

Figure 6. Generated cokriging mean relative air humidity map

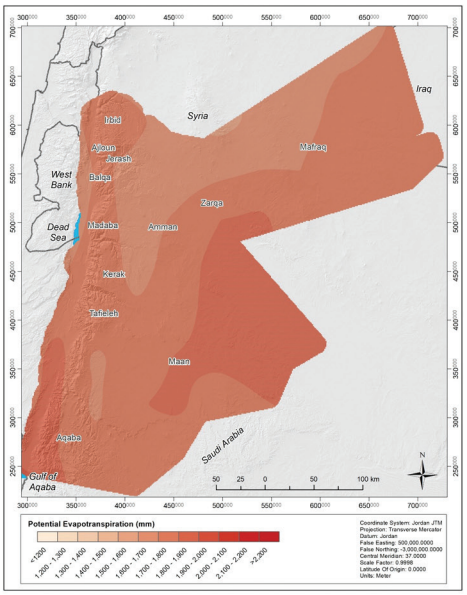

Figure 7. Generated cokriging potential evapotranspiration map

Conclusions

Climatic variability in Jordan is spatially and temporally dependent, varying at both national and local micro-climatic levels. Understanding the spatial variation of climatic factors is very important for a better future planning and management. Also, increasing the accuracy of the spatial predictions of the climatic variables with the aid of the available ancillary data is quite helpful, especially in complex terrains like Jordan.

Mann-Kendall rank and linear regression trend tests for long historical data about 143 stational points indicated that the climatic variability in Jordan has specific site-base trends which confirm the warming generated by the impacts of climate change. Annual precipitation decreasing trends vary by space with an average rate of 1.2 mm/year. On the contrary, maximum air temperature tends more likely to increase by 0.01°C/year, while the minimum air temperature is very likely to increase by 0.03 °C/year, respectively. As a result, the potential evapotraspiration will eventually increase by an estimated rate of 17mm/year threatening the water availability which is already exerbated by the growing needs for crop-water.

Integrating the Geographic Information System and a geostatistic approach for the spatial interpolation of selected climatic variables was promising through generating cokriging fine resolution maps by integrating climatic variables with elevation as an auxiliary variable. Cross-validations between the auxiliary variable and the climatic variables were very satisfactory, and provided good advantages that enabled the reduction of significant prediction errors, therefore, improving the prediction accuracy as indicated by the high coefficients of determination and the low root mean square errors.

References

[1] Abandeh, A. 1999. Climate trends and climate change scenarios, vulnerability and Adaptation to Climate Change in Jordan, Project No. JOR/95/G31/IG/99, 1, Al-Shamil Engineering: Amman, Jordan.

[2] Adhikary S.K., Muttil N., Yilmaz A.G. 2017. Cokriging for enhanced spatial interpolation of rainfall in two Australian catchments. Hydrological Processes. 31:2143–2161.

[3] Al-Ansari, N., Salameh, E., and Al-Omari, H. 1999. Analysis of rainfall in the Badia region, Jordan, Research Paper, 1. Al-al-Bayt University, Jordan.

[4] Al-Houri Z. 2014. Detecting Variability and Trends in Daily Rainfall Characteristics in Amman-Zarqa Basin, Jordan. International Journal of Applied Science and Technology, 4(6):11-23.

[5] Al-Qinna M., Hammouri N., Obeidat M., Ahmad F. 2011. Drought Analysis in Jordan under Current and Future Climates. Journal of Climatic Change, 106(3):421-440.

[6] Bani-Domi, M. 2005. Trend analysis of temperatures and precipitation in Jordan, Umm Al-Qura University Journal of Educational, Social Sciences & Humanities, 17(1), 15-36.

[7] Dahamsheh, A., and Aksoy H. 2007. Structural characteristics of annual precipitation data in Jordan. Theoretical Applied Climatology, 88, 201–212.

[8] Diodato N. 2005. The Influence of Topographic Co-Variables on the Spatial Variability of Precipitation Over Small Regions of Complex Terrain. Int. J. Climatol. 25: 351–363.

[9] ESRI. 2017. ArcGIS software version 10.3. ESRI Inc., Redlands, California, USA

[10] FAO (Food and Agricultural Organization). 2012. Assessment of the risks from climate change and water scarcity on food productivity in Jordan.

[11] Fiebrich, C.A., Morgan, C.R., McCombs, A.G., Hall, P.K., Jr., and McPherson, R.A. 2010. Quality assurance procedures for mesoscale meteorological data. Journal of Atmospheric and Oceanic Technology 27(10):1565 – 1582.

[12] Freiwan M. and Kadioğlu M. 2008a. Spatial and temporal analysis of climatology in Jordan. Int. J. Climatol., 28:521 – 535.

[13] Freiwan, M. and Kadioğlu, M. 2008b. Climate variability in Jordan. Int. J. Climatol. 28: 69 – 89.

[14] Freiwan, M. and Kadioğlu, M. 2006. Contemporary Climate Change in Jordan. 1st International Conference on Climate Change and the Middle East: Past, Present and Future 20-23 November 2006, Istanbul Technical University, Istanbul, Turkey.

[15] Ghanem A. 2013. Case Study: Trends and Early Prediction of Rainfall in Jordan. American Journal of Climate Change, 2013, 2, 203-208.

[16] Ghanem, A. 2010. Climatology of the areal precipitation in Amman/Jordan, International Journal of Climatology, 31(9), 1328-1333.

[17] Ghanem, A. 2011. Trends in mean seasonal and annual rainfall amounts over Jordan. Dirasat, University of Jordan, Vol. 8, 2011, pp. 1041-1049.

[18] Goovaerts P. 1997. Geostatistics for natural resources evaluation. Oxford University Press, New York

[19] Goovaerts, P. 2000. Geostatistical approaches for incorporating elevation into the spatial interpolation of rainfall, J Hydrol. 228, 113—129.

[20] Grzymala-Busse J.W. and Hu M. 2001. A Comparison of Several Approaches to Missing Attribute Values in Data Mining, RSCTC 2000, LNAI 2005, pp. 378−385, 2001.

[21] Guttman, N., Karl, C., Reek, T., and Shuler, V. 1988. Measuring the performance of data validators. Bulletin of the American Meteorological Society 69(12):1448 – 1452.

[22] IPCC (Intergovernmental Panel on Climate Change). 2007: Technical Summary. In: Climate Change 2007: The Physical Science Basis. Contribution of Working Group I to the Fourth Assessment Report of the Intergovernmental Panel on Climate Change [Solomon, S., D. Qin, M. Manning, Z. Chen, M. Marquis, K.B. Averyt, M. Tignor and H.L. Miller (eds.)]. Cambridge University Press, Cambridge, United Kingdom and New York, NY, USA.

[23] IPCC (Intergovernmental Panel on Climate Change). 2013. Climate Change 2013: The Physical Science Basis. Contribution of Working Group I to the Fifth Assessment Report of the Intergovernmental Panel on Climate Change [Stocker, T.F., D. Qin, G.-K. Plattner, M. Tignor, S.K. Allen, J. Boschung, A. Nauels, Y. Xia, V. Bex and P.M. Midgley (eds.)]. Cambridge University Press, Cambridge, United Kingdom and New York, NY, USA, 1535 pp.

[24] IPCC (Intergovernmental Panel on Climate Change). 2014. Summary for Policymakers. Climate Change 2014: Synthesis Report. Contribution of Working Groups I, II and III to the Fifth Assessment Report of the Intergovernmental Panel on Climate Change. http://doi.org/10.1017/CBO9781107415324

[25] Isaaks, E.H. and Srivastava, R.M. 1989. An Introduction to Applied Geostatistics. Oxford, UK: Oxford University Press.

[26] JMP. 2014. JMP statistical Software Guide Book, SAS Institute Inc., Cary, NC, USA.

[27] Journel, A.G. 1986. Geostatistics: Models and Tools for Earth Sciences. Math. Geol. 18: 119.

[28] Journel, A.G. 1989. Fundamentals of Geostatistics in Five Lessons. Short Course in Geology, AGU, Washington, DC, 8, 40.

[29] Kendall, M. 1975. Rank correlation methods, 4th edition, Charles Griffin, London.

[30] Kotsiantis S., A. Kostoulas, S. Lykoudis, A. Argiriou, K. Menagias. 2006. Filling Missing Temperature Values In Weather Data Banks. 2nd IEE International Conference on Intelligent Environments, 5-6 July, 2006, Athens, Greece, 1:327-334.

[31] Mann, H. 1945. Non-parametric tests against trend, Econometrica, 13, 163-171.

[32] Matouqa, M., El-Hasan,T., Al-Bilbisi, H., Abdelhadi, M., Hindiyeh, M., Eslamian, S., and Duheisat, S. 2013. The climate change implication on Jordan: A case study using GIS and Artificial Neural Networks for weather forecasting, Journal of Taibah University for Science, 7, 44–55.

[33] MoEnv (Ministry of Environment). 1999. Jordan's First National Communication to the UNFCCC. Ministry of Environment, Amman, Jordan.

[34] MoEnv (Ministry of Environment). 2006. National Capacity Self Assessment for Global Environmental Management (NCSA) - Jordan National Capacity: Assessment Report and Action Plan, GEF and UNDP project, Amman, Jordan.

[35] MoEnv (Ministry of Environment). 2009. Jordan's Second National Communication to the UNFCCC. Ministry of Environment, Amman, Jordan.

[36] MoEnv (Ministry of Environment). 2012. Climate Change Adaptation in the Zarqa River Basin: Assessment of Direct and Indirect Impacts of Climate Change Scenarios, (Water Resources Study, Vol. l). Ministry of Environment, Funded by UNDP, Amman, Jordan.

[37] MoEnv (Ministry of Environment). 2013. The National Climate Change Policy of the Hashemite Kingdom of Jordan 2013-2020. Sector Strategic Guidance Framework. Supported by Global Environment Facility (GEF) and the United Nations Development Programme (UNDP), Amman, Jordan.

[38] MoEnv (Ministry of Environment). 2014a. Intended Nationally Determined Contribution (INDC) submitted by the Hashemite Kingdom of Jordan to UNFCCC, Amman, Jordan.

[39] MoEnv (Ministry of Environment). 2014b. Jordan's Third National Communication on Climate Change Submitted to The united nations Framework Convention on Climate Change (UNFCCC). Ministry of Environment, Amman, Jordan.

[40] Nelsen, R. 2001. Kendall tau metric, Hazewinkel, Michiel, Encyclopedia of Mathematics, Springer.

[41] Ragab, R. and Prudhomme, C. 2002. Climate change and water resources management in arid and semi arid regions: prospective and challenges of the 21st century. Biosystem Engineering, 81(1): 3- 34.

[42] Salahat M.A. and Al-Qinna M.I. 2015. Rainfall Fluctuation for Exploring Desertification and Climate Change: New Aridity Classification. Jordan Journal of Earth and Environmental Sciences. 7(1): 27-35.

[43] Scott H.D. 2000. Soil physics: agricultural and environmental applications. Iowa State University Press, Iowa, USA.

[44] Selker J.S., Keller C.K., McCord J.T. 1999. Vadose zone processes. Lewis Publishers/CRC Press LLC, Florida, USA.

[45] Shulski, M.D., J. You, J.R. Krieger, W. Baule, J. Zhang, X. Zhang and W. Horowitz. 2014. Quality Assessment of Meteorological Data for the Beaufort and Chukchi Sea Coastal Region using Automated Routines. ARCTIC, 67(1):104–112.

[46] Smadi, M., and Zghoul, A. 2006. A sudden change in rainfall characteristics in Amman, Jordan during the mid 1950s, American Journal of Environmental Sciences, 2 (3), 84-91.

[47] Tarawneh Q. and Kadioğlu M. 2002. An analysis of precipitation climatology in Jordan. Theoretical and Applied Climatology. 74: 123-136.

[48] UN (United Nation). 2009. Guidance on Water and Adaptation to Climate Change. Economic Commission for Europe Convention on the Protection and Use of Transboundary Watercourses and International Lakes.

[49] Wackernagel, H. 1995. Multivariate Geostatistics: An Introduction with Applications. Berlin, Germany: Springer-Verlag.

[50] Wang X., Lv J., Wei C., Xie D. 2011. Modeling Spatial Pattern of Precipitation with GIS and Multivariate Geostatistical Methods in Chongqing Tobacco Planting Region, China. In: Li D., Liu Y., Chen Y. (eds) Computer and Computing Technologies in Agriculture IV. CCTA 2010. IFIP Advances in Information and Communication Technology, vol 346. Springer, Berlin, Heidelberg.

المملكة الأردنية الهاشمية

صندوق دعم البحث العلمي

الجامعة الهاشمية

المجلة الأردنية
لعلوم الأرض والبيئة

JJEES

مجلة علمية عالمية محكمة

المجلد (٩) العدد (١)

http:// jjees.hu.edu.jo/

ISSN 1995-6681

المجلة الأردنية لعلوم الأرض والبيئة

مجلة علمية عالمية محكمة

المجلة الأردنية لعلوم الأرض والبيئة: مجلة علمية عالمية محكمة ومفهرسة ومصنفة، تصدر عن عمادة البحث العلمي في الجامعة الهاشمية وبدعم من صندوق البحث العلمي - وزارة التعليم العالي والبحث العلمي، الأردن.

ترسل البحوث إلكترونيا إلى البريد الإلكتروني التالي:

رئيس تحرير المجلة الأردنية لعلوم الأرض والبيئة

jjees@hu.edu.jo

لمزيد من المعلومات والأعداد السابقة يرجى زيارة موقع المجلة على شبكة الانترنت على الرابط التالي:

www.jjees.hu.edu.jo

المملكة الأردنية الهاشمية
صندوق دعم البحث العلمي
الجامعة الهاشمية

المجلة الأردنية لعلوم الأرض والبيئة

JJEES

مجلة علمية عالمية محكمة

تصدر بدعم من صندوق دعم البحث العلمي

http://jjees.hu.edu.jo/

المجلد (٩) العدد (١) ISSN 1995-6681 نيسان ٢٠١٨ / شعبان ١٤٣٩